

Dear Editor,

We appreciate the careful consideration of our manuscript by the reviewers. We have carefully responded to all of the [point-by-point](#) comments and issues raised by the reviewers and have revised the manuscript accordingly. These revisions are described in detail below.

Reviewer 1#

The work by Liu et al present field measurements of HONO, a key source of radicals in the boundary layer, along with supplementary gas and particle-phase measurements in over a 5-month period in Beijing. The authors used this dataset to probe the sources and their contributions to ambient HONO, with a focus on pollution events. Using a steady state approach, the authors calculated the contributions of different sources to the HONO budget and concluded that traffic emission (via direct emission and conversion of NO by homogenous reactions) was the key source of HONO during winter pollution events. Liu et al present a comprehensive and interesting long-term dataset that enables the authors to perform a budget analysis to investigate the main sources of HONO. The main sources of HONO in Beijing and urban area in general is an open research topic, and consequently this work would be of interest to the community, particularly their HONO budget analysis of the haze events.

Response: Thank you so much for your positive comments.

There are, however, a few issues that in my opinion should be addressed prior to publication. While the manuscript is mostly well written, it is long. For example, Section 3.1 and 3.2 could be much shorter. In my opinion much of the text in these sections is unnecessary and could be reduced, without losing the key points.

Response: Thank you so much for your instructive suggestions. We have revised the redundant descriptions in Section 3.1 and 3.2.

In Section 3.1, the paragraph “In particular, the frequency of severe polluted episodes in March was obviously higher than that in the rest months (Fig. 1 and S3), resulting in the highest monthly mean concentration of PM_{2.5} ($88.5 \pm 60.0 \mu\text{g m}^{-3}$) and NR-PM_{2.5} ($67.0 \pm 56.8 \mu\text{g m}^{-3}$). This can be explained by both intensive emission during the heating season, which is supported

by the high concentration of primary pollutants including CO, SO₂ and BC (Table S1), and the stagnant meteorological conditions that physically and chemically promote the accumulation of pollutants. For example, the low wind speed (<2 m s⁻¹) mainly from south-based directions accompanied with the low planetary boundary layer (PBL) height frequently occurred in March compared with other months (Fig. S4A).” has been shortened as “Both the frequency of severe polluted episodes and the mean mass concentration of PM_{2.5} and NR-PM_{2.5} were obviously higher in March than that in the rest months (Fig. 1 and S3). This can be explained by both the intensive emission during the heating season as evidenced by the high concentration of primary pollutants including CO, SO₂ and BC (Table S1) and the stagnant meteorological conditions supported by the low wind speed (<2 m s⁻¹) and the low planetary boundary layer (PBL) height in March (Fig. S4A)” from lines 249 to 255 in the revised manuscript. In addition, we also deleted the sentences “It should be noted that the median mass concentrations of nitrate and OA also were higher in March than that in other months (Fig. S4C). The median mass concentrations of nitrate were 1.42, 8.76, 6.30, 3.15, and 3.23 μg m⁻³ from February to June, respectively. And the corresponding OA concentrations were 4.78, 14.04, 11.64, 13.89, and 14.08 μg m⁻³. Secondary formation is the major source of OA and nitrate in the atmosphere” from line 232 to 237 in the original version of the manuscript.

In Section 3.2, we deleted the following sentences “The hourly averaged $P_{\text{OH-HONO}}/P_{\text{OH-O}_3}$ ratio varied in the range of 1-25.4 during the daytime, while it varied from 0.3 to 2.8 from April to June” (lines 284-288, in the original manuscript), “Although the high loading of fine particles in polluted days could reduce the surface solar radiation (Li et al., 2017), subsequently, the OH concentration, the noon-time OH radical concentrations observed in polluted wintertime of Beijing were $2.4 \times 10^6 \text{ cm}^{-3}$ compared with $3.6 \times 10^6 \text{ cm}^{-3}$ in clean days (Tan et al., 2018). It was around 2 times compared to places such as Tokyo (Kanaya et al., 2007) and New York City (Ren et al., 2006)” (lines 295-300, in the original manuscript), and “ This implies that oxidation of atmospheric trace gases by OH may still be highly effective even in wintertime, thereby facilitating the vigorous formation of secondary pollutants in Beijing” (lines 301-304, in the original manuscript).

The most interesting work is presented in Section 3.3, where a detailed and comprehensive budget analysis is presented. However, throughout section 3.3 some of the calculations and equations need more explanation, as it was not always clear from section 2.2 how they were performed. Some examples are given below in the minor comments. It would also help the reader if the equation used to calculate the rates of emission for each source (I.e. the eqn numbers) were referenced throughout section 3.3.

Response: Thank you for your good suggestions. We have referenced all the equation numbers throughout the revised manuscript. For example, in [line 389](#) in the revised manuscript, “The E_{vehicle} was calculated **according to Eq. (2)** using the relative emission rate of HONO to NO_x and the emission inventory of NO_x from vehicles”; In [lines 446-448](#) in the revised manuscript, “The lower limit, the middle value and the upper limit of **the E_{soil} are $0.0032\pm 0.0027-0.013\pm 0.014$, $0.0046\pm 0.0039-0.020\pm 0.020$ and $0.0057\pm 0.0047-0.025\pm 0.024$ ppbv h⁻¹, respectively, **calculated according to Eq. (2)**”; In [lines 473-475](#) in the revised manuscript, “Thus, the lower limit, the middle value and the upper limit of $P_{\text{NO-OH}}$ were **$0.007\pm 0.019-0.43\pm 0.26$, $0.026\pm 0.053-0.99\pm 0.79$ and $0.028\pm 0.053-2.14\pm 1.71$ ppbv h⁻¹, respectively, **calculated according to Eqs. (3) and (4)**”; In [lines 495-498](#) in the revised manuscript, “Therefore, the corresponding daytime lower limit, the middle value and the upper limit of HONO from photolysis of nitrate were **$0.0011\pm 0.0021-0.096\pm 0.092$, $0.0072\pm 0.0021-0.66\pm 0.092$ and $0.042\pm 0.082-3.86\pm 0.008$ ppbv h⁻¹, respectively, **calculated in the light of Eqs. (3) and (8)**”; And in [lines 499-501](#) in the revised manuscript, “The production of HONO from heterogeneous reactions of NO_2 on aerosol surface was calculated according to **Eqs. (3) and (5)**”.******

We also added the more details about budget calculations. For example, we added the following paragraphs “**Oswald et al. (2013) measured the emission flux of HONO from 17 soil samples, including eucalyptus forest, tropical rain forest, coniferous forest, pasture, woody savannah, grassland, stone desert, maize field, wheat field, jujube field and cotton field etc. Tropical rain forest, coniferous forest and grassland are the typical plants in downtown Beijing (Huang et al., 2017a). At the same time, their emission fluxes of HONO are comparable (Oswald et al., 2013). Thus, we used the emission flux from grassland to calculate the emission rate of HONO from soil in Beijing because the temperature and water holding content dependent emission flux of HONO was available for grassland soil**” [lines 433-441](#); “The

method for the photolysis rates calculation were shown in the SI and the time series of the photolysis rates were shown in Fig. S7” in lines 458-460; “The time series of the measured nitrate concentration and the middle value of J_{nitrate} were shown in Fig. 1 and Fig. S7, respectively” in lines 493-495; “The A_s of aerosols varied from 1×10^{-4} to $4.8 \times 10^{-3} \text{ m}^{-1}$ with a mean value of $1.4 \pm 0.5 \times 10^{-3} \text{ m}^{-1}$ during pollution events. This value is comparable with that used in modeling studies (Zhang et al., 2016; Aumont et al., 2003). The A_s of ground surface which was calculated according to Eq. (6) and (7) varied from 1.5×10^{-3} to $3.85 \times 10^{-2} \text{ m}^{-1}$ with a mean value of $1.3 \pm 0.9 \times 10^{-2} \text{ m}^{-1}$ during pollution events. The surface roughness was 3.85 calculated according to Eq. (7). The Y_{HONO} was set to 0.5 because of the hydrolysis reaction of NO_2 (Liu et al., 2015), while it was 0.8 for light enhanced reaction (Liu et al., 2019; Ndour et al., 2008) and on BC (Han et al., 2013)” in lines 523-530 in the revised manuscript.

My major comment is from Section 3.3, the way the OH concentration was estimated is problematic in my opinion. As the authors rightly point out, to measure OH is difficult and requires highly specialized kit and therefore as they did not have access to these instruments, OH concentration needs to be estimated for this study. I am not sure about the way the OH concentration was calculated, as the equations they use (e.g. 13), use the levels of ozone and NO_2 . The problem is that during winter, the main source of OH in Beijing is HONO photolysis, as the authors themselves state earlier in the manuscript (Section 3.2, line 288, with references), and is in fact one of their conclusions from Fig 2. Therefore, without considering OH produced from HONO photolysis, how can they be sure that their estimated OH concentration is reasonable, especially in winter? I think that for an atmosphere as chemically complex as Beijing, to estimate the OH concentration requires a box-model approach. It is important as the estimated OH concentration will affect the budget analysis, both sources and loss terms, and therefore the conclusions drawn from it. If this is not possible, then the uncertainties with their approach to estimating OH concentrations should at least be discussed/quantified.

Response: Thank you for your instructive suggestion. We agree with you that OH concentration is an important parameter when calculating the HONO source from homogenous reaction between NO and OH. Some uncertainties of OH concentration should be resulted from the estimation approaches used in this work. In strictly speaking, it is better to directly measure

OH concentration using a LIF or a CIMS. However, these instruments are unavailable at the present time. A box-model simulation is another choice as you suggested because both the source and sink terms can be considered. A comprehensive sheet of VOCs including different isomers is required when doing box-model simulation because the reactivity varies greatly among different isomers even with the same mass to charge ratio (m/z). Unfortunately, the VOCs concentration was measured using a SPI-MS in this work. Similar to a PTR-MS, this instrument cannot separate the isomers with the same m/z . Therefore, we did not simulate OH concentration using a box-model. If we had the measured or modeled OH concentration, we could parameterize the J_{HONO} and C_{HONO} into the Eq. (15).

We indirectly verified the estimated OH concentration by comparison with diurnal curves of OH concentration in this work and that reported in literatures (Tan et al., 2019). Overall, the estimated OH concentration was comparable with that measured in the literature (Fig. S10). In addition, we further compared it with the OH concentration derived from the measured H_2SO_4 concentration using a nitrate-CIMS from December 2019 to February 2020. In a box model, we considered the daytime source of H_2SO_4 from oxidation of SO_2 by OH and the sinks of H_2SO_4 using the measured concentration of the monomer and the dimer of H_2SO_4 , the condensation sink (CS, from 1 nm to 10 μm of aerosol) and the meteorological parameters. Then, OH concentration was calculated using a steady state method. As shown in Fig. R1, the predicted OH concentrations were generally comparable between these two different methods. This means the estimated OH concentration in this work is overall credible.

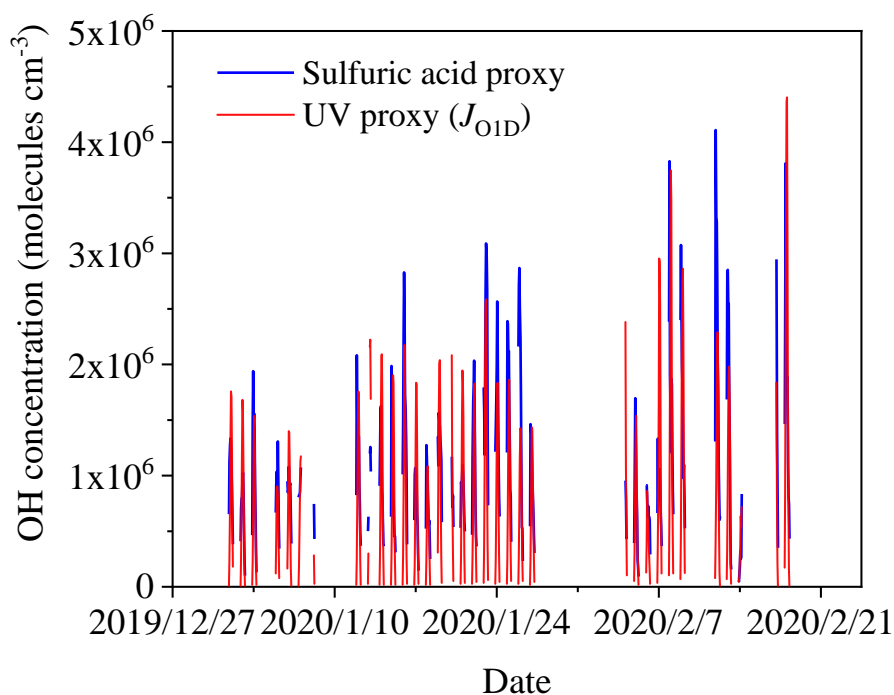


Fig. R1. Comparison of OH concentration between UV proxy method and H₂SO₄ proxy method.

In the revised manuscript (lines 482-488), we added the discussion about the uncertainties from OH concentration estimation as you suggested. “It should be noted that OH concentration was estimated based on J_{O1D} (Tan et al., 2019; Tan et al., 2018) or J_{O1D} and J_{NO2} (Li et al., 2018). As discussed in Section 3.2, HONO was an important primary OH source in the daytime. Unfortunately, it could not be parameterized for calculating OH concentration because the measured or modelled OH concentration was unavailable in this work. This might underestimate the early daytime OH concentration, subsequently, the contribution of homogeneous reaction of NO with OH to HONO source. This need to be further investigated in the future”.

Minor comments Line 82: I assume you mean nitrous acid not nitric acid?

Response: Thank you. It is nitrous acid. We have corrected this error in line 81 in the revised manuscript..

Line 112: it would be good to specify that your ACSM was configured for PM_{2.5}, as many of these instruments measure PM₁

Response: Thank you. It has been pointed out in the revised manuscript in [lines 136-137](#) as “Then a Time-of-Flight Aerosol Chemical Speciation Monitor **equipped a PM_{2.5} aerodynamic lens** (ToF-ACSM, Aerodyne)”.

Line 207: Why does it matter if PM_{2.5} is above 75 ug m⁻³? I assume you are referring to the regulatory limits, but it is good to be clear on this.

Response: Thank you. Yes, it the regulatory limits. The air quality is in pollution level if the PM_{2.5} concentration is above 75 ug m⁻³ according to the national air quality standards. In the revised manuscript ([lines 247-249](#)), we revised the sentences “During the observation period, 20-60% of hourly PM_{2.5} concentration was higher than 75 μg m⁻³ (**the criterion for pollution according to the national air quality standards**) in each month (Fig. S3A)”

Line 211: I am a bit confused by your explanation for there being more pollution episodes and higher concentrations of BC, CO and PM_{2.5} in March, as it was the heating season. But isn't February just as cold? So why would there more heating in March?

Response: Thank you for your comments. In Beijing, the air quality is always determined by both the emission and meteorological conditions. In both February and March are in heating season. However, in March the meteorological condition is more favorable for haze formation due to low wind speed and low PBL height. This is a long sentence in the original manuscript. We revised it as “**This can be explained by both the intensive emission during the heating season as evidenced by the high concentration of primary pollutants including CO, SO₂ and BC (Table S1) and the stagnant meteorological conditions supported by the low wind speed (<2 m s⁻¹) and the low planetary boundary layer (PBL) height, in particular, in March (Fig. S4A)**” in [lines 251-255](#) in the revised manuscript.

Line 222: Are the percentages listed for nitrate, chloride and ammonium also monthly means?

Response: Yes, they are monthly means. It has been pointed out in the revised manuscript. “At the same time, **the monthly mean fraction of** nitrate and chloride decreased from 26.7±8.8 % to 16.7±12.8 % and from 7.7±6.1 % to 0.3±0.2 %, respectively” in [lines 260-262](#) in the revised manuscript.

Line 226: I am bit surprised that fireworks is regionally transported from Tangshan, are there no fireworks in Beijing?

Response: Thanks. According to the regulation on fireworks of Beijing government, firework burning is totally forbidden within the fifth ring road of Beijing. Based on back trajectory analysis of air masses, we found that firework burning in Tangshan should also contribute to the high mass concentration of chloride in Beijing during Chinese New Year.

Line 232-240: As example to one of my main comments above, I found that this paragraph was repeating much of the information presented in the preceding one. Perhaps these two paragraphs could be edited and combined.

Response: Thank you for your suggestion. We deleted the paragraph “It should be noted that the median mass concentrations of nitrate and OA also were higher in March than that in other months (Fig. S4C). The median mass concentrations of nitrate were 1.42, 8.76, 6.30, 3.15, and 3.23 $\mu\text{g m}^{-3}$ from February to June, respectively. And the corresponding OA concentrations were 4.78, 14.04, 11.64, 13.89, and 14.08 $\mu\text{g m}^{-3}$. Secondary formation is the major source of OA and nitrate in the atmosphere” in [lines 232-237](#) in the original manuscript.

Line 272: why have you chosen to subset the data based on ‘when the $\text{PM}_{2.5}$ concentration was larger than $50 \mu\text{g m}^{-3}$ and the RH was less than 90 %’. Furthermore, as you state ‘Under these conditions, local chemistry should be more important as 75 % of the wind speed was less than 1.0 m s^{-1} ’. Why not then subset the data based solely on wind speed if local sources are of interest?

Response: Thank you for your comment. Because the aim of this paper is to understand the influence of HONO on secondary aerosol formation and the possible HONO source during pollution events. The dataset based solely on wind speed less than 1.0 m^{-1} could be also meaningful to discuss local chemistry. However, there are around one third data with low wind speed ($<1.0 \text{ m}^{-1}$) and low $\text{PM}_{2.5}$ concentration ($< 50 \mu\text{g m}^{-3}$). Therefore, the concentration of $\text{PM}_{2.5}$ was considered as one of the standards in this work. In the revised manuscript ([lines 307-311](#)), we revised it as “We simply compared the OH production via photolysis of HONO (P_{OH}).

$J_{\text{HONO}}=J_{\text{HONO}}\times C_{\text{HONO}}$) and O_3 ($P_{\text{OH-O}_3}=J_{\text{O1D}}\times C_{\text{O}_3}$) in Fig. 2 when the $\text{PM}_{2.5}$ concentration was larger than $50 \mu\text{g m}^{-3}$ and the RH was less than 90 % to understand the chemistry in pollution events”.

Line 275: How were these maximal $P_{\text{OH-HONO}}$ and $P_{\text{OH-O}_3}$ values calculated? I could not find the equation in the methods or reference.

Response: Thank you for your comment. They were calculated according to $P_{\text{OH-HONO}}=J_{\text{HONO}}\times C_{\text{HONO}}$ and $P_{\text{OH-O}_3}=J_{\text{O1D}}\times C_{\text{O}_3}$. In lines 307-311 in the revised manuscript, we defined them. “We simply compared the OH production via photolysis of HONO ($P_{\text{OH-HONO}}=J_{\text{HONO}}\times C_{\text{HONO}}$) and O_3 ($P_{\text{OH-O}_3}=J_{\text{O1D}}\times C_{\text{O}_3}$) in Fig. 2 when the $\text{PM}_{2.5}$ concentration was larger than $50 \mu\text{g m}^{-3}$ and the RH was less than 90 % to understand the chemistry in pollution events”. In addition, the J values were also added in Fig. S7 and Fig. R2.

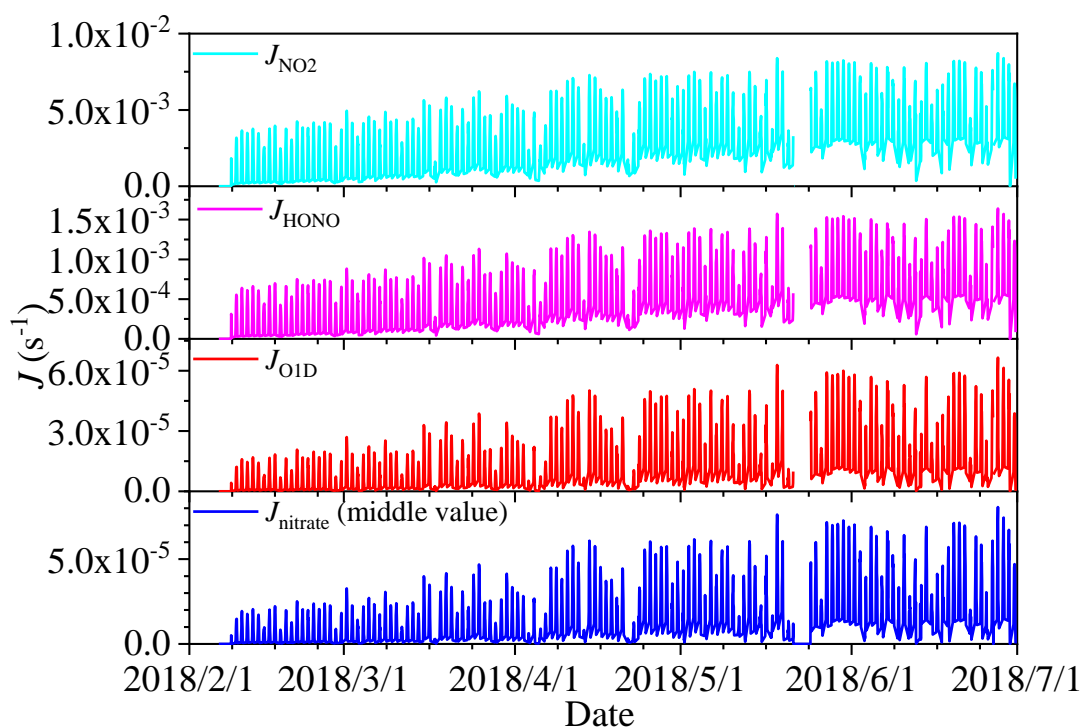


Fig. R2. The photolysis rate of NO_2 , HONO, O_3 (O1D) and nitrate (middle value) from 8:00 am to 6:00 pm.

Line 304: Is it not the production of the OH that changes in winter relative to summer, rather than the rate of oxidation of VOC by OH? Please clarify

Response: Thank you. We mean OH production from photolysis of HONO will compensate the relative weak sunlight in winter. As you suggested above, we removed this redundant sentences (This implies that oxidation of atmospheric trace gases by OH may still be highly effective even in winter, thereby facilitating the vigorous formation of secondary pollutants in Beijing) in [lines 301-304](#) in the original manuscript.

Line 318-20 and Fig 2: I am not so sure that is 'reasonable to mainly ascribe the increase of OA concentration to local secondary formation initiated by OH radical from HONO photolysis'. This is because if only OH from HONO photolysis was driving secondary formation, then shouldn't the OA/CO peak earlier, as the ambient HONO is essentially run out by 10am?

Response: Thank you for your instructive comment. During pollution events in winter in Beijing, the absolute HONO concentration was still above 0.6 ppb at noon ([Fig. R3](#)). The instrument automatically carried out zero point calibration twice per day during our observation. The measured HONO concentration at noon was much higher than the detection limit (10 ppt). Therefore, it reflected the real HONO concentration. Thus, it means that a photochemical steady state should be achieved between the daytime HONO sources and sinks and OH from photolysis of HONO should play an important role in initiation the HO_x and RO_x chemistry even after 10:00 am. In [lines 350-353](#) in the revised manuscript, we revised this sentence to "...it was reasonable to ascribe the increase of OA concentration to local secondary formation initiated by OH radical **and photolysis of HONO should play an important role in initiation the HO_x and RO_x chemistry**".

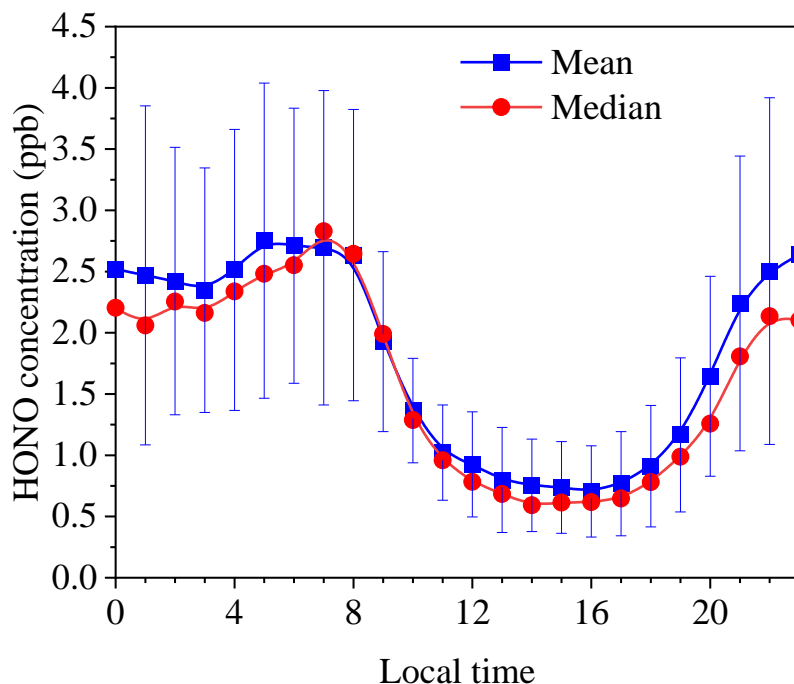


Fig. R3. The diurnal curve of HONO concentration during pollution events in winter.

Line 324: But can't there also be anthropogenic sources of alkenes? For example, isoprene can also be from vehicle emissions (See e.g. Zou et al 2019).

Response: Thank you. We agree with you that vehicles can also emit isoprene. In August, 2019, we measured the isoprene using a GC-FID, the mean isoprene concentration was 0.35 ppb. And the mean concentration was 0.5 ± 0.3 ppb at noon and 0.11 ± 0.11 ppb in night, respectively. The nighttime isoprene concentration was comparable with that in winter (0.13 ppb) in Guangzhou (Zou et al., 2019). If we assume the isoprene concentration in winter being equivalent to the nighttime concentration in August, the SOA formation potential of isoprene is $0.015 \pm 0.015 \mu\text{g m}^{-3}$. This contributes less than 0.5 % to the typical increase of OA concentration observed in this work. Therefore, we think the contribution of isoprene to the observed increase of OA concentration should be unimportant. In lines 358-360 in the revised manuscript, we added a sentence as “Although vehicles can emit isoprene (Zou et al., 2019), the contribution of isoprene to the observed increase of OA concentration should be unimportant due to the low concentration of isoprene in winter (Zou et al., 2019)”.

Line 379: at the start of the sentence, you state that hourly NO_x EI were available, yet than go

to give a yearly emission factor? Why wasn't hourly EI used, and did you consider your measured NO_x concentrations, as the diurnal variation in NO_x would be important? Please clarify in more detail how the Vehicle was calculated Especially as emission inventories can have significant bias (See for example very recent work for Beijing by Squires et al, 2020).

Response: Thank you for your good suggestion. In this work, we used the hourly emission inventory of NO_x (Fig. R4A) (Yang et al., 2019) to calculate the emission rate of HONO from vehicles. When calculating the emission rate of HONO, we converted the the hourly emission inventory (*EI*) to hourly emission flux ($F=EI/A$, where *A* is the area of Beijing). Then, the emission flux was normalized to the hourly mean PBL height according to Eq. (2). This resulted into the diurnal variation of NO_x. If the annual emission inventory was used to calculate the emission rate of HONO, the daily emission inventory was required to normalize to the measured NO_x concentration to catch the diurnal variation. As shown in Fig. R4B, the emission rate of HONO using these two methods are overall comparable, but the daytime emission rate of HONO based on the hourly emission inventory is higher than that calculated using the annual emission inventory. We used the hourly emission inventory because it contained the traffic details on road such as emission factor of NO_x for vehicle category, speed, traffic volume and congestion map and so on (Yang et al., 2019).

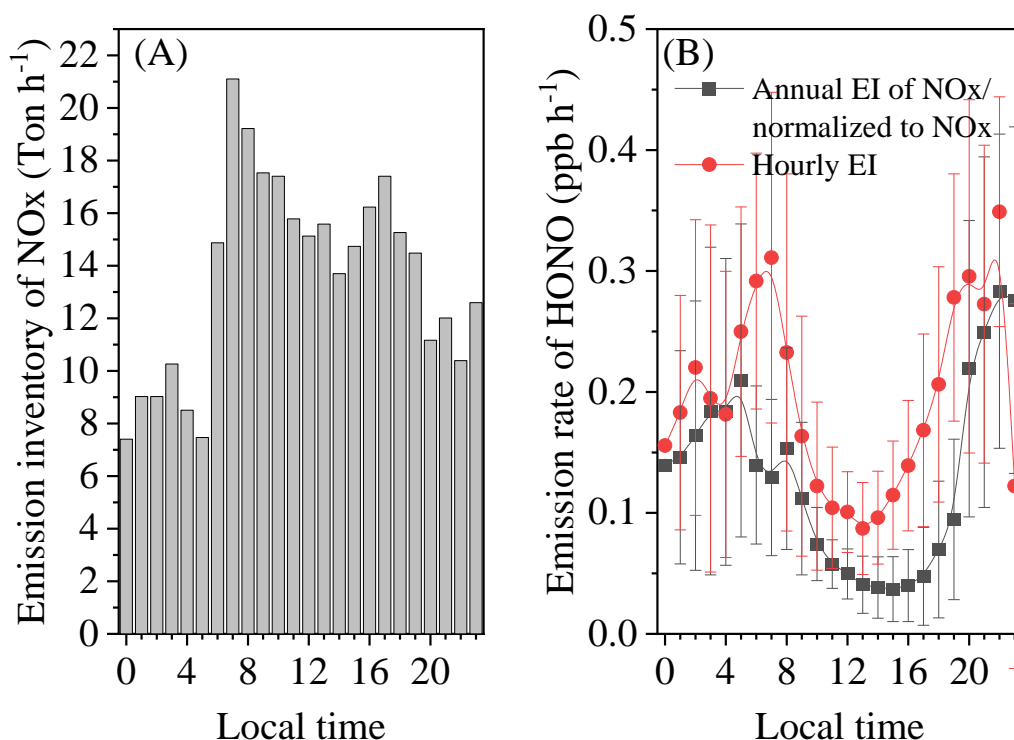


Fig. R4. (A) Hourly emission inventory of NO_x from vehicles in Beijing (Yang et al., 2019) and calculated emission rate of HONO from vehicles using different methods.

To make it clearer, in lines 180-185 the revised manuscript, we added more details as “The emission rate (E_{HONO} , ppbv h⁻¹) was calculated based on the emission flux ($F_{\text{HONO}}=EI_{\text{HONO}}/A$, g m⁻² s⁻¹) and PBL height (H , m) according to the following equation,

$$E_{\text{HONO}} = \frac{\alpha \cdot F_{\text{HONO}}}{H} \quad (2)$$

where, EI_{HONO} , is the emission inventory of HONO (g s⁻¹), A is the urban area of Beijing (m²), α is the conversion factor ($\alpha = \frac{1 \times 10^9 \cdot 3600 \cdot R \cdot T}{M \cdot P} = \frac{2.99 \times 10^{13} \cdot T}{M \cdot P}$), M is the molecular weight (g mol⁻¹), T is the temperature (K) and P is the atmospheric pressure (Pa)”.

In lines 421- 423 in the revised manuscript, we revised the sentence “The E_{vehicle} was calculated using the hourly NO_x emission inventory from vehicles in Beijing (Yang et al., 2019) after converted to emission flux of HONO ($F_{\text{HONO}}=F_{\text{NO}_x} \times \text{HONO}/\text{NO}_x$) and the PBL height as described in Section 2.2”

We agree with you that a bias should exist for the emission inventory. According to the most recent work, the MEIC 2013 emissions inventory might significantly overestimate the emission of NO_x in Beijing (Squires et al., 2020). In this work, we used the newest emission inventory (Yang et al., 2019) but not the MEIC 2013. We compared the wintertime emission flux of NO_x calculated using the emission inventory from Yang et al. (2019) with the emission flux reported by Squires et al. (2020) (Fig. R5). The former emission flux is as 2.4±0.5 times as the later one. This will introduce an additional uncertainty to our estimation. In lines 712-716 in the revised manuscript, we added a paragraph “The source of HONO from vehicles was calculated based on the emission inventories, which should have a significant bias (Squires et al., 2020). For example, the emission flux of NO_x calculated using the emission inventory from Yang et al. (2019) is as 2.4±0.5 times as the reported emission flux reported by Squires et al. (2020).”.

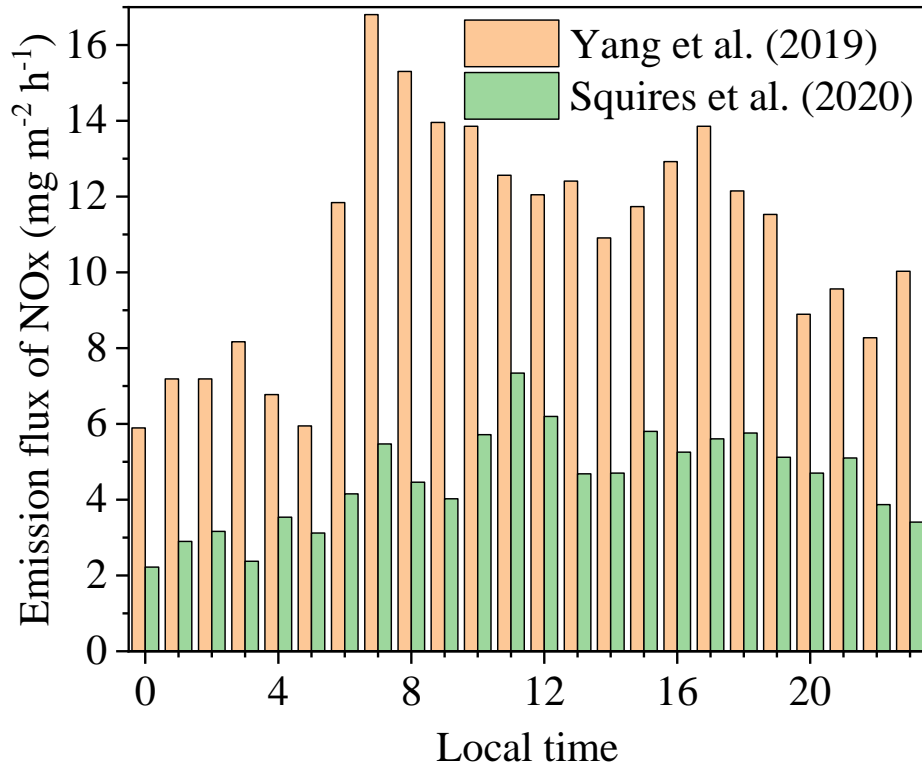


Fig. R5. Comparison of the wintertime emission flux of NO_x based on different emission inventory.

Line 381: This may be related to the above comment, but how did you report a range for calculated middle value of vehicle, when the NO_x EI rate is constant and the HONO/NO_x is constant? Furthermore, what does the middle value refer to? Daily avg? hourly avg? please specify. This applies throughout this section

Response: Thank you. As discussed above, the hourly emission of NO_x reflected the diurnal variation vehicle emission. In addition, the variation of PBL height was considered when we calculating the emission rate. Although the HONO/NO_x was constant, the emission rate should show a diurnal variation. Three different emission rates of HONO were calculated because we chose three levels of HONO/NO_x, i.e., the lower limit is 0.18% measured using a Chassis dynamometer test (Liu et al., 2017), 1.17% calculated using the low limit correlation of field data and 1.8 % using the empirical analysis of field data in this work. We called “middle value” for the emission rate calculated using HONO/NO_x=1.17%. In [lines 423-425](#) in the revised manuscript, we added a sentence “**Thus the calculated emission rate reflected the diurnal**

variation of both the emission inventory and the PBL height”. In lines 425-427 in the revised manuscript, the sentence was revised “The calculated hourly middle value of E_{vehicle} using the HONO/NO_x of 1.17% was from 0.085 ± 0.038 to 0.34 ± 0.15 ppbv h⁻¹, which was slightly higher than the daytime emission rate of HONO in Xi’an (Huang et al., 2017b)”.

Line 386: the reported range for the upper limit is the same as reported for the lower limit, I’m guessing a typo?

Response: Thank you. From line 428 to 431 in the revised manuscript, “The lower limit of E_{vehicle} was $0.013\pm 0.006-0.053\pm 0.023$ ppbv h⁻¹, which was close to the estimated emission rate of HONO in Jinan (Li et al., 2018). The upper limit was in the range of $0.13\pm 0.06-0.53\pm 0.23$ ppbv h⁻¹”. The upper limit is one order of magnitude higher than the lower limit because the corresponding HONO/NO_x is 0.18 % and 1.8%.

Line 389: Please give the reference for the emission flux you used, the value and also why grassland was the most appropriate.

Response: Thank you. Oswald et al. measured the emission flux of HONO from 17 soil samples, including eucalyptus forest, tropical rain forest, coniferous forest, pasture, woody savannah, grassland, stone desert, maize field, wheat field, jujube field and cotton field etc. (Oswald et al., 2013). Tropical rain forest, coniferous forest and grassland are the typical plants in downtown Beijing (Huang et al., 2017a). At the same time, their emission fluxes of HONO are comparable (Oswald et al., 2013). Thus, we used the emission flux from grassland to calculate the emission rate of HONO from soil in Beijing because the temperature and water holding content dependent emission flux of grassland was available (Fig. R6). We added this paragraph “Oswald et al. (2013) measured the emission flux of HONO from 17 soil samples, including eucalyptus forest, tropical rain forest, coniferous forest, pasture, woody savannah, grassland, stone desert, maize field, wheat field, jujube field and cotton field etc. Tropical rain forest, coniferous forest and grassland are the typical plants in downtown Beijing (Huang et al., 2017a). At the same time, their emission fluxes of HONO are comparable (Oswald et al., 2013). Thus, we used the emission flux from grassland to calculate the emission rate of HONO from soil in Beijing because the temperature and water holding content dependent emission flux of

HONO from grassland soil was available” in lines 433-441 in the revised manuscript.

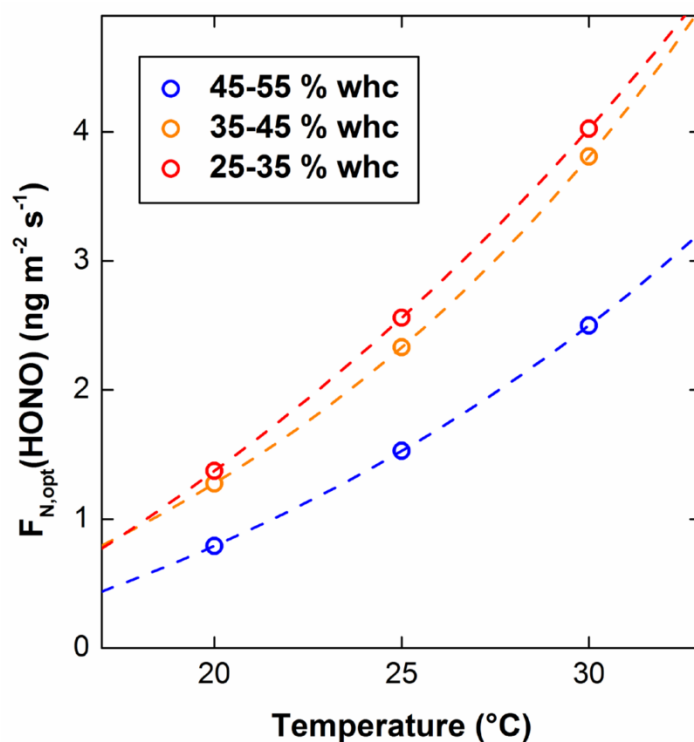


Fig. R6. The emission flux of HONO from grassland at different temperature and water holding capacity (Oswald et al., 2013).

Line 397: why does only the middle values for E_{soil} have uncertainty calculated? Also how did you estimate the uncertainty for E_{soil} ? And why did you use a range of soil water content for lower, middle and upper, why not just use a single value?

Response: Thank you. We added the uncertainties of other values in lines 446-448 in the revised manuscript. “The lower limit, the middle value and the upper limit of the E_{soil} are $0.0032 \pm 0.0027 - 0.013 \pm 0.014$, $0.0046 \pm 0.0039 - 0.020 \pm 0.20$ and $0.0057 \pm 0.0047 - 0.025 \pm 0.024$ ppbv h⁻¹, respectively, calculated according to Eq. (2)”. The uncertainty is the standard deviation when calculating the diurnal curve. We didn’t measure the water content of the soil, while it should vary with seasons. Thus, we used a range of soil water content rather than a single value. For other sources, we also added all the uncertainties in the revised manuscript.

Line 416: Please provide more information on the night time temperature dependence of OH concentration, and the equations used in this calculation.

Response: Thank you. In the night, OH concentration usually varied from 1.0×10^5 molecules cm^{-3} (Li et al., 2012; Tan et al., 2018) in winter to 5×10^5 molecules cm^{-3} in summer (Tan et al., 2017). In the original manuscript, we linearly calculated the nighttime OH from 1×10^5 to 4×10^5 molecules m^{-3} according to

$$c_{OH,night} = 1 \times 10^5 + 4 \times 10^5 \times \frac{T - T_{min,night}}{T_{max,night} - T_{min,night}} \quad (\text{R1}).$$

In the revised manuscript, we updated the calculation method as suggested by another reviewer. Because the nighttime OH is mainly generated from reaction of O_3 with alkenes measured with the SPIMS, we changed the estimation method using

$$c_{OH,night} = 1 \times 10^5 + 4 \times 10^5 \times \frac{(c_{O_3} \times c_{alkenes})_{night} - (c_{O_3} \times c_{alkenes})_{night,min}}{(c_{O_3} \times c_{alkenes})_{night,max} - (c_{O_3} \times c_{alkenes})_{night,min}} \quad (\text{R2}).$$

In lines 468-471 in the revised manuscript, we changed it as “**The nighttime OH concentration was estimated linearly correlated with the product of nighttime O_3 concentration and alkenes concentration, namely,**

$$c_{OH,night} = 1 \times 10^5 + 4 \times 10^5 \times \frac{(c_{O_3} \times c_{alkenes})_{night} - (c_{O_3} \times c_{alkenes})_{night,min}}{(c_{O_3} \times c_{alkenes})_{night,max} - (c_{O_3} \times c_{alkenes})_{night,min}} \quad (16)”$$

Line 419: Please give the reported OH concentrations by Li et al (2018) and Huang et al (2017) and if they were calculated or measured OH levels.

Response: Thank you. Here we compared the production rate of HONO from homogenous reaction between NO and OH among different researches but not OH concentration. In lines 475-478 in the revised manuscript, we added the corresponding $P_{\text{NO-OH}}$ as “The calculated middle value of $P_{\text{NO-OH}}$ (with mean daytime value of $0.49 \pm 0.35 \text{ ppb h}^{-1}$) was comparable with these estimated values by Li et al. (2018) (0.4 ppb h^{-1}) and Huang et al. (2017b) (0.28 ppb h^{-1})”.

Line 433: How was the HONO form nitrate photolysis calculated? Which equation (give number)? What do these ranges represent?

Response: Thank you. HONO formation from nitrate photolysis was calculated according to Eqs (3) and (8). Bao et al. reported the J_{nitrate} at zenith angle of 0° . We normalized the J_{nitrate} with the zenith angle at our observation station. The time series of the middle value was shown in Fig. R2 and was also added in Fig. S7. In lines 489-495 in the revised manuscript, we revised

it. “A recent work reported the photolysis rate of nitrate (J_{nitrate}) in ambient $\text{PM}_{2.5}$ at a solar zenith angle of 0° (Bao et al., 2018). The J_{nitrate} varied from 1.22×10^{-5} to $4.84 \times 10^{-4} \text{ s}^{-1}$ with the mean value of $8.24 \times 10^{-5} \text{ s}^{-1}$. These values were further normalized according to the zenith angle and UV light at our observation station to calculate the low limit, the upper limit and the middle J_{nitrate} . The time series of the measured nitrate concentration and the middle value of J_{nitrate} were shown in Fig. 1 and Fig. S7, respectively”. In addition, the equation numbers was pointed out in line 498 in the revised manuscript. “The corresponding daytime lower limit, the middle value and the upper limit of HONO from photolysis of nitrate were $0.0011 \pm 0.0021 - 0.096 \pm 0.092$, $0.0072 \pm 0.0021 - 0.66 \pm 0.092$ and $0.042 \pm 0.082 - 3.86 \pm 0.008$ ppbv h^{-1} , respectively, calculated in the light of Eqs. (3) and (8)”.

Line 447: by the end of this paragraph, it was not at all clear to me which uptake co-efficient you actually used. Please clarify.

Response: Thank you. In the dark, the low limit, middle value and upper limit of P_{aerosol} were calculated using the RH dependent γ_{NO_2} on kaolin ($4.47 \times 10^{39} / (1.75 \times 10^{46} + 1.93 \times 10^{45} \text{RH})$) (Liu et al., 2015), the fixed γ_{NO_2} (1.2×10^{-8}) recommended by Crowley et al. (Crowley et al., 2010) and the RH dependent γ_{NO_2} on kaolin on hematite ($\gamma_{\text{NO}_2} = 4.46 \times 10^{39} / (6.73 \times 10^{44} + 3.48 \times 10^{44} \text{RH})$) (Liu et al., 2015), respectively, along with the γ_{NO_2} on black carbon (1.17×10^{-5}). In the daytime, the light enhanced uptake γ of NO_2 (1.9×10^{-6}) on mineral dust was parameterized (Ndour et al., 2008) after normalized to the solar radiation intensity in Beijing. For P_{ground} , the low limit, middle value and upper limit of P_{ground} were calculated using the same γ_{NO_2} as P_{aerosol} in night, while γ_{NO_2} of NO_2 on urban regime ($\gamma_{\text{NO}_2} = 7.4 \times 10^{-7} + 5.5 \times 10^{-8} \text{RH}$) (Liu et al., 2019) was used after normalized to the light intensity at BUCT in the daytime. In the revised manuscript, we pointed out these equations as “($\gamma_{\text{NO}_2} = 4.47 \times 10^{39} / (1.75 \times 10^{46} + 1.93 \times 10^{45} \text{RH})$)”, “($\gamma_{\text{NO}_2} = 4.46 \times 10^{39} / (6.73 \times 10^{44} + 3.48 \times 10^{44} \text{RH})$)” and “($\gamma_{\text{NO}_2} = 7.4 \times 10^{-7} + 5.5 \times 10^{-8} \text{RH}$)” in lines 507-508, 509 and 521, respectively.

Line 477-9: the authors state that ‘Heterogeneous reactions of NO_2 on aerosol surface and ground surfaces were unimportant compared with other sources because of the very low uptake coefficient’. What do you mean by the very low uptake coefficient, low compared to what? Is

the issue more that you used the wrong co-efficient?

Response: Thank you. For heterogeneous reaction of NO₂ on aerosol surface, the production rate is determined by the uptake coefficient according to Eqs. (3)-(5). Modelling studies have found that a given chemical process should be important in the tropospheric chemistry if the uptake coefficient of a trace gas on particles is greater than 10⁻⁵ (Zhang and Carmichael, 1999;Zheng et al., 2015). As discussed in this work, the typical uptake coefficient of NO₂ on aerosol is on the order of 10⁻⁷-10⁻⁸. It was it was recommended to be 1.2×10⁻⁸ (Crowley et al., 2010). Furthermore, we also performed laboratory studies about uptake of NO₂ on kaolin, hematite and soot particles. The uptake coefficient on mineral dust is on the order of 10⁻⁷-10⁻⁸ (Liu et al., 2015). In addition, we found that the $\gamma_{\text{NO}_2, \text{BET}}$ at steady state (or after aged in air) was one order of magnitude lower than that of fresh sample. Therefore, we chose the $\gamma_{\text{NO}_2, \text{BET}}$ 10⁻⁷-10⁻⁸ in this work. It was lower than that (10⁻⁶) used in modeling studies (Zhang et al., 2016;Aumont et al., 2003).

We double checked the parameters for budget calculation. We found a bug when calculating the heterogeneous reaction of NO₂ on black carbon. A conversion factor of time from second to hour was missed. So, the contribution of heterogeneous reaction to HONO source was underestimated. Now, the P_{aerosol} was 0.038±0.030-0.088±0.072. It was on the same orders as soil emission. In the revised manuscript, we updated Figs. 3-5 and the corresponding numbers in section 3.3.

In lines 544-554 the revised manuscript, we added a paragraph “It should be pointed out that HONO production from heterogeneous reaction of NO₂ on both aerosol and ground surface greatly depend on the $\gamma_{\text{NO}_2, \text{BET}}$ and A_s . The A_s of aerosols was comparable with the modeling input. However, the small nighttime $\gamma_{\text{NO}_2, \text{BET}}$ (10⁻⁸ - 10⁻⁷) on dust were used in this work rather than the $\gamma_{\text{NO}_2, \text{BET}}$ (1×10⁻⁶) used in modelling studies (Zhang et al., 2016;Aumont et al., 2003;Gall et al., 2016). This leads to a lower production rate of HONO from heterogeneous reaction of NO₂ on aerosols. As for heterogeneous reaction of NO₂ on ground surface, besides the small $\gamma_{\text{NO}_2, \text{BET}}$ used in this work, the A_s of ground surface (0.0015 to 0.0385 m⁻¹) calculated using the surface roughness and PBL height was also significantly lower than the fixed value of 0.3 m⁻¹ in modeling studies that might overestimate the contribution of HONO production from heterogeneous reaction of NO₂ on ground surface”. In lines 558-561 in the revised

manuscript, we revised the sentences as “These results mean that heterogeneous reaction might not be a major HONO source. This is consistent with a recent work that heterogeneous reaction should be unimportant when compared with traffic emission during haze events in winter in Beijing (Zhang et al., 2019)”. And in lines 605-607 in the revised manuscript, we also revised the sentence “Heterogeneous reactions of NO₂ on aerosol surface and ground surfaces were not the major HONO source during night unlike the modelled results (Zhang et al., 2016; Aumont et al., 2003).”.

Fig 2D: if you take the bottom and top points in Feb/Mar (blue), I am not sure there this a correlation. It would be good to check if you get a similar slope and r² without these 2 points.

Response: Thank you. If we remove these two points as you suggested, the correlation coefficient will decrease from 0.74 to 0.31. A positive correlation can be still observable when the uncertainty is taken into consideration (Fig. R7). We think it is unreasonable to remove them because these data points are valid. We agree with you that it should be better if more data points are available. This will be further investigated in the future.

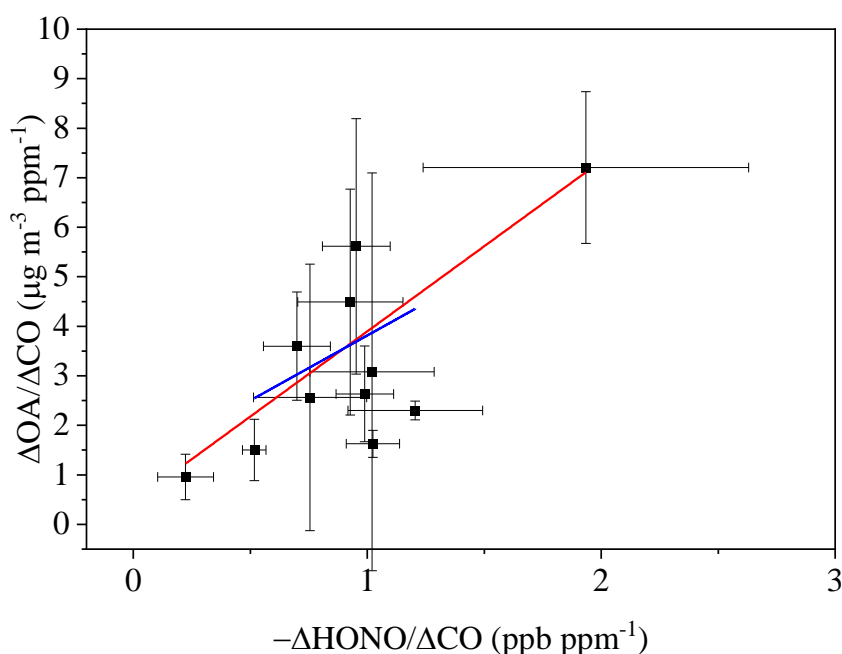


Fig. R7 Correlation of the daytime OA/CO increased and consumed HONO/CO in March.

References

Aumont, B., Chervier, F., and Laval, S.: Contribution of HONO sources to the NO_x/HO_x/O₃ chemistry in the polluted boundary layer, *Atmos. Environ.*, 37, 487-498, [https://doi.org/10.1016/S1352-2310\(02\)00920-2](https://doi.org/10.1016/S1352-2310(02)00920-2), 2003.

Bao, F., Li, M., Zhang, Y., Chen, C., and Zhao, J.: Photochemical Aging of Beijing Urban PM_{2.5}: HONO Production, *Environ. Sci. Technol.*, 52, 6309-6316, [10.1021/acs.est.8b00538](https://doi.org/10.1021/acs.est.8b00538), 2018.

Crowley, J. N., Ammann, M., Cox, R. A., Hynes, R. G., Jenkin, M. E., Mellouki, A., Rossi, M. J., Troe, J., and Wallington, T. J.: Evaluated kinetic and photochemical data for atmospheric chemistry: Volume V – heterogeneous reactions on solid substrates, *Atmos. Chem. Phys.*, 10, 9059-9223, doi: 10.5194/acp-10-9059-2010, 2010.

Gall, E. T., Griffin, R. J., Steiner, A. L., Dibb, J., Scheuer, E., Gong, L., Rutter, A. P., Cevik, B. K., Kim, S., Lefter, B., and Flynn, J.: Evaluation of nitrous acid sources and sinks in urban outflow, *Atmos. Environ.*, 127, 272-282, <https://doi.org/10.1016/j.atmosenv.2015.12.044>, 2016.

Han, C., Liu, Y., and He, H.: Role of Organic Carbon in Heterogeneous Reaction of NO₂ with Soot, *Environ. Sci. Technol.*, 47, 3174-3181, [10.1021/es304468n](https://doi.org/10.1021/es304468n), 2013.

Huang, H., Chen, Y., Clinton, N., Wang, J., Wang, X., Liu, C., Gong, P., Yang, J., Bai, Y., Zheng, Y., and Zhu, Z.: Mapping major land cover dynamics in Beijing using all Landsat images in Google Earth Engine, *Remote Sensing of Environment*, 202, 166-176, <https://doi.org/10.1016/j.rse.2017.02.021>, 2017a.

Huang, R.-J., Yang, L., Cao, J., Wang, Q., Tie, X., Ho, K.-F., Shen, Z., Zhang, R., Li, G., Zhu, C., Zhang, N., Dai, W., Zhou, J., Liu, S., Chen, Y., Chen, J., and O'Dowd, C. D.: Concentration and sources of atmospheric nitrous acid (HONO) at an urban site in Western China, *Sci. Total Environ.*, 593, 165-172, [10.1016/j.scitotenv.2017.02.166](https://doi.org/10.1016/j.scitotenv.2017.02.166), 2017b.

Kanaya, Y., Cao, R., Akimoto, H., Fukuda, M., Komazaki, Y., Yokouchi, Y., Koike, M., Tanimoto, H., Takegawa, N., and Kondo, a. Y.: Urban photochemistry in central Tokyo: 1. Observed and modeled OH and HO₂ radical concentrations during the winter and summer of 2004, *J. Geophys. Res.- Atmos.*, 112, [10.1029/2007JD008670](https://doi.org/10.1029/2007JD008670), 2007.

Li, D., Xue, L., Wen, L., Wang, X., Chen, T., Mellouki, A., Chen, J., and Wang, W.: Characteristics and sources of nitrous acid in an urban atmosphere of northern China: Results from 1-yr continuous observations, *Atmos. Environ.*, 182, 296-306, <https://doi.org/10.1016/j.atmosenv.2018.03.033>, 2018.

Li, X., Brauers, T., H'aseler, R., Bohn, B., Fuchs, H., Hofzumahaus, A., Holland, F., Lou, S., Lu, K. D., Rohrer, F., Hu, M., Zeng, L. M., Zhang, Y. H., Garland, R. M., Su, H., Nowak, A., Wiedensohler, A., Takegawa, N., Shao, M., and Wahner, A.: Exploring the atmospheric chemistry of nitrous acid (HONO) at a rural site in Southern China, *Atmos. Chem. Phys.*, 12, 1497-1513, 2012.

Li, Z. Q., Guo, J. P., Ding, A. J., Liao, H., Liu, J. J., Sun, Y. L., Wang, T. J., Xue, H. W., Zhang, H. S., and Zhu, B.: Aerosol and boundary-layer interactions and impact on air quality, *Natl. Sci. Rev.*, 4, 810-833, [10.1093/nsr/nwx117](https://doi.org/10.1093/nsr/nwx117), 2017.

Liu, J., Li, S., Mekic, M., Jiang, H., Zhou, W., Loisel, G., Song, W., Wang, X., and Gligorovski, S.: Photoenhanced Uptake of NO₂ and HONO Formation on Real Urban Grime, *Environmental Science & Technology Letters*, 6, 413-417, [10.1021/acs.estlett.9b00308](https://doi.org/10.1021/acs.estlett.9b00308), 2019.

Liu, Y., Han, C., Ma, J., Bao, X., and He, H.: Influence of relative humidity on heterogeneous kinetics of NO₂ on kaolin and hematite, *Phys. Chem. Chem. Phys.*, 17, 19424-19431, doi: 10.1039/C5CP02223A, 2015.

Liu, Y., Lu, K., Ma, Y., Yang, X., Zhang, W., Wu, Y., Peng, J., Shuai, S., Hu, M., and Zhang, Y.: Direct emission of nitrous acid (HONO) from gasoline cars in China determined by vehicle chassis dynamometer experiments, *Atmos. Environ.*, 169, 89-96, [10.1016/j.atmosenv.2017.07.019](https://doi.org/10.1016/j.atmosenv.2017.07.019), 2017.

Ndour, M., D'Anna, B., George, C., Ka, O., Balkanski, Y., K., J., S., and K., A., M.: Photoenhanced uptake of NO₂ on mineral dust: Laboratory experiments and model simulations, *Geophys. Res. Lett.*, 35, L05812, doi:05810.101029/02007GL032006, 2008.

Oswald, R., Behrendt, T., Ermel, M., Wu, D., Su, H., Cheng, Y., Breuninger, C., Moravek, A., Mougín, E., Delon, C., Loubet, B., Pommerening-Röser, A., Sörgel, M., Pöschl, U., Hoffmann, T., Andreae, M. O., Meixner, F. X., and Trebs, I.: HONO Emissions from Soil Bacteria as a Major Source of Atmospheric Reactive Nitrogen, *Science*, 341, 1233-1235, 10.1126/science.1242266, 2013.

Ren, X., Brune, W. H., Mao, J., Mitchell, M. J., Lesher, R. L., Simpas, J. B., Metcalf, A. R., Schwab, J. J., Cai, C., Li, Y., Demerjian, K. L., Felton, H. D., Boynton, G., Adams, A., Perry, J., He, Y., Zhou, X., and Hou, J.: Behavior of OH and HO₂ in the winter atmosphere in New York City, *Atmos. Environ.*, 40, 252-263, <https://doi.org/10.1016/j.atmosenv.2005.11.073>, 2006.

Squires, F. A., Nemitz, E., Langford, B., Wild, O., Drysdale, W. S., Acton, W. J. F., Fu, P., Grimmond, C. S. B., Hamilton, J. F., Hewitt, C. N., Hollaway, M., Kotthaus, S., Lee, J., Metzger, S., Píngintha-Durden, N., Shaw, M., Vaughan, A. R., Wang, X., Wu, R., Zhang, Q., and Zhang, Y.: Measurements of traffic dominated pollutant emissions in a Chinese megacity, *Atmos. Chem. Phys. Discuss.*, 2020, 1-33, 10.5194/acp-2019-1105, 2020.

Tan, Z., Fuchs, H., Lu, K., Hofzumahaus, A., Bohn, B., Broch, S., Dong, H., Gomm, S., Häsel, R., He, L., Holland, F., Li, X., Liu, Y., Lu, S., Rohrer, F., Shao, M., Wang, B., Wang, M., Wu, Y., Zeng, L., Zhang, Y., Wahner, A., and Zhang, Y.: Radical chemistry at a rural site (Wangdu) in the North China Plain: observation and model calculations of OH, HO₂ and RO₂ radicals, *Atmos. Chem. Phys.*, 17, 663-690, 10.5194/acp-17-663-2017, 2017.

Tan, Z., Rohrer, F., Lu, K., Ma, X., Bohn, B., Broch, S., Dong, H., Fuchs, H., Gkatzelis, G. I., Hofzumahaus, A., Holland, F., Li, X., Liu, Y., Liu, Y., Novelli, A., Shao, M., Wang, H., Wu, Y., Zeng, L., Hu, M., Kiendler-Scharr, A., Wahner, A., and Zhang, Y.: Wintertime photochemistry in Beijing: observations of RO_x radical concentrations in the North China Plain during the BEST-ONE campaign, *Atmos. Chem. Phys.*, 18, 12391-12411, 10.5194/acp-18-12391-2018, 2018.

Tan, Z. F., Lu, K. D., Jiang, M. Q., Su, R., Wang, H. L., Lou, S. R., Fu, Q. Y., Zhai, C. Z., Tan, Q. W., Yue, D. L., Chen, D. H., Wang, Z. S., Xie, S. D., Zeng, L. M., and Zhang, Y. H.: Daytime atmospheric oxidation capacity in four Chinese megacities during the photochemically polluted season: a case study based on box model simulation, *Atmos. Chem. Phys.*, 19, 3493-3513, 10.5194/acp-19-3493-2019, 2019.

Yang, D., Zhang, S., Niu, T., Wang, Y., Xu, H., Zhang, K. M., and Wu, Y.: High-resolution mapping of vehicle emissions of atmospheric pollutants based on large-scale, real-world traffic datasets, *Atmos. Chem. Phys.*, 2019, 8831-8843, 10.5194/acp-2019-32, 2019.

Zhang, L., Wang, T., Zhang, Q., Zheng, J., Xu, Z., and Lv, M.: Potential sources of nitrous acid (HONO) and their impacts on ozone: A WRF-Chem study in a polluted subtropical region, *Journal of Geophysical Research-Atmospheres*, 121, 3645-3662, 10.1002/2015jd024468, 2016.

Zhang, W., Tong, S., Ge, M., An, J., Shi, Z., Hou, S., Xia, K., Qu, Y., Zhang, H., Chu, B., Sun, Y., and He, H.: Variations and sources of nitrous acid (HONO) during a severe pollution episode in Beijing in winter 2016, *The Science of the total environment*, 648, 253-262, 10.1016/j.scitotenv.2018.08.133, 2019.

Zhang, Y., and Carmichael, G.: Interactions of mineral aerosol with tropospheric chemistry, *J Appl. Meteor.*, 38, 353-366, 1999.

Zheng, B., Zhang, Q., Zhang, Y., He, K. B., Wang, K., Zheng, G. J., Duan, F. K., Ma, Y. L., and Kimoto, T.: Heterogeneous chemistry: a mechanism missing in current models to explain secondary inorganic aerosol formation during the January 2013 haze episode in North China, *Atmos. Chem. Phys.*, 15, 2031-2049, doi: 10.5194/acp-15-2031-2015, 2015.

Zou, Y., Deng, X. J., Deng, T., Yin, C. Q., and Li, F.: One-Year Characterization and Reactivity of Isoprene and Its Impact on Surface Ozone Formation at A Suburban Site in Guangzhou, China, *Atmosphere*, 10, 10.3390/atmos10040201, 2019.

Reviewer 2#

This paper reports the possible promotion effect of nitrous acid (HONO) on the formation of secondary organic aerosol (SOA) and nitrate in winter based on a five-month comprehensive observation in urban Beijing. Evidence for the relationship between secondary aerosol formation and the consumed HONO was obtained from the observations. The detailed budget of ambient HONO was explored, and vehicle emission was proposed as a significant source of HONO in Beijing. Overall, the manuscript is logically organized and well written, and the measurement data are much valuable. I would like to recommend that it can be considered for publication after the following major and specific comments being properly addressed.

Response: Thank you so much for your positive comments.

Section 2.2. HONO budget calculation: the description of the budget calculation is not clear enough. Firstly, the method used in this study was the budget analysis, other than the stationary state analysis. For a thorough budget analysis, physical terms (such as vertical and horizontal transport) should be considered for equations (1) and (12). At least, the authors need to evaluate if the physical processes were negligible for the analysis presented here. Secondly, a number of parameters (e.g., F_{HONO} , COH , γ , Y_{HONO} , $J_{nitrate}$, J_{HONO} , etc.) are required for the analysis. It is not clear how these parameters were obtained or approximated in this study. Although they were described more or less in the following Section 3.3, the authors may need clearly state the data source and uncertainties of these key parameters at their first appearance. This may help the readers better understand the overall methodology of this study.

Response: Thank you for your good suggestions. We revised the “stationary state HONO concentration” to “HONO budget” in line 171 in the revised manuscript.

The vertical and horizontal transport have been added in Eq. (1) and (12) from line 171 to 179 in the revised manuscript. “The HONO budget could be calculated by,

$$\frac{dc_{HONO}}{dt} = E_{HONO} + P_{HONO} - L_{HONO} + T_{vertical} + T_{horizontal} \quad (1)$$

where $\frac{dc_{HONO}}{dt}$ is the observed change rate of HONO mixing ratios (ppbv h^{-1}); E_{HONO} represents the emission rate of HONO from different sources (ppbv h^{-1}); P_{HONO} is the *in-situ* production

rate of HONO in the troposphere (ppbv h⁻¹); L_{HONO} is the loss rate of HONO (ppbv h⁻¹) (Li et al., 2018); T_{vertical} and $T_{\text{horizontal}}$ are the vertical and horizontal transport (Soergel et al., 2011), which can mimic source or sink terms depending on the HONO mixing ratios of the advected air relative to that of the measurement site and height (Soergel et al., 2011)”.

In addition, we added two paragraphs to discuss the transport in lines 222-232 “Vertical transport by advection (T_{vertical}), which is an important sink of HONO in the night (Gall et al., 2016; Meng et al., 2019), can be calculated according to equation (12).

$$T_{\text{vertical}} = -K_h(z, t) \frac{\partial c(z, t)}{\partial z} \frac{1}{h} \quad (12)$$

where $K_h(z, t)$ is the eddy diffusivity of heat (m² s⁻¹) at height z (m) and time t , h is the height of the second layer (18 m in this study) (Gall et al., 2016). On the other hand, both the vertical and horizontal transport can be estimate according to Eq. (13),

$$T_{\text{vertical}} = k_{\text{dilution}}(C_{\text{HONO}} - C_{\text{HONO,background}}) \quad (13)$$

where k_{dilution} is a dilution rate (0.23 h⁻¹, including both vertical and horizontal transport) (Dillon et al., 2002), C_{HONO} and $C_{\text{HONO,background}}$ is the HONO concentration at the observation site and background site, respectively (Dillon et al., 2002)” and lines 574-598 “As pointed in Section 2.2, vertical transport by advection is an important nocturnal sink of HONO (Gall et al., 2016). In this work, the vertical distribution of HONO concentration is unavailable. Recently, Meng et al. (2019) measured the vertical distribution of HONO in Beijing in December, 2016. The concentration of HONO showed nearly flat profiles from ground level to 240 m in pollution events after sunset, while negative profiles of HONO were observed in pollution events during night (Meng et al., 2019). The nighttime concentration gradient was 0.0047±0.0025 ppb m⁻¹ derived from the nighttime dataset (Meng et al., 2019). In the daytime, we assume a zero concentration gradient. On the other hand, the eddy diffusivity of heat in urban environment was measured in New Delhi, Indian (Yadav et al., 2003). Using their dataset with the wind speed lower than 2.0 m s⁻¹, we derived the relationship between the K_h and the wind speed (WS) ($K_h=0.9389 \times \text{WS} - 0.3374$ m² s⁻¹). The nighttime T_{vertical} changed from 0.15 to 0.37 ppbv h⁻¹ in winter, while it was from 0.12 to 0.68 ppbv h⁻¹ according to Eq. (12) from April to June. Because the wind speed was usually lower than 1.0 m s⁻¹ in pollution events (Fig. S6), horizontal transport should have little influence on the daytime sources or sinks of HONO

because of the short lifetime of HONO. In the night, 79 % of the wind speed was lower than 1.0 m s^{-1} in winter, thus the air masses from suburban areas should have influence on the sources and sinks of HONO in Beijing. If the HONO concentration at background was zero, the vertical and horizontal transport rate of HONO varied from 0.17 to 0.61 ppbv h^{-1} which is calculated in the light of Eq. (13) on haze days in winter and from 0.15 to 0.74 ppbv h^{-1} in pollution events from April to June. These values were higher than that calculated according to Eq. (12). Because the background HONO concentration was unavailable, we only considered the nighttime transport calculated according to Eq. (12) in the following section”. At the same time, the relative contribution of each source in Section 3.3 was updated based on the total sinks.

We added a sentence “The E_{vehicle} was calculated using the hourly NO_x emission inventory from vehicles in Beijing (Yang et al., 2019) after converted to emission flux of HONO ($F_{\text{HONO}}=F_{\text{NO}_x} \times \text{HONO}/\text{NO}_x$) and the PBL height as described in Section 2.2” to make it clearer about F_{HONO} in lines 421-423 in the revised manuscript.

The OH concentration was estimated based on $J_{\text{O}_1\text{D}}$ (Tan et al., 2019; Tan et al., 2018a) or $J_{\text{O}_1\text{D}}$ and J_{NO_2} (Li et al., 2018). Photolysis rate constants of NO_2 (J_{NO_2}), HONO (J_{HONO}) and O_3 (J_{O_3}) for clear sky conditions were calculated according to the solar zenith angle and the location using a box model (FACSIMILE 4). NO_2 photolysis sensor (J_{NO_2} , Metcon) was unavailable during our observation study. However, it was available from Aug 17 to Sep 16, 2018. Calibration function between the measured UVB light intensity and J_{NO_2} from Aug 17 to Sep 16, 2008 was established to correct the influence the climatological O_3 column, aerosol optical depth and cloud cover on surface UV light intensity. As shown in Fig. S10A, the model well predicted the J_{NO_2} . Then the J_{NO_2} during this campaign study was predicted using the model. The details about photolysis rates are shown in the Supplement Information. In lines 458-460 in the revised manuscript, we added a sentence “The method for the photolysis rates calculation were shown in SI and the time series of the photolysis rates were shown in Fig. S7”. In lines 472-473 in the revised manuscript, we added a sentence “The time series of OH concentration calculated using different methods was shown in Fig. S11”.

Three kinds of OH concentration was used in this work. In lines 460-466 in the revised manuscript, we revised it as “On polluted days, high concentration of NO_2 resulted into lower

OH concentrations estimated using the Eq. (13). Therefore, the corresponding $P_{\text{NO-OH}}$ was taken as the low limit for homogeneous reaction between NO and HONO because polluted events were discussed in this work, while $P_{\text{NO-OH}}$ calculated using the OH concentration ($J_{\text{O1D}} \times 4.33 \times 10^{11}$ molecules cm^{-3}) (Tan et al., 2018a) was taken as the upper limit and $P_{\text{NO-OH}}$ calculated using the OH concentration ($J_{\text{O1D}} \times 2 \times 10^{11}$ molecules cm^{-3}) (Tan et al., 2019) was the middle value”.

As for J_{nitrate} , we added the number as “The J_{nitrate} varied from 1.22×10^{-5} to 4.84×10^{-4} s^{-1} with the mean value of 8.24×10^{-5} s^{-1} ” in line 490-491 in the revised manuscript. About γ_{NO_2} on aerosol and ground surface, we pointed out from line 502 to 510 in the revised manuscript “The uptake coefficient (γ) of NO_2 on different particles varied from 5×10^{-9} to 9.6×10^{-6} (Ndour et al., 2009; Underwood et al., 2001; Underwood et al., 1999), while it was recommended to be 1.2×10^{-8} (Crowley et al., 2010), which was used to calculate the P_{aerosol} in the base case. It has been found that the γ highly depends on the relative humidity (RH). The low limit bound of P_{aerosol} was calculated based on the RH dependent uptake coefficient of NO_2 on kaolinite ($\gamma_{\text{NO}_2} = 4.47 \times 10^{39} / (1.75 \times 10^{46} + 1.93 \times 10^{45} \text{RH})$), while the upper limit of P_{aerosol} was calculated according to the RH dependent γ on hematite ($\gamma_{\text{NO}_2} = 4.46 \times 10^{39} / (6.73 \times 10^{44} + 3.48 \times 10^{44} \text{RH})$) (Liu et al., 2015)”. In the night, Y_{HONO} was set to 0.5 because of the hydrolysis reaction of NO_2 , while it was 0.8 for light enhanced reaction. It has been added “The Y_{HONO} was set to 0.5 because of the hydrolysis reaction of NO_2 (Liu et al., 2015), while it was 0.8 for light enhanced reaction (Liu et al., 2019a; Ndour et al., 2008) and on BC (Han et al., 2013)” in lines 528-530 in the revised manuscript.

Section 3.3 and Figures 3&4: following the first comment, the description and discussion of the HONO budget are also not clear and need clarification. The contributions of heterogeneous reactions of NO_2 on aerosol and ground surfaces were too low, and they were even lower than the OH+NO reactions during the nighttime. This is unusual. Is it reasonable to approximate the nighttime OH concentrations linearly with the temperature? Furthermore, the heterogeneous reactions of NO_2 on aerosol and ground surfaces were highly dependent on the NO_2 concentrations, the uptake coefficients, and surface density, some of which are highly uncertain. It is not clear what values were actually adopted for the uptake coefficients of NO_2 on aerosol

and ground surfaces, and how much were the ambient NO₂ levels and surface density? More details about the calculation of HONO budget are needed.

Response: Thank you for your good suggestion and comments. HONO production from heterogeneous reactions of NO₂ on both aerosol surface and ground surface greatly depend on the uptake coefficient ($\gamma_{\text{NO}_2, \text{BET}}$) and the surface to volume ratio (S/V). The mean and median surface to volume ratio of aerosols are 1.33×10^{-3} and $1.36 \times 10^{-3} \text{ m}^{-1}$ during pollution events. This is comparable with the input parameters in modeling studies (Zhang et al., 2016). However, as discussed from [line 501 to 503](#) in the revised manuscript, the $\gamma_{\text{NO}_2, \text{BET}}$ on aerosols varied from 5×10^{-9} to 9.6×10^{-6} . The $\gamma_{\text{NO}_2, \text{BET}}$ on pure oxides was usually higher than on composite oxides. The selection of a proper $\gamma_{\text{NO}_2, \text{BET}}$ is quite tricky. For example, a fixed $\gamma_{\text{NO}_2, \text{BET}}$ was set to 1×10^{-6} in nighttime and 2×10^{-5} in daytime due to photochemical reaction of NO₂ on soot surface in a modelling study (Zhang et al., 2016; Aumont et al., 2003). The nighttime $\gamma_{\text{NO}_2, \text{BET}}$ is ~2 orders of magnitude higher than ours (1.2×10^{-8}) as suggested by Crowley et al. (Crowley et al., 2010). In our previous work, we have measured the $\gamma_{\text{NO}_2, \text{BET}}$ on kaolin and hematite (Liu et al., 2015) and soot (Han et al., 2013). The initial $\gamma_{\text{NO}_2, \text{BET}}$ on kaolin is $4.85 \pm 0.39 \times 10^{-8}$ at 47 % RH. It should be pointed out that the $\gamma_{\text{NO}_2, \text{BET}}$ decreases significantly with exposure time due to surface saturation. [Fig. R8](#) shows the typical uptake curve of NO₂ and the $\gamma_{\text{NO}_2, \text{obs}}$ which is not normalized to the specific surface area. The $\gamma_{\text{NO}_2, \text{BET}}$ at steady state (2.56×10^{-9} to 4.56×10^{-9} on kaolin and 1.23×10^{-8} to 1.50×10^{-8} on hematite) is around one order of magnitude lower than the initial $\gamma_{\text{NO}_2, \text{BET}}$ as shown in [Fig. R9](#). Therefore, we used the recommended value (1.2×10^{-8}) (Crowley et al., 2010) in the base case. On the other hand, the $\gamma_{\text{NO}_2, \text{BET}}$ decreases with RH due to competitive adsorption (Liu et al., 2015). High mass concentration of PM_{2.5} usually accompanied with high RH in winter in Beijing. Thus, we calculated the RH dependent $\gamma_{\text{NO}_2, \text{BET}}$ according to the equation we determined previously (Liu et al., 2015) and the measured ambient RH in this work. This should be more reasonable than a fixed uptake coefficient used in modeling studies.

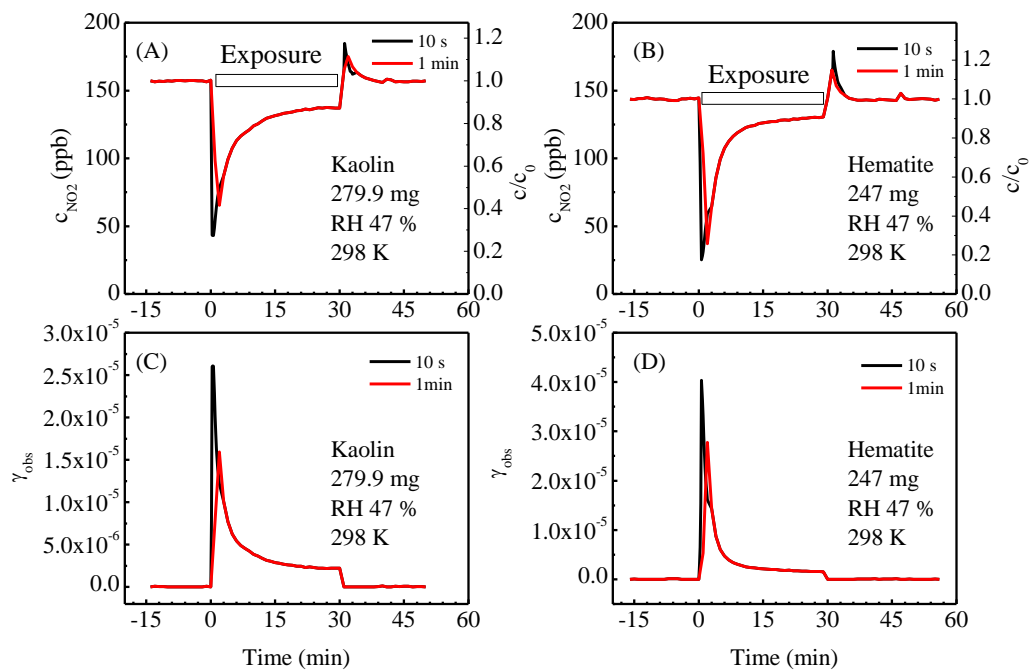


Fig. R8. Uptake curves of NO_2 on (A) kaolin and (B) hematite; and evolution of the observed uptake coefficient on (C) kaolin and (D) hematite at 298 K and at 47 % of RH (Liu et al., 2015).

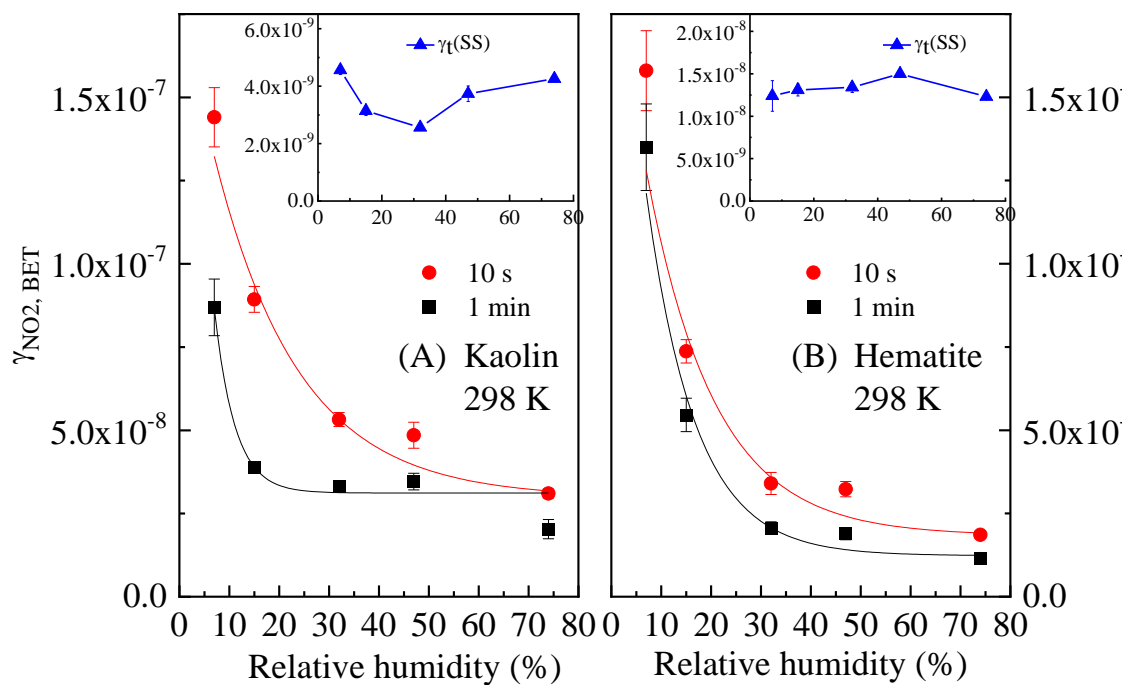


Fig. R9. The dependence of $\gamma_{\text{NO}_2, \text{BET}}$ on relative humidity (Liu et al., 2015).

In the original version of manuscript, we found a bug when calculating the heterogeneous reaction of NO₂ on black carbon. A conversion factor of time from second to hour was missed. So, the contribution of heterogeneous reaction to HONO source was underestimated in the original version. Now, the P_{aerosol} was 0.038 ± 0.030 - 0.088 ± 0.072 , which was dominated by the heterogeneous reaction of NO₂ on black carbon. It was on the same orders as soil emission. However, this was still significantly lower than the contribution of vehicle emission. In the revised manuscript, we updated Figs. 3-5 and the corresponding numbers in section 3.3.

As for heterogeneous reaction of NO₂ on ground surface, we used the same $\gamma_{\text{NO}_2,\text{BET}}$ on dust aerosol in the night, which is similar to the methodology used in modelling studies (Zhang et al., 2016; Aumont et al., 2003). As pointed out in Section 2.2 from [line 197 to 209](#) in the revised manuscript, the S/V was estimated using the surface roughness calculated in the light of satellite image of Beijing. The calculated surface roughness is 3.85, which is slightly higher than the value (2.2) used by Li et al. (2017). Thus, the calculated S/V varied from 0.0015 to 0.0385 m^{-1} (with a mean value of 0.0125 m^{-1}) because of the variation of the PBL height during pollution events. However, a fixed S/V of ground surface was set to 0.3 m^{-1} in the modeling studies (Zhang et al., 2016). This corresponds to a surface roughness ~ 92 , which means the surface area is ~ 92 times of the projected area of ground. It's too high. If both the $\gamma_{\text{NO}_2,\text{BET}}$ (1×10^{-6}) and surface roughness are increased to the values used in modeling studies, the nighttime production rate of HONO via heterogeneous reaction of NO₂ on ground surface will be 2.9 ppb h^{-1} . This means a large sink missed if this number is reasonable. In [lines 558-561](#) in the revised manuscript, we also revised the sentence “These results mean that heterogeneous reaction might not be a major HONO source. This is consistent with a recent work that heterogeneous reaction should be unimportant when compared with traffic emission during haze events in winter in Beijing (Zhang et al., 2019c)” and in [lines 605-607](#) in the revised manuscript, “Heterogeneous reactions of NO₂ on aerosol surface and ground surfaces were not the major HONO source during night unlike the modelled results (Zhang et al., 2016; Aumont et al., 2003) ”.

During the Chinese New Year (CNY) and the COVID-19 event in 2020, traffic emission decreased significantly in Beijing. This provides us a unique opportunity to verify the relative importance of each HONO source. We only analyzed the nocturnal data from January 1 to

February 29 because the HONO sources related to photochemical reactions could be avoided. The CNY vacation was from January 23 to February 2. These results are in preparation for a separate paper. Fig. R10 shows the relative change of the concentrations of HONO, NO_x and non-refractory PM_{2.5} (NR-PM_{2.5}). The traffic index and the chemical age of the air masses which is defined as $-\log(\text{NO}_x/\text{NO}_y)$ are also shown in Fig. R10. NO_y was measured with a NO_y analyzer (Thermo 42i-Y). The concentration of nighttime HONO decreased significantly during the CNY and after the CNY accompanied with the reduction in vehicle emission as supported by both the concentration of NO_x and traffic index (Fig. R10B). Interestingly, the NR-PM_{2.5} concentration during and after the CNY increased obviously when compared with that before the CNY. The effective conversion of NO₂ aerosol surface was almost constant because both the promotion effect of increased PM_{2.5} concentration and the inhibition effect of reduced NO₂ concentration during and after the CNY as shown in Fig. R10C. On the other hand, we found that the nighttime chemical age of the air masses during and after the CNY was also obviously larger than that before the CNY (Fig. R10D). This means that heterogeneous reaction of NO₂ on both aerosol surface and ground surface should be more effective due to longer residence of the air masses during and after the CNY than that before the CNY. When the reduction of NO₂ concentration was taken into consideration, the product of NO₂ concentration and $-\log(\text{NO}_x/\text{NO}_y)$ in COVID-19 epidemic periods increased slightly (Fig. R11). Therefore, the observed HONO concentration should decreased in COVID-19 epidemic or at least be constant in different periods and be independent on the reduction of vehicle emission if heterogeneous reaction of NO₂ on aerosol and ground surfaces dominates nighttime HONO source or if the vehicle emission is a minor HONO source. However, we observed the decrease of HONO along with reduction of vehicle emission (Fig.R10A). This well supports our (and other researchers' (Meng et al., 2019;Zhang et al., 2019c) conclusion that vehicle emission is an important source of HONO in Beijing.

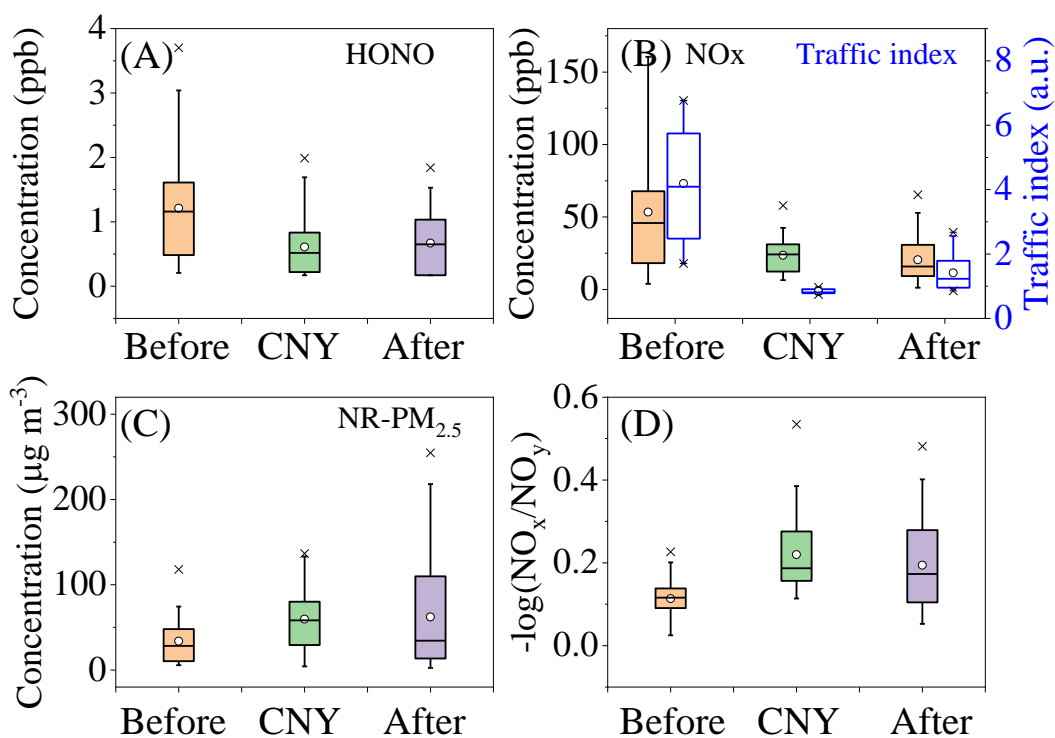


Fig. R10. Relative change of nighttime (A) HONO concentration, (B) NO_x concentration and the traffic index, (C) non-refractory PM_{2.5} (NR-PM_{2.5}) concentration and (D) relative chemical age ($-\log(\text{NO}_x/\text{NO}_y)$) of air masses before Chinese New Year (CNY) (2020.1.1-2020.1.22), during CNY (2020.1.23-2020.2.1) and after CNY (2020.2.2-2020.2.29).

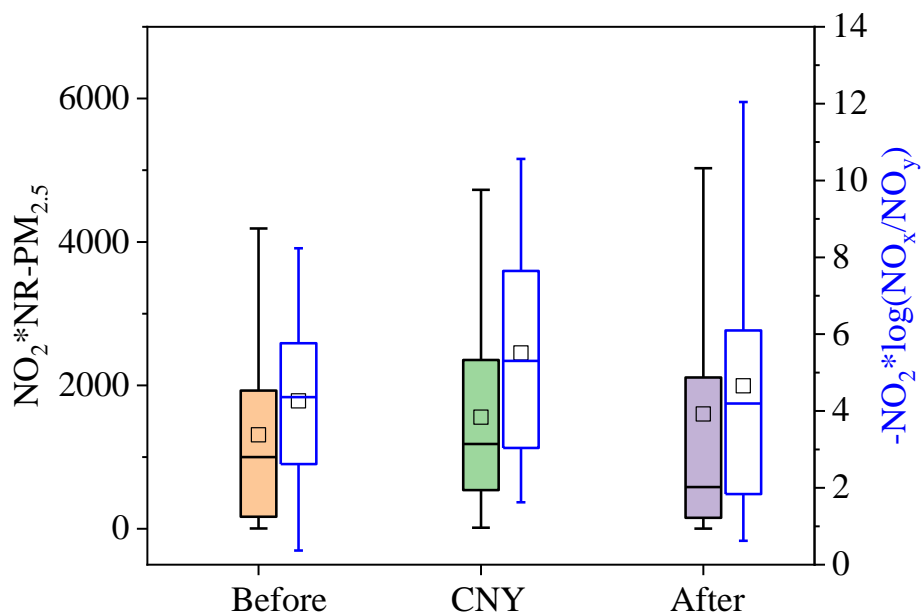


Fig. R11. Relative change of nighttime the product of NO₂ and NR-PM_{2.5} concentration and

the product of NO₂ concentration and $-\log(\text{NO}_x/\text{NO}_y)$ in different periods.

In lines 523-528 in the revised manuscript, we pointed out “The A_s of aerosols which was measured using a DMPS varied from 1×10^{-4} to $4.8 \times 10^{-3} \text{ m}^{-1}$ with a mean value of $1.4 \pm 0.5 \times 10^{-3} \text{ m}^{-1}$ during pollution events. This value is comparable with that used in modeling studies (Zhang et al., 2016; Aumont et al., 2003). The A_s of ground surface which was calculated according to Eq. (6) and (7) varied from 1.5×10^{-3} to $3.85 \times 10^{-2} \text{ m}^{-1}$ with a mean value of $1.3 \pm 0.9 \times 10^{-2} \text{ m}^{-1}$ during pollution events. The surface roughness was 3.85 calculated according to Eq. (7)”. And from line 544 to 554 in the revised manuscript, we added a paragraph to discuss the reason why we obtained the low production rate of HONO via heterogeneous reaction of NO₂ on ground and aerosol surfaces as “It should be pointed out that HONO production from heterogeneous reaction of NO₂ on both aerosol and ground surface greatly depend on the $\gamma_{\text{NO}_2, \text{BET}}$ and A_s . The A_s of aerosols is comparable with the modeling input. However, the small nighttime $\gamma_{\text{NO}_2, \text{BET}}$ ($10^{-8} - 10^{-7}$) were used in this work rather than the $\gamma_{\text{NO}_2, \text{BET}}$ (1×10^{-6}) used in modelling studies (Zhang et al., 2016; Aumont et al., 2003). This leads to a lower production rate of HONO from heterogeneous reaction of NO₂ on aerosols. As for heterogeneous reaction of NO₂ on ground surface, besides the small $\gamma_{\text{NO}_2, \text{BET}}$ used in this work, the A_s of ground surface (0.0015 to 0.0385 m^{-1}) calculated using the surface roughness and PBL height was also significantly lower than the fixed value of 0.3 m^{-1} used in modeling studies that might overestimate the contribution of HONO production from heterogeneous reaction of NO₂ on ground surface”.

As for nighttime OH concentration, we revised it to using the proxy of alkene and O₃ concentration to normalize it from 1×10^5 to 4×10^5 molecules cm^{-3} . In lines 468-472 in the revised manuscript, we revised it as “The nighttime OH concentration was estimated linearly correlated with the product of nighttime O₃ concentration and alkenes concentration, namely,

$$c_{\text{OH}, \text{night}} = 1 \times 10^5 + 4 \times 10^5 \times \frac{(c_{\text{O}_3} \times c_{\text{alkenes}})_{\text{night}} - (c_{\text{O}_3} \times c_{\text{alkenes}})_{\text{night}, \text{min}}}{(c_{\text{O}_3} \times c_{\text{alkenes}})_{\text{night}, \text{max}} - (c_{\text{O}_3} \times c_{\text{alkenes}})_{\text{night}, \text{min}}} \quad (16)$$

The time series of OH concentration calculated using different methods was shown in Fig. S11”

At the same time, we updated the data in Figs. 3-5 in the revised manuscript.

The authors attempted to quantify the contributions of vehicle-emitted NO to ambient HONO via NO+OH reaction based on the source apportionment of NO emissions. This is not

convincing because the homogeneous HONO formation is generally limited by OH other than NO. This means that the produced HONO should be not linearly dependent to the NO emissions. It can be concluded that vehicle emission should contribute significantly to not only direct HONO emission but also HONO formation through reactions of NO and NO₂. However, the current quantification analysis needs be more careful.

Response: Thank you so much for your comment. We agree with you that the production rate of HONO ($P_{\text{NO-OH}}$) from this reaction is greatly dependent on or determined by OH concentration as shown in Fig. 3 because the variation degree of OH concentration from nighttime to daytime is obviously larger than that of NO concentration. However, we think $P_{\text{NO-OH}}$ actually reflects both the variations of OH concentration and the emission of NO from vehicles. From the point view of HONO sources, it still represents the indirect source of HONO related to traffic emission although the diurnal variation of OH concentration is mainly determined by light intensity. In the revised manuscript, we added a sentence to discuss this point “As shown in Fig.3, although the diurnal curve of $P_{\text{NO-OH}}$ coincided well with that of OH concentration (Fig. S10), which means the $P_{\text{NO-OH}}$ should be mainly determined by OH concentration, the $P_{\text{NO-OH}}$ should still reflect the indirect contribution of traffic related emission to HONO source because the ambient NO concentration was used to calculate the $P_{\text{NO-OH}}$.” in lines 637-641 in the revised manuscript.

Specific Comments:

Line 44: fine particulate matter with diameter less than or equal to 2.5...

Response: Thank you. It has been corrected in line 44 in the revised manuscript.

Line 78: on polluted days

Response: Thank you. It has been corrected throughout the paper.

Lines 84-94: to my knowledge, there have been a number of observational studies of HONO in recent years in China, and similar HONO budget analyses were performed. I suggest the authors to comprehensively review the existing results about the HONO sources in China and compare them against the source analysis results obtained in the present study.

Response: Thank you for your good suggestion. In the revised manuscript, we added two paragraphs to review the previous results. “The HONO concentration has been measured with a wide range from 0.18 to 9.71 ppbv at different locations, such as Beijing (Zhang et al., 2019c; Hu et al., 2002; Hendrick et al., 2014; Wang et al., 2017), Shanghai (Wang et al., 2013; Zhang et al., 2019a), Guangdong (Hu et al., 2002; Su et al., 2008a), Hongkong (Xu et al., 2015), Shandong (Li et al., 2018), Xi’an (Huang et al., 2017) and so on in China since 2000” in lines 85-89 and “At the present time, the study of the HONO budget is still far from closed, which would require a significant effort on both the accurate measurement of HONO and the determination of related kinetic parameters for its production pathways (Liu et al., 2019b). For example, photo-enhanced conversion of NO₂ (Su et al., 2008b) and photolysis of particulate nitrate were found to be the two major mechanisms with large potential of HONO formation during noontime, but the associated uncertainty may reduce their importance (Liu et al., 2019b). Some other researches proposed that heterogeneous reactions on ground/aerosol surfaces were important during nighttime (Wang et al., 2017; Zhang et al., 2019b) and daytime in Beijing-Tianjin-Hebei (BTH) (Zhang et al., 2019b). But the heterogeneous reaction was unimportant in Ji’an compared with the unknown sources and the homogeneous reaction between NO and OH (Li et al., 2018). In addition, the traffic emission was proposed to be an important HONO source during nighttime but not significant during daytime in BTH (Zhang et al., 2019b). However, it was proposed that direct emission of HONO from vehicles should contribute about 51.1 % (Meng et al., 2019) and 52 % of nighttime HONO in Beijing (Zhang et al., 2019c). These results mean that more studies are still required on the HONO budget” in lines 99-115.

Line 138: replace “nitrous acid” by “nitric acid”

Response: Thank you. It has been corrected in line 81 in the revised manuscript.

Line 146: Equation (1) describes the budget analysis other than the stationary state analysis. Both methods are different. Transport terms need be considered here.

Response: Thank you. It has been corrected in line 171 in the revised manuscript.

Lines 198-202 and Fig. 1: it would be much better if the authors could also plot the other related

parameters, such as NO_x and meteorological parameters, in Fig. 1. It is difficult for the readers to look at the same measurements separately from main text and supplement.

Response: Thank you for your suggestion. We have combined these parameters in Fig. 1 and Fig. R12.

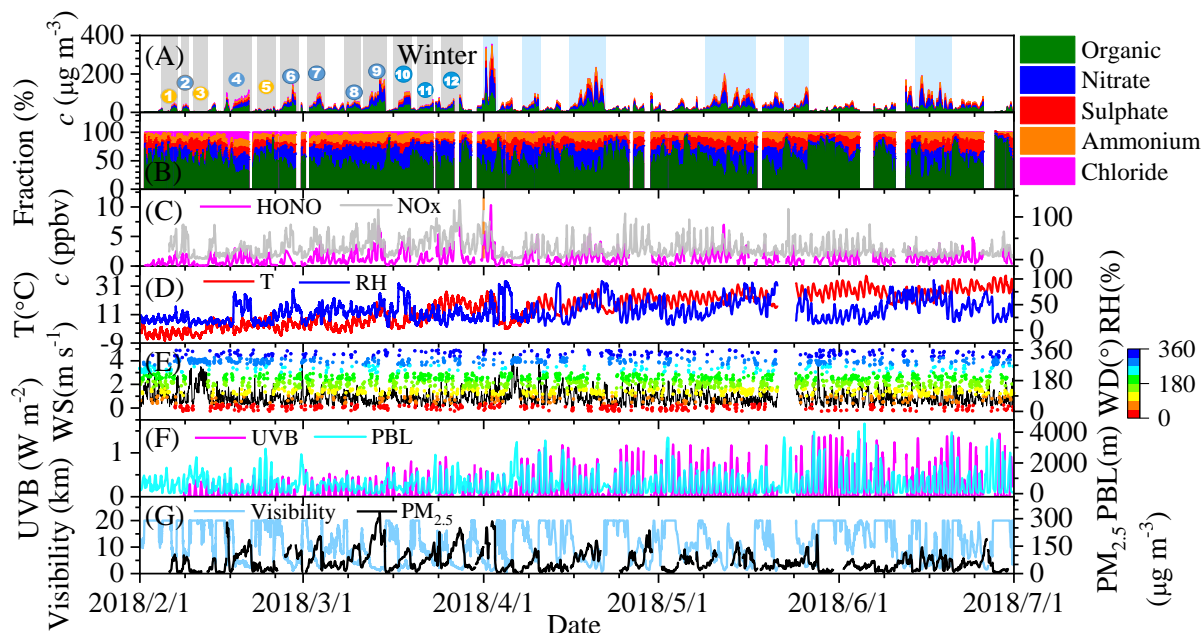


Fig. R12. An overviewed measurement of non-refractory-PM_{2.5} (NR-PM_{2.5}), HONO, NO_x, PM_{2.5} and meteorological parameters from Feb. 1 to July 1, 2018. (A) the mass concentration of different components of PM_{2.5}, (B) the mass fraction of individual component, (C) HONO and NO_x concentration, (D) temperature and RH, (E) wind speed and wind direction, (F) UVB and PBL height and (G) visibility and PM_{2.5} concentration during observation.

Line 228: the increase in temperature...

Response: Thank you. It has been corrected in [line 268](#) in the revised manuscript.

Line 262: what does “in RO₂ chemistry” mean? Rephrase this sentence.

Response: Thank you. We revised it to “**the reaction between NO and HO₂**” in [line 298](#) in the revised manuscript. It means the reaction: HO₂ + NO → OH + NO₂.

Line 266: replace “dominating” by “dominant”

Response: Thank you. It has been corrected in [line 303](#) in the revised manuscript.

Lines 270-282: it is not clear how the $P_{\text{OH-HONO}}$ and $P_{\text{OH-O}_3}$ were calculated from the current discussion. The calculated $P_{\text{OH-HONO}}$ and $P_{\text{OH-O}_3}$ levels in winter and April-June seem to be too high. Detailed calculation methods should be given here. Usually, the OH+NO reactions should be subtracted from the photolysis of HONO to denote the real contribution of HONO to the OH source.

Response: Thank you for your good suggestions. The photolysis rates of $\text{NO}_2(J_{\text{NO}_2})$, $\text{HONO}(J_{\text{HONO}})$ and $\text{O}_3(J_{\text{O}_3})$ under clear sky conditions were calculated according to the solar zenith angle and the location using a box model (FACSIMILE 4). NO_2 photolysis sensor (J_{NO_2} , Metcon) was unavailable, while UVB is always available during our observation study. However, the J_{NO_2} sensor was available from Aug 17 to Sep 16, 2018. A calibration function between the measured UVB light intensity and the J_{NO_2} was established to correct the influence the climatological O_3 column, aerosol optical depth and cloud cover on surface UV light intensity from Aug 17 to Sep 16, 2008. As shown in Fig. S10, the model well predicted the J_{NO_2} . Then, the J_{NO_2} during this campaign study was predicted using the measured UVB light and the modelled photolysis rates. These information has been shown in the SI. The time series of the daytime photolysis rates were added in the SI (Fig. S7) and shown in Fig. R2. Overall, the J values are comparable with literature data during the similar season in Beijing (Tan et al., 2018b; Zhang et al., 2019c). In addition, we recently compared the OH concentration using the $J_{\text{O}_1\text{D}}$ with that derived from measured H_2SO_4 concentration using a box model. We found the OH concentration calculated with the two methods are comparable as shown in Fig. R1.

In lines 313-314 in the revised manuscript, we added a sentence “The details about the J_{HONO} and $J_{\text{O}_1\text{D}}$ calculation were shown in the Supplement Information and their time series were shown in Fig. S7”.

Line 291: photolysis of HCHO is actually the primary source of HO_2 .

Response: Thank you. OH is formed from the reaction between NO and HO_2 , which is related to HCHO photolysis (Alicke et al., 2003). We revised it as “...,while photolysis of O_3 and HCHO related reactions usually dominated primary OH production in summer (Alicke et al., 2003)” in lines 330-331 in the revised manuscript.

Line 330: delete “and”.

Response: Thank you. It has been corrected in [line 366](#) in the revised manuscript.

Lines 333-336: Several recent papers about the nitrate aerosol trend and formation mechanisms in China are highly relevant to this study, and should be acknowledged.

Wen et al., Summertime fine particulate nitrate pollution in the North China Plain: increasing trends, formation mechanisms, and implications for control policy, *Atmospheric Chemistry and Physics*, 18, 11261-11275, 2018.

Sun et al., Two years of online measurement of fine particulate nitrate in the western Yangtze River Delta: influences of thermodynamics and N₂O₅ hydrolysis, *Atmospheric Chemistry and Physics*, 18, 17177-17190, 2018.

Response: Thank you so much. These work have been cited in the revised manuscript ([lines 369-370](#)).

Line 363: high or low HONO concentration?

Response: Thank you. We think is should be low HONO concentration if the secondary formation is unimportant.

Line 408: Tan et al., (2019)

Response: Thank you. It has been corrected in [line 453](#) in the revised manuscript.

Line 407-408: it would be better if the authors could provide the estimated OH levels here.

Response: Thank you. The calculated OH concentration was added in the revised SI (Fig. S11) and [Fig. R13](#). And in [lines 472-473](#) in the revised manuscript, we added a sentence “**The time series of OH concentration calculated using different methods was shown in Fig. S11**”.

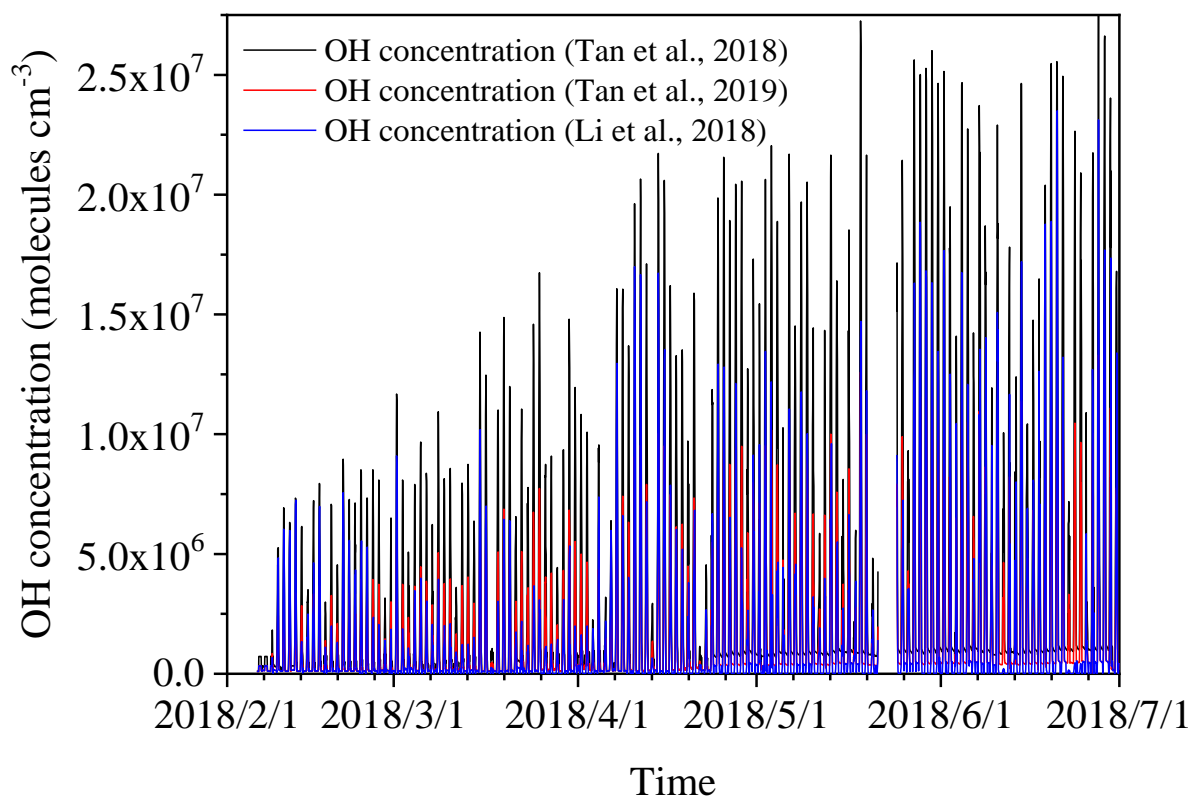


Fig. R13. Estimated OH concentration using different methods.

Lines 430-431: it is not clear how the photolysis frequency of nitrate was corrected? Details are needed here. What are the J values used finally?

Response: Thank you. In the literature (Bao et al., 2018), the authors measured the photolysis of $PM_{2.5}$ samples under irradiation by a Xenon lamp. The authors adjusted the J value to ambient sunlight condition at solar zenith angle of 0° . We additionally normalized this value according to the solar zenith angle during our observation according to the latitude, the date and the observed sunlight intensity. They reported a series of J_{nitrate} which varied from 1.22×10^{-5} to $4.84 \times 10^{-4} \text{ s}^{-1}$ with a mean value of $8.24 \times 10^{-5} \text{ s}^{-1}$. Thus, we used these three values to calculate the lower limit, higher limit and middle value of the J_{nitrate} . The time series of the middle value has been added as an example in Fig. S7 in the revised SI and Fig. R2. We added a sentence as “The time series of the measured nitrate concentration and the middle value of J_{nitrate} were shown in Fig. 1 and Fig. S7, respectively” in lines 493-495 in the revised manuscript.

Line 553-554: again, it is budget analysis other than stationary state calculation.

Response: Thank you. It has been corrected in [line 683](#) in the revised manuscript.

Line 568: indirect production

Response: Thank you. It has been corrected in [line 698](#) in the revised manuscript.

References:

- Alicke, B., Geyer, A., Hofzumahaus, A., Holland, F., Konrad, S., Patz, H. W., Schafer, J., Stutz, J., Volz-Thomas, A., and Platt, U.: OH formation by HONO photolysis during the BERLIOZ experiment, *Journal of Geophysical Research-Atmospheres*, 108, 17, 10.1029/2001jd000579, 2003.
- Aumont, B., Chervier, F., and Laval, S.: Contribution of HONO sources to the NO_x/HO_x/O₃ chemistry in the polluted boundary layer, *Atmos. Environ.*, 37, 487-498, [https://doi.org/10.1016/S1352-2310\(02\)00920-2](https://doi.org/10.1016/S1352-2310(02)00920-2), 2003.
- Bao, F., Li, M., Zhang, Y., Chen, C., and Zhao, J.: Photochemical Aging of Beijing Urban PM_{2.5}: HONO Production, *Environ. Sci. Technol.*, 52, 6309-6316, 10.1021/acs.est.8b00538, 2018.
- Crowley, J. N., Ammann, M., Cox, R. A., Hynes, R. G., Jenkin, M. E., Mellouki, A., Rossi, M. J., Troe, J., and Wallington, T. J.: Evaluated kinetic and photochemical data for atmospheric chemistry: Volume V – heterogeneous reactions on solid substrates, *Atmos. Chem. Phys.*, 10, 9059-9223, doi: 10.5194/acp-10-9059-2010, 2010.
- Dillon, M. B., Lamanna, M. S., Schade, G. W., Goldstein, A. H., and Cohen, R. C.: Chemical evolution of the Sacramento urban plume: Transport and oxidation, *J. Geophys. Res.- Atmos.*, 107, ACH 3-1-ACH 3-15, 10.1029/2001jd000969, 2002.
- Gall, E. T., Griffin, R. J., Steiner, A. L., Dibb, J., Scheuer, E., Gong, L., Rutter, A. P., Cevik, B. K., Kim, S., Lefer, B., and Flynn, J.: Evaluation of nitrous acid sources and sinks in urban outflow, *Atmos. Environ.*, 127, 272-282, <https://doi.org/10.1016/j.atmosenv.2015.12.044>, 2016.
- Han, C., Liu, Y., and He, H.: Role of Organic Carbon in Heterogeneous Reaction of NO₂ with Soot, *Environ. Sci Technol.*, 47, 3174-3181, 10.1021/es304468n, 2013.
- Hendrick, F., Muller, J. F., Clemer, K., Wang, P., De Maziere, M., Fayt, C., Gielen, C., Hermans, C., Ma, J. Z., Pinardi, G., Stavrou, T., Vlemmix, T., and Van Roozendaal, M.: Four years of ground-based MAX-DOAS observations of HONO and NO₂ in the Beijing area, *Atmos. Chem. Phys.*, 14, 765-781, 10.5194/acp-14-765-2014, 2014.
- Hu, M., Zhou, F., Shao, K., Zhang, Y., Tang, X., and Slanina, J.: Diurnal variations of aerosol chemical compositions and related gaseous pollutants in Beijing and Guangzhou, *Journal of Environmental Science and Health, Part A*, 37, 479-488, 10.1081/ESE-120003229, 2002.
- Huang, R.-J., Yang, L., Cao, J., Wang, Q., Tie, X., Ho, K.-F., Shen, Z., Zhang, R., Li, G., Zhu, C., Zhang, N., Dai, W., Zhou, J., Liu, S., Chen, Y., Chen, J., and O'Dowd, C. D.: Concentration and sources of atmospheric nitrous acid (HONO) at an urban site in Western China, *Sci. Total Environ.*, 593, 165-172, 10.1016/j.scitotenv.2017.02.166, 2017.
- Li, D., Xue, L., Wen, L., Wang, X., Chen, T., Mellouki, A., Chen, J., and Wang, W.: Characteristics and sources of nitrous acid in an urban atmosphere of northern China: Results from 1-yr continuous observations, *Atmos. Environ.*, 182, 296-306, <https://doi.org/10.1016/j.atmosenv.2018.03.033>, 2018.
- Liu, J., Li, S., Mekic, M., Jiang, H., Zhou, W., Loisel, G., Song, W., Wang, X., and Gligorovski, S.: Photoenhanced Uptake of NO₂ and HONO Formation on Real Urban Grime, *Environmental Science &*

Technology Letters, 6, 413-417, 10.1021/acs.estlett.9b00308, 2019a.

Liu, Y., Han, C., Ma, J., Bao, X., and He, H.: Influence of relative humidity on heterogeneous kinetics of NO₂ on kaolin and hematite, *Phys. Chem. Chem. Phys.*, 17, 19424-19431, doi: 10.1039/C5CP02223A, 2015.

Liu, Y. H., Lu, K. D., Li, X., Dong, H. B., Tan, Z. F., Wang, H. C., Zou, Q., Wu, Y. S., Zeng, L. M., Hu, M., Min, K. E., Kecorius, S., Wiedensohler, A., and Zhang, Y. H.: A Comprehensive Model Test of the HONO Sources Constrained to Field Measurements at Rural North China Plain, *Environ. Sci. Technol.*, 53, 3517-3525, 10.1021/acs.est.8b06367, 2019b.

Meng, F., Qin, M., Tang, K., Duan, J., Fang, W., Liang, S., Ye, K., Xie, P., Sun, Y., Xie, C., Ye, C., Fu, P., Liu, J., and Liu, W.: High resolution vertical distribution and sources of HONO and NO₂ in the nocturnal boundary layer in urban Beijing, China, *Atmos. Chem. Phys. Discuss.*, 2019, 1-34, 10.5194/acp-2019-613, 2019.

Ndour, M., D'Anna, B., George, C., Ka, O., Balkanski, Y., K., J., S., and K., A., M.: Photoenhanced uptake of NO₂ on mineral dust: Laboratory experiments and model simulations, *Geophys. Res. Lett.*, 35, L05812. doi:05810.01029/02007GL032006, 2008.

Ndour, M., Nicolas, M., D'Anna, B., Ka, O., and George, C.: Photoreactivity of NO₂ on mineral dusts originating from different locations of the Sahara desert, *Phys. Chem. Chem. Phys.*, 11, 1312-1319, 2009.

Soergel, M., Regelin, E., Bozem, H., Diesch, J. M., Drewnick, F., Fischer, H., Harder, H., Held, A., Hosaynali-Beygi, Z., Martinez, M., and Zetzsch, C.: Quantification of the unknown HONO daytime source and its relation to NO₂, *Atmos. Chem. Phys.*, 11, 10433-10447, 10.5194/acp-11-10433-2011, 2011.

Su, H., Cheng, Y. F., Cheng, P., Zhang, Y. H., Dong, S., Zeng, L. M., Wang, X., Slanina, J., Shao, M., and Wiedensohler, A.: Observation of nighttime nitrous acid (HONO) formation at a non-urban site during PRIDE-PRD2004 in China, *Atmos. Environ.*, 42, 6219-6232, 10.1016/j.atmosenv.2008.04.006, 2008a.

Su, H., Cheng, Y. F., Shao, M., Gao, D. F., Yu, Z. Y., Zeng, L. M., Slanina, J., Zhang, Y. H., and Wiedensohler, A.: Nitrous acid (HONO) and its daytime sources at a rural site during the 2004 PRIDE-PRD experiment in China, *Journal of Geophysical Research-Atmospheres*, 113, 10.1029/2007jd009060, 2008b.

Tan, Z., Rohrer, F., Lu, K., Ma, X., Bohn, B., Broch, S., Dong, H., Fuchs, H., Gkatzelis, G. I., Hofzumahaus, A., Holland, F., Li, X., Liu, Y., Liu, Y., Novelli, A., Shao, M., Wang, H., Wu, Y., Zeng, L., Hu, M., Kiendler-Scharr, A., Wahner, A., and Zhang, Y.: Wintertime photochemistry in Beijing: observations of RO_x radical concentrations in the North China Plain during the BEST-ONE campaign, *Atmos. Chem. Phys.*, 18, 12391-12411, 10.5194/acp-18-12391-2018, 2018a.

Tan, Z. F., Rohrer, F., Lu, K. D., Ma, X. F., Bohn, B., Broch, S., Dong, H. B., Fuchs, H., Gkatzelis, G. I., Hofzumahaus, A., Holland, F., Li, X., Liu, Y., Liu, Y. H., Novelli, A., Shao, M., Wang, H. C., Wu, Y. S., Zeng, L. M., Hu, M., Kiendler-Scharr, A., Wahner, A., and Zhang, Y. H.: Wintertime photochemistry in Beijing: observations of RO_x radical concentrations in the North China Plain during the BEST-ONE campaign, *Atmos. Chem. Phys.*, 18, 12391-12411, 10.5194/acp-18-12391-2018, 2018b.

Tan, Z. F., Lu, K. D., Jiang, M. Q., Su, R., Wang, H. L., Lou, S. R., Fu, Q. Y., Zhai, C. Z., Tan, Q. W., Yue, D. L., Chen, D. H., Wang, Z. S., Xie, S. D., Zeng, L. M., and Zhang, Y. H.: Daytime atmospheric oxidation capacity in four Chinese megacities during the photochemically polluted season: a case study based on box model simulation, *Atmos. Chem. Phys.*, 19, 3493-3513, 10.5194/acp-19-3493-2019, 2019.

Underwood, G. M., Miller, T. M., and Grassian, V. H.: Transmission FT-IR and Knudsen Cell Study of the Heterogeneous Reactivity of Gaseous Nitrogen Dioxide on Mineral Oxide Particles, *J. Phys. Chem. A*, 103, 6184-6190, 1999.

Underwood, G. M., Song, C. H., Phadnis, M., Carmichael, G. R., and Grassian, V. H.: Heterogeneous reactions of NO₂ and HNO₃ on oxides and mineral dust: A combined laboratory and modeling study, *J. Geophys. Res.-Atmos.*, 106, 18055-18066, 10.1029/2000jd900552, 2001.

- Wang, J., Zhang, X., Guo, J., Wang, Z., and Zhang, M.: Observation of nitrous acid (HONO) in Beijing, China: Seasonal variation, nocturnal formation and daytime budget, *Sci. Total Environ.*, 587, 350-359, 10.1016/j.scitotenv.2017.02.159, 2017.
- Wang, S., Zhou, R., Zhao, H., Wang, Z., Chen, L., and Zhou, B.: Long-term observation of atmospheric nitrous acid (HONO) and its implication to local NO₂ levels in Shanghai, China, *Atmos. Environ.*, 77, 718-724, 10.1016/j.atmosenv.2013.05.071, 2013.
- Xu, Z., Wang, T., Wu, J., Xue, L., Chan, J., Zha, Q., Zhou, S., Louie, P. K. K., and Luk, C. W. Y.: Nitrous acid (HONO) in a polluted subtropical atmosphere: Seasonal variability, direct vehicle emissions and heterogeneous production at ground surface, *Atmos. Environ.*, 106, 100-109, 10.1016/j.atmosenv.2015.01.061, 2015.
- Yadav, A. K., Raman, S., and Niyogi, D. D. S.: A note on the estimation of eddy diffusivity and dissipation length in low winds over a tropical urban terrain, *Pure and Applied Geophysics*, 160, 395-404, 10.1007/s00024-003-8785-4, 2003.
- Yang, D., Zhang, S., Niu, T., Wang, Y., Xu, H., Zhang, K. M., and Wu, Y.: High-resolution mapping of vehicle emissions of atmospheric pollutants based on large-scale, real-world traffic datasets, *Atmos. Chem. Phys.*, 2019, 8831-8843, 10.5194/acp-2019-32, 2019.
- Zhang, J., Chen, J., Xue, C., Chen, H., Zhang, Q., Liu, X., Mu, Y., Guo, Y., Wang, D., Chen, Y., Li, J., Qu, Y., and An, J.: Impacts of six potential HONO sources on HO_x budgets and SOA formation during a wintertime heavy haze period in the North China Plain, *Sci. Total Environ.*, 681, 110-123, <https://doi.org/10.1016/j.scitotenv.2019.05.100>, 2019a.
- Zhang, J. W., Chen, J. M., Xue, C. Y., Chen, H., Zhang, Q., Liu, X. G., Mu, Y. J., Guo, Y. T., Wang, D. Y., Chen, Y., Li, J. L., Qu, Y., and An, J. L.: Impacts of six potential HONO sources on HO_x budgets and SOA formation during a wintertime heavy haze period in the North China Plain, *Sci. Total Environ.*, 681, 110-123, 10.1016/j.scitotenv.2019.05.100, 2019b.
- Zhang, L., Wang, T., Zhang, Q., Zheng, J., Xu, Z., and Lv, M.: Potential sources of nitrous acid (HONO) and their impacts on ozone: A WRF-Chem study in a polluted subtropical region, *Journal of Geophysical Research-Atmospheres*, 121, 3645-3662, 10.1002/2015jd024468, 2016.
- Zhang, W., Tong, S., Ge, M., An, J., Shi, Z., Hou, S., Xia, K., Qu, Y., Zhang, H., Chu, B., Sun, Y., and He, H.: Variations and sources of nitrous acid (HONO) during a severe pollution episode in Beijing in winter 2016, *The Science of the total environment*, 648, 253-262, 10.1016/j.scitotenv.2018.08.133, 2019c.

Reviewer 3#

The title of this paper is very intriguing that (1) wintertime HONO promotes aerosol formation and (2) >50% of observed HONO is traffic related in Beijing. After reviewing this paper, I think it will be a grave mistake if the editor decides to publish this paper with these two conclusions in any form. The conclusions are pure speculations. I find no evidence to support either of the two claims in this paper.

Response: Thank you for your comments. We will answer your questions in the following section point by point.

The discussion for conclusion (1) is in section 3.2. One of the many mistakes in this section is that the authors do not understand that the largest source of OH is from the reaction of $\text{HO}_2 + \text{NO}$. Even when OH production from HONO photolysis is larger than from O_3 photolysis, the effect on OH is much smaller than the photolysis rate comparison. Line 301-304 is based on another paper; the data in this paper do not either support or dispute that oxidation by OH promotes aerosol formation. Figure 2D is used at the observation evidence supporting conclusion (1). There are many reasons that HONO/CO correlates with OA/CO. For example, CO is primary in winter in Beijing. If HONO and OA variations are from secondary sources, there will be high correlations as shown. Line 318 states “: : : it was reasonable to mainly ascribe the increase of OA concentration to local secondary formation initiated by OH radical from HONO photolysis.” It is a pure speculation. The observation data in this paper do not support this statement. It is the same with Line 328. The vague statement cannot be supported by the data in this paper. Line 332 is again a speculation. Ammonia is mostly neutralized by sulfate in Beijing. Line 338-400 is another speculative and ambiguous statement. Line 345-345 cites other people’s work but is not supported by the data in this work.

Response: Thank you for your instructive comment. The budget of HO_x or RO_x radical has been investigated at several locations in China based on field measurements and modelling studies (Tan et al., 2018; Tan et al., 2017; Tan et al., 2019; Tang et al., 2015). Using WRF-Chem model, Tang et al (2015) proposed that $\text{HO}_2 + \text{NO}$ was the major OH source, followed by HONO photolysis and O_3 photolysis in Beijing, Shanghai and Guangzhou when both primary and

secondary OH sources were taken into consideration (Fig. R14). As shown in this figure, however, photolysis of HONO was still an important OH sources and the dominate primary OH source in Beijing. Other studies also confirmed that HONO photolysis is an important OH sources, in particular, dominated the primary OH source at various locations (Fig. R15) (Tan et al., 2019; Liu et al., 2019; Tan et al., 2018; Tan et al., 2017).

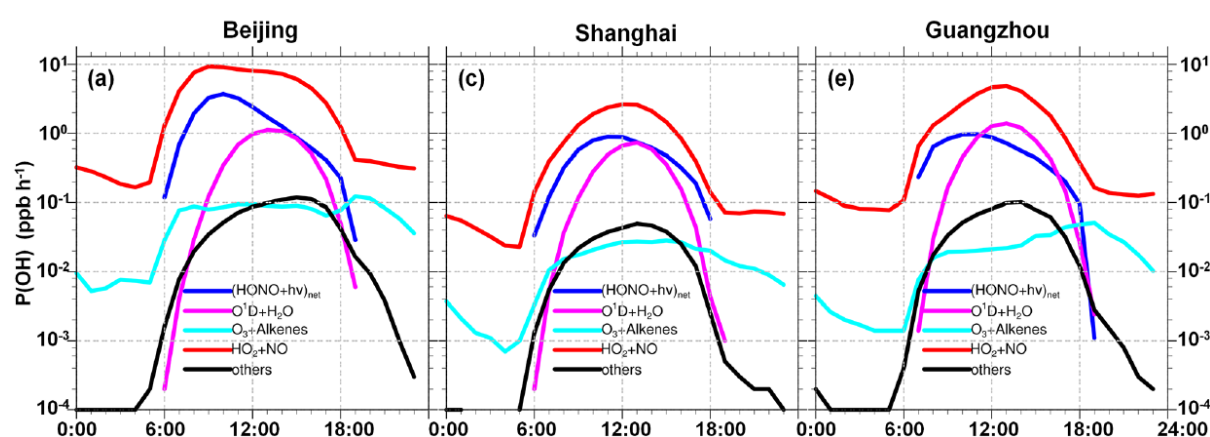


Fig. R14. Averaged production rate of OH in Beijing, Shanghai and Guangzhou (Tang et al., 2015).

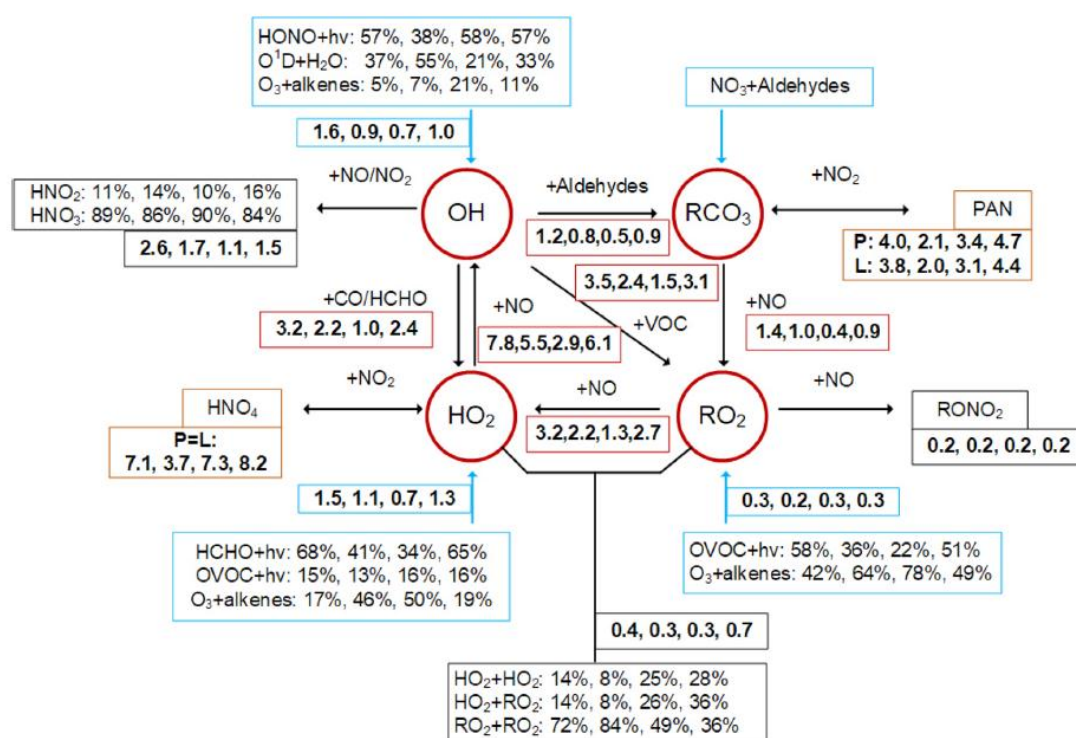


Fig. R15. Comparison of the OH–HO₂–RO₂ radical budget in four cities under daytime conditions (06:00 to 18:00 LT). The numbers are sorted from left to right in the order of Beijing, Shanghai, Guangzhou, and Chongqing. The blue, black, red, and yellow boxes denote the

primary radical sources, radical termination, radical propagation, and equilibrium between radicals and reservoir species, respectively (Tan et al., 2019).

We agree with you that HO_2+NO is the major OH source when both the primary and secondary OH sources are taken into consideration. In section 3.2, we were not going to discuss the budget of OH or RO_x . We want to confirm that HONO should play an important role in the initiation of RO_x chemistry during our observation. From [line 285 to 289](#), in the original version of the manuscript, we may mislead you because of the improper statements (“This means that the photolysis of HONO dominates the daytime OH production in polluted days in winter, while photolysis of O_3 behaves as a bigger OH source from April to June. This is consistent with the previous findings that HONO photolysis is the dominant OH source in winter of BTH”). In [lines 324-328](#) in the revised manuscript, we revised it “**These results mean that the photolysis of HONO should play an important role in the initiation of the daytime HO_x and RO_x chemistry on polluted days in winter, while photolysis of O_3 becomes more important from April to June.** This is consistent with the previous findings that **HONO photolysis dominates the primary OH source in winter of BTH...**”. At the same time, a sentence has also been added in [lines 305-307](#) in the revised manuscript “**In addition, it has been confirmed that HONO dominates the primary OH source at various locations (Tan et al., 2018;Liu et al., 2019;Tan et al., 2017;Aumont et al., 2003)**”.

We agree that the relationship among different pollutants are very complicated in the atmosphere because many variables are entangled. So, it is difficult to isolate the cause and effect relationship between two variables. In both laboratory and modeling studies, one can change the experiment conditions or the input parameters to test the sensitivity of a target parameter to a given variable. For example, a modeler can change the HONO concentration to simulate the change of aerosol concentration and quantify the influence of HONO on secondary aerosol formation. However, this is impossible for field measurements. Thus, correlation analysis is a common method to reasonably deduce the possible mechanism occurring in the atmosphere based on existing knowledge and reasonable assumptions in field measurements (it does so even in modeling studies and laboratory studies). For example, based on correlation analysis, it has been proposed that amines play a crucial role in new particle formation (Kirkby et al., 2011;Almeida et al., 2013) and NH_3/NO_2 can promote sulfate formation in aqueous phase

(Wang et al., 2016).

It has been well recognized that secondary organic aerosol is formed via multiple steps oxidation of VOCs (Kroll and Seinfeld, 2008). At the same time, HOx and ROx play very important role in VOCs oxidation (Atkinson et al., 2006). As discussed above, HONO is the important source of primary OH in the atmosphere. It also has been found that HONO is responsible for the initiation of photochemical reactions in chamber studies (Rohrer et al., 2005). In addition, modelling studies have confirmed that HONO can enhance secondary aerosols formation in Beijing-Tianjin-Hebei (BTH) region (Zhang et al., 2019b) and Pearl-River-Delta (PRD) region of China (Zhang et al., 2019a; Xing et al., 2019). Therefore, it is reasonable to deduce that the increase of OA concentration (Δ_{COA}) should be related to the OH from HONO photolysis (Δ_{CHONO}) after normalized to CO as supported by the linear correlation between $\Delta_{COA/CCO}$ and $-\Delta_{CHONO/CCO}$ in Fig. 2D. CO is a primary pollutant and a stable species in the atmosphere like BC. Thus, it was used to partially alleviate the influence of PBL variation (Cheng et al., 2016). In addition, $\Delta_{COA/BC}$ has also been used to characterize SOA formation during air mass transport (Liggio et al., 2016). Therefore, we correlated the $\Delta_{COA/CCO}$ with the $-\Delta_{CHONO/CCO}$ rather than the COA with the $CHONO$. This has been pointed out as in [lines 291-293](#) in the revised manuscript “After partially ruling out the possible influence of PBL variation by normalizing the concentrations of all pollutants to CO (Cheng et al., 2016) or BC (Liggio et al., 2016)...”.

It should be noted that the daytime lifetime of HONO is very short due to photolysis. This means regional transport should have little influence on local HONO concentration. However, OA concentration is ready to be affected by regional transport. Thus, we chose these pollution events under stagnant meteorological conditions. Therefore, we pointed out that “As the meteorological condition was stagnant during these cases as indicated by the low wind speed ($< 1.0 \text{ m s}^{-1}$, Fig. S5D), it was reasonable to mainly ascribe the increase of OA concentration to local secondary formation initiated by OH radical from HONO photolysis” from [line 317 to 319](#) in the original versions of the manuscript. It has been recognized that oxidation of NO_2 by OH dominates the daytime nitrate formation (Tian et al., 2019). Thus, we can deduce that OH from photolysis of HONO should promote nitrate formation because of the good correlation between the $\Delta_{\text{nitrate}/CCO}$ and $-\Delta_{CHONO/CCO}$ in [lines 375-377](#) in the revised manuscript.

In North China Plain, NH_3 is enough to neutralize both sulfate and nitrate due to the intensive emission of NH_3 . Fig. R16A shows the correlation between the charge of NH_4^+ and anions (including sulfate, nitrate and chloride) in non-refractory $\text{PM}_{2.5}$ measured using the ACSM in this work. In general, ammonium can neutralize both nitrate and sulfate. In addition, as shown in Fig. R16B, the cations can also neutralize the anions measured using a MARGA in Shijiazhuang from March, 2018 to April, 2019. Therefore, the increase of $\Delta C_{\text{ammonium}}/CCO$ and $-\Delta C_{\text{HONO}}/CCO$ can be ascribed to the fact that ammonium keeps the pace of nitrate through neutralization. In the revised SI, we added the correlation of the charge between the cations and anions in Fig. S8. In the revised manuscript (lines 368-371), we also pointed out that “We explained the increased ammonium as the result of enhanced neutralization of HNO_3 by NH_3 (Wang et al., 2018; Wen et al., 2018; Sun et al., 2018) because NH_4^+ was adequate to neutralize both sulfate and nitrate as shown in Fig.S8”.

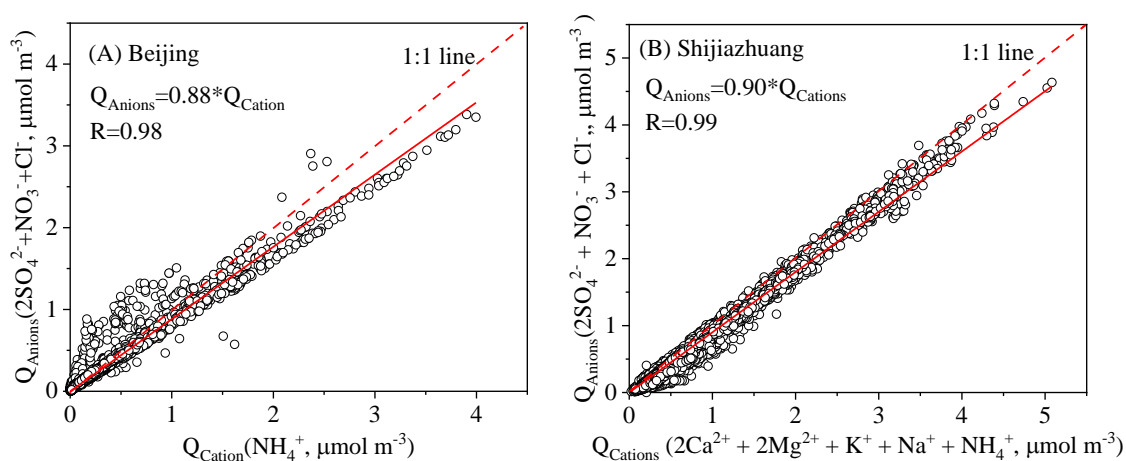


Fig. R16. Correlation of the charge between inorganic anions and cations (A) in non-refractory $\text{PM}_{2.5}$ in Beijing and (B) in soluble $\text{PM}_{2.5}$ in Shijiazhuang.

From line 338 to 340 in the original manuscript, we concluded that promotion effect of HONO photolysis on nitrate formation could not be excluded. From line 240 to 347, we proposed that HONO photolysis has little influence on sulfate formation based on the correlation between $\Delta C_{\text{sulfate}}/CCO$ and $-\Delta C_{\text{HONO}}/CCO$ as well as the previous studies, and then made a conclusion that photolysis of HONO could promote aerosol formation during pollution events in winter. From line 348 to 400, we showed the calculation details about HONO emission from vehicle and soil after referring to literatures. From line 345 to 348, we cited the results of

modeling studies. We pointed out that “this work well supported the recent modeling results that HONO could obviously promote the aerosol production in winter (Zhang et al., 2019a;Zhang et al., 2019b;Xing et al., 2019;An et al., 2013) from the point of view of observation”. So, we need to cite these previous work.

Conclusion (2) is based on some calculation that was not described in the paper. Line 376-378 states that the mean emission factor is 1.17% with a lower limit of 0.18% and an upper limit of 1.8%. (Why is the mean so close to the upper limit and 6.6 times larger than the lower limit?) The mean value is similar to previous studies and is not the reason for conclusion (2). Line 381 gives a vehicle HONO emission rate of 0.085 to 0.34 ppbv/h. The unit implies some volume was used in the calculation. No discussion was given on what volume was used and how it varied in a day. Another important factor not considered in this study is the outflow of vehicle HONO and NO_x by advection at night. It is the largest sink at night but is not included in the budget discussion. The nighttime source of NO₂ from the ground is 38 times less than vehicle emissions. However, no other paper I know of found that HONO concentrations at night cannot be explained mostly by a ground source. It led me to conclude that the vehicle HONO emission source in this paper is overestimated by 10-100 times. The authors should look at previous modeling papers that included vehicle HONO emissions. What they found is that the effect of vehicle HONO emissions is small.

Response: Thank you for your comments. As for the contribution of vehicle-related emission to HONO source, the details have been discussed in both [Section 2.2 and 3.3](#). In this work, we used two different methods to estimate the emission ratio of HONO to NO_x (HONO/NO_x) from vehicle exhaust. 1.8 % was calculated based on empirical analysis of field data, while 1.17% was obtained by using the low limit correlation of field data. Table R1 and Table S3 summaries the emission ratio from vehicles estimated or measured in China. The lowest value is 0.18% based on chassis dynamometer tests. From [line 376 to 378](#) in the original manuscript we described as “Thus, three levels of vehicle emission factor were considered. $1.17\pm 0.05\%$ was taken as the middle value, while 0.18% (Liu et al., 2017) and 1.8 % were the lower limit and the upper limit, respectively”. Here, we used a “middle value” (using the low limit correlation method of filed data) but not a “mean value”. Actually, this value is very close to

the mean emission ratio (1.21) if we consider all these reported values in Table R1. In the revised manuscript, we revised this sentence “Thus, three levels of vehicle emission factor were considered. $1.17\pm 0.05\%$ was taken as the middle value **which was very close to the mean emission ratio (1.21) for all of these reported values in China** (Li et al., 2018; Xu et al., 2015; Yang et al., 2014; Liu et al., 2017; Gall et al., 2016; Meng et al., 2019), while 0.18% (Liu et al., 2017) and 1.8 % were the lower limit and the upper limit, respectively” from [line 415 to 420](#) in the revised manuscript.

Table R1. Summary of the measured emission ratio of HONO to NO_x from vehicles in China.

Time	Place	Methods	$\Delta\text{HONO}/\Delta\text{NO}_x$		Reference
			Range	Mean	
2015/9/1- 2016/8/31	Ji'nan, Shandong	Empirical analysis of field data	0.19%- 0.87%	0.53±0.20%	(Li et al., 2018)
2011/8/3- 2012/5/31	Hongkong	Empirical analysis of field data	0.5%- 1.6%	1.2±0.4%	(Xu et al., 2015)
2015/3/11- 2015/3/21	Hongkong	Tunnel experiment	-	1.24±0.35%	(Liang et al., 2017)
2014	Beijing	Tunnel experiment	-	2.1%	(Yang et al., 2014)
2017	Beijing	Chassis dynamometer test	0.03%- 0.42%	0.18%	(Liu et al., 2017)
2016/12/16 - 2016/12/24	Beijing	Empirical analysis of field data	-	1.3%	(Zhang et al., 2019c)
2016/12/7- 2016/12/13	Beijing	Low limit correlation of field data	-	1.41%	(Meng et al., 2019)
2018/2/1- 2018/6/30	Beijing	Empirical analysis of field data	1.3-2.4%	1.8±0.5%	This study
2018/2/1- 2018/6/30	Beijing	Low limit correlation of field data	-	1.17±0.05%	This study

In [Section 2.2](#), we defined the calculation method for the emission rate of HONO from vehicles “The emission rate (E_{HONO} , ppbv h⁻¹) was calculated based on the emission flux (F_{HONO} , g m⁻² s⁻¹) and PBL height (H , m) according to the following equation,

$$E_{\text{HONO}} = \frac{\alpha \cdot F_{\text{HONO}}}{H} \quad (2)$$

where, α is the conversion factor ($\alpha = \frac{1 \times 10^9 \cdot 3600 \cdot R \cdot T}{M \cdot P} = \frac{2.99 \times 10^{13} \cdot T}{M \cdot P}$), M is the molecular weight

(g mol⁻¹), T is the temperature (K) and P is the atmospheric pressure (Pa)” from line 152 to 156 in the original manuscript. The emission flux of HONO was calculated according to the the hourly emission flux of NO_x from vehicle sector (Yang et al., 2019) and the relative emission ratio of HONO to NO_x as discussed above. It was pointed out as “The hourly NO_x emission inventory from vehicles in Beijing, with an annual emission rate of 109.9 Gg yr⁻¹ (Yang et al., 2019), was used when calculating the E_{vehicle} in this work.” from line 379 to 381 in the original manuscript. To make it clearer, we revised this sentence “The E_{vehicle} was calculated using the hourly NO_x emission inventory from vehicles in Beijing (Yang et al., 2019) after converted to emission flux of HONO ($F_{\text{HONO}}=F_{\text{NO}_x}\times \text{HONO/NO}_x$) and the PBL height as described in Section 2.2. Thus, the calculated emission rate reflected the diurnal variation of both the emission inventory and the PBL height” in lines 421-425 in the revised manuscript.

As you suggested, the outflow HONO by advection is an important sink of HONO in the night (Gall et al., 2016;Meng et al., 2019). The the loss of HONO ($T_{\text{advection}}$) via vertical advection can be calculated according to the following equation,

$$T_{\text{vertical}} = -K_h(z, t) \frac{\partial c(z,t)}{\partial z} \frac{1}{h} \quad (\text{R3})$$

where $K_h(z,t)$ is the eddy diffusivity of heat (m² s⁻¹) at height z (m) and time t , h is the height of the second layer (Gall et al., 2016). We added two paragraphs to discuss the transport in lines 222-232 “Vertical transport by advection (T_{vertical}), which is an important sink of HONO in the night (Gall et al., 2016;Meng et al., 2019), can be calculated according to equation (12).

$$T_{\text{vertical}} = -K_h(z, t) \frac{\partial c(z,t)}{\partial z} \frac{1}{h} \quad (12)$$

where $K_h(z,t)$ is the eddy diffusivity of heat (m² s⁻¹) at height z (m) and time t , h is the height of the second layer (18 m in this study) (Gall et al., 2016). On the other hand, both the vertical and horizontal transport can be estimate according to Eq. (13),

$$T_{\text{vertical}} = k_{\text{dilution}}(C_{\text{HONO}} - C_{\text{HONO,background}}) \quad (13)$$

where k_{dilution} is a dilution rate (0.23 h⁻¹, including both vertical and horizontal transport) (Dillon et al., 2002), C_{HONO} and $C_{\text{HONO,background}}$ is the HONO concentration at the observation site and background site, respectively (Dillon et al., 2002)” and lines 574-598 “As pointed in Section 2.2, vertical transport by advection is an important nocturnal sink of HONO (Gall et al., 2016). In this work, the vertical distribution of HONO concentration is unavailable.

Recently, Meng et al. (2019) measured the vertical distribution of HONO in Beijing in December, 2016. The concentration of HONO showed nearly flat profiles from ground level to 240 m in pollution events after sunset, while negative profiles of HONO were observed in pollution events during night (Meng et al., 2019). The nighttime concentration gradient was 0.0047 ± 0.0025 ppb m^{-1} derived from the nighttime dataset (Meng et al., 2019). In the daytime, we assume a zero concentration gradient. On the other hand, the eddy diffusivity of heat in urban environment was measured in New Delhi, Indian (Yadav et al., 2003). Using their dataset with the wind speed lower than 2.0 $m\ s^{-1}$, we derived the relationship between the K_h and the wind speed (WS) ($K_h = 0.9389 \times WS - 0.3374$ $m^2\ s^{-1}$). The nighttime $T_{vertical}$ changed from 0.15 to 0.37 ppbv h^{-1} in winter, while it was from 0.12 to 0.68 ppbv h^{-1} according to Eq. (12) from April to June. Because the wind speed was usually lower than 1.0 $m\ s^{-1}$ in pollution events (Fig. S6), horizontal transport should have little influence on the daytime sources or sinks of HONO because of the short lifetime of HONO. In the night, 79 % of the wind speed was lower than 1.0 $m\ s^{-1}$ in winter, thus the air masses from suburban areas should have influence on the sources and sinks of HONO in Beijing. If the HONO concentration at background was zero, the vertical and horizontal transport rate of HONO varied from 0.17 to 0.61 ppbv h^{-1} calculated according to Eq. (13) on haze days in winter and from 0.15 to 0.74 ppbv h^{-1} in pollution events from April to June. These values are higher than that calculated according to Eq. (12). Because the background HONO concentration was unavailable, we only considered the nighttime transport calculated according to Eq. (12) in the following section". At the same time, the relative contribution of each source in Section 3.3 was updated based on the total sinks.

HONO production from heterogeneous reactions of NO_2 on both aerosol surface and ground surface greatly depend on the uptake coefficient ($\gamma_{NO_2, BET}$) and the surface to volume ratio (S/V). The mean and median surface to volume ratio of aerosols are 1.33×10^{-3} and 1.36×10^{-3} m^{-1} during pollution events. This is comparable with the input parameters in modeling studies (Zhang et al., 2016). However, as discussed from [line 501 to 503](#) in the revised manuscript, the $\gamma_{NO_2, BET}$ on aerosols varied from 5×10^{-9} to 9.6×10^{-6} . The $\gamma_{NO_2, BET}$ on pure oxides was usually higher than on composite oxides. The selection of a proper $\gamma_{NO_2, BET}$ is quite tricky. For example, a fixed $\gamma_{NO_2, BET}$ was set to 1×10^{-6} in nighttime and 2×10^{-5} in daytime due to photochemical reaction of NO_2 on soot surface in a modelling study (Zhang et al.,

2016;Aumont et al., 2003). The nighttime $\gamma_{\text{NO}_2, \text{BET}}$ is ~ 2 orders of magnitude higher than ours (1.2×10^{-8}) as suggested by Crowley et al. (Crowley et al., 2010). In our previous work, we have measured the $\gamma_{\text{NO}_2, \text{BET}}$ on kaolin and hematite (Liu et al., 2015) and soot (Han et al., 2013). The initial $\gamma_{\text{NO}_2, \text{BET}}$ on kaolin is $4.85 \pm 0.39 \times 10^{-8}$ at 47 % RH. It should be pointed out that the $\gamma_{\text{NO}_2, \text{BET}}$ decreases significantly with exposure time due to surface saturation. Fig. R8 shows the typical uptake curve of NO_2 and the $\gamma_{\text{NO}_2, \text{obs}}$ which is not normalized to the specific surface area. The $\gamma_{\text{NO}_2, \text{BET}}$ at steady state (2.56×10^{-9} to 4.56×10^{-9} on kaolin and 1.23×10^{-8} to 1.50×10^{-8} on hematite) is around one order of magnitude lower than the initial $\gamma_{\text{NO}_2, \text{BET}}$ as shown in Fig. R9. Therefore, we used the recommended value (1.2×10^{-8}) (Crowley et al., 2010) as the base case. On the other hand, the $\gamma_{\text{NO}_2, \text{BET}}$ decreases with RH due to competitive adsorption (Liu et al., 2015). High mass concentration of $\text{PM}_{2.5}$ usually accompanied with high RH in winter in Beijing. Thus, we calculated the RH dependent $\gamma_{\text{NO}_2, \text{BET}}$ according to the equation we determined previously (Liu et al., 2015) and the measured ambient RH in this work. This should be more reasonable than a fixed uptake coefficient used in modeling studies.

In the original version of manuscript, we found a bug when calculating the heterogeneous reaction of NO_2 on black carbon. A conversion factor of time from second to hour was missed. So, the contribution of heterogeneous reaction to HONO source was underestimated in the original version. Now, the P_{aerosol} was 0.038 ± 0.030 - 0.088 ± 0.072 , which was dominated by the heterogeneous reaction of NO_2 on black carbon. It was on the same orders as soil emission. However, this was still significantly lower than the contribution of vehicle emission. In the revised manuscript, we updated Figs. 3-5 and the corresponding numbers in section 3.3.

As for heterogeneous reaction of NO_2 on ground surface, we used the same $\gamma_{\text{NO}_2, \text{BET}}$ on dust aerosol in the night, which is similar to the methodology used in modelling studies (Zhang et al., 2016;Aumont et al., 2003). As pointed out in Section 2.2 from [line 197 to 209](#) in the revised manuscript, the S/V was estimated using the surface roughness calculated in the light of satellite image of Beijing. The calculated surface roughness is 3.85, which is slightly higher than the value (2.2) used by Li et al. (2017). Thus, the calculated S/V varied from 0.0015 to 0.0385 m^{-1} (with a mean value of 0.0125 m^{-1}) because of the variation of the PBL height during pollution events. However, a fixed S/V of ground surface was set to 0.3 m^{-1} in the modeling studies (Zhang et al., 2016). This corresponds to a surface roughness ~ 92 , which means the

surface area is ~92 times of the projected area of ground. It's too high. If both the $\gamma_{\text{NO}_2,\text{BET}}$ (1×10^{-6}) and surface roughness are increased to the values used in modeling studies, the nighttime production rate of HONO via heterogeneous reaction of NO_2 on ground surface will be 2.9 ppb h^{-1} . This means a large sink missed if this number is reasonable. In lines 558-561 in the revised manuscript, we also revised the sentence “These results mean that heterogeneous reaction might not be a major HONO source. This is consistent with a recent work that found heterogeneous reaction being unimportant when compared with traffic emission during haze events in winter in Beijing (Zhang et al., 2019c)” and in lines 605-607 in the revised manuscript, “Heterogeneous reactions of NO_2 on aerosol surface and ground surfaces were not the major HONO source during night unlike the modelled results (Zhang et al., 2016; Aumont et al., 2003) ”.

During the Chinese New Year (CNY) and the COVID-19 epidemic in 2020, traffic emission decreased significantly in Beijing. This provides us a unique opportunity to verify the relative importance of each HONO source. We only analyzed the nocturnal data from January 1 to February 29 because the HONO sources related to photochemical reactions could be avoided. The CNY vacation was from January 23 to February 2. These results are in preparation for a separate paper. Fig. R10 shows the relative change of the concentrations of HONO, NO_x and non-refractory $\text{PM}_{2.5}$ (NR- $\text{PM}_{2.5}$). The traffic index and the chemical age of the air masses which is defined as $-\log(\text{NO}_x/\text{NO}_y)$ are also shown in Fig. R10. NO_y was measured with a NO_y analyzer (Thermo 42i-Y). The concentration of nighttime HONO decreased significantly during the CNY and after the CNY accompanied with the reduction in vehicle emission as supported by both the concentration of NO_x and traffic index (Fig. R10B). Interestingly, the NR- $\text{PM}_{2.5}$ concentration during and after the CNY increased obviously when compared with that before the CNY. The effective conversion of NO_2 aerosol surface was almost constant because both the promotion effect of increased $\text{PM}_{2.5}$ concentration and the inhibition effect of reduced NO_2 concentration during and after the CNY as shown in Fig. R10C. On the other hand, we found that the nighttime chemical age of the air masses during and after the CNY was also obviously larger than that before the CNY (Fig. R10D). This means that heterogeneous reaction of NO_2 on both aerosol surface and ground surface should be more effective due to longer residence of the air masses during and after the CNY than that before the CNY. When

the reduction of NO₂ concentration was taken into consideration, the product of NO₂ concentration and $-\log(\text{NO}_x/\text{NO}_y)$ in different periods increased slightly (Fig. R11). Therefore, the observed HONO concentration should be at least constant in different periods and independent on the reduction of vehicle emission if heterogeneous reaction of NO₂ on aerosol and ground surfaces dominates nighttime HONO source or if the vehicle emission is a minor HONO source. However, we observed the decrease of HONO along with reduction of vehicle emission (Fig.R10A). This well supports our (and other researchers' (Meng et al., 2019;Zhang et al., 2019c) conclusion that vehicle emission is an important source of HONO in Beijing.

In lines 523-528 in the revised manuscript, we pointed out “The A_s of aerosols which was measured using a DMPS varied from 1×10^{-4} to $4.8 \times 10^{-3} \text{ m}^{-1}$ with a mean value of $1.4 \pm 0.5 \times 10^{-3} \text{ m}^{-1}$ during pollution events. This value is comparable with that used in modeling studies (Zhang et al., 2016;Aumont et al., 2003). The A_s of ground surface which was calculated according to Eq. (6) and (7) varied from 1.5×10^{-3} to $3.85 \times 10^{-2} \text{ m}^{-1}$ with a mean value of $1.3 \pm 0.9 \times 10^{-2} \text{ m}^{-1}$ during pollution events. The surface roughness was 3.85 calculated according to Eq. (7)”. And from line 544 to 554 in the revised manuscript, we added a paragraph to discuss the reason why we obtained the low production rate of HONO via heterogeneous reaction of NO₂ on ground and aerosol surfaces as “It should be pointed out that HONO production from heterogeneous reaction of NO₂ on both aerosol and ground surface greatly depend on the $\gamma_{\text{NO}_2, \text{BET}}$ and A_s . The A_s of aerosols is comparable with the modeling input. However, the small nighttime $\gamma_{\text{NO}_2, \text{BET}}$ ($10^{-8} - 10^{-7}$) were used in this work rather than the $\gamma_{\text{NO}_2, \text{BET}}$ (1×10^{-6}) used in modelling studies (Zhang et al., 2016;Aumont et al., 2003). This leads to a lower production rate of HONO from heterogeneous reaction of NO₂ on aerosols. As for heterogeneous reaction of NO₂ on ground surface, besides the small $\gamma_{\text{NO}_2, \text{BET}}$ used in this work, the A_s of ground surface (0.0015 to 0.0385 m^{-1}) calculated using the surface roughness and PBL height was also significantly lower than the fixed value of 0.3 m^{-1} used in modeling studies that might overestimate the contribution of HONO production from heterogeneous reaction of NO₂ on ground surface”.

In summary, I think that the calculation and reasoning of this paper are either incorrect or ambiguous. It does seem likely that any revision can correct the flaws in the two main conclusions. I suggest that the authors scratch the conclusions and redo the analysis of their

observation data.

Response: Thank you for your comments again. We have answered your questions above.

References:

- Almeida, J., Schobesberger, S., Kurten, A., Ortega, I. K., Kupiainen-Maatta, O., Praplan, A. P., Adamov, A., Amorim, A., Bianchi, F., Breitenlechner, M., David, A., Dommen, J., Donahue, N. M., Downard, A., Dunne, E., Duplissy, J., Ehrhart, S., Flagan, R. C., Franchin, A., Guida, R., Hakala, J., Hansel, A., Heinritzi, M., Henschel, H., Jokinen, T., Junninen, H., Kajos, M., Kangasluoma, J., Keskinen, H., Kupc, A., Kurten, T., Kvashin, A. N., Laaksonen, A., Lehtipalo, K., Leiminger, M., Leppa, J., Loukonen, V., Makhmutov, V., Mathot, S., McGrath, M. J., Nieminen, T., Olenius, T., Onnela, A., Petaja, T., Riccobono, F., Riipinen, I., Rissanen, M., Rondo, L., Ruuskanen, T., Santos, F. D., Sarnela, N., Schallhart, S., Schnitzhofer, R., Seinfeld, J. H., Simon, M., Sipila, M., Stozhkov, Y., Stratmann, F., Tome, A., Trostl, J., Tsagkogeorgas, G., Vaattovaara, P., Viisanen, Y., Virtanen, A., Vrtala, A., Wagner, P. E., Weingartner, E., Wex, H., Williamson, C., Wimmer, D., Ye, P., Yli-Juuti, T., Carslaw, K. S., Kulmala, M., Curtius, J., Baltensperger, U., Worsnop, D. R., Vehkamäki, H., and Kirkby, J.: Molecular understanding of sulphuric acid-amine particle nucleation in the atmosphere, *Nature*, 502, 359-363, doi: 10.1038/nature12663, 2013.
- An, J., Li, Y., Chen, Y., Li, J., Qu, Y., and Tang, Y.: Enhancements of major aerosol components due to additional HONO sources in the North China Plain and implications for visibility and haze, *Adv. Atmos. Sci.*, 30, 57-66, 10.1007/s00376-012-2016-9, 2013.
- Atkinson, R., Baulch, D. L., Cox, R. A., Crowley, J. N., Hampson, R. F., Hynes, R. G., Jenkin, M. E., Rossi, M. J., Troe, J., and Subcommittee, I.: Evaluated kinetic and photochemical data for atmospheric chemistry: Volume II - gas phase reactions of organic species, *Atmos. Chem. Phys.*, 6, 3625-4055, doi:10.5194/acp-6-3625-2006, 2006.
- Aumont, B., Chervier, F., and Laval, S.: Contribution of HONO sources to the NO_x/HO_x/O₃ chemistry in the polluted boundary layer, *Atmos. Environ.*, 37, 487-498, [https://doi.org/10.1016/S1352-2310\(02\)00920-2](https://doi.org/10.1016/S1352-2310(02)00920-2), 2003.
- Cheng, Y., Zheng, G., Wei, C., Mu, Q., Zheng, B., Wang, Z., Gao, M., Zhang, Q., He, K., Carmichael, G., Poschl, U., and Su, H.: Reactive nitrogen chemistry in aerosol water as a source of sulfate during haze events in China, *Sci. Adv.*, 2, 10.1126/sciadv.1601530, 2016.
- Dillon, M. B., Lamanna, M. S., Schade, G. W., Goldstein, A. H., and Cohen, R. C.: Chemical evolution of the Sacramento urban plume: Transport and oxidation, *J. Geophys. Res.- Atmos.*, 107, ACH 3-1-ACH 3-15, 10.1029/2001jd000969, 2002.
- Gall, E. T., Griffin, R. J., Steiner, A. L., Dibb, J., Scheuer, E., Gong, L., Rutter, A. P., Cevik, B. K., Kim, S., Lefer, B., and Flynn, J.: Evaluation of nitrous acid sources and sinks in urban outflow, *Atmos. Environ.*, 127, 272-282, <https://doi.org/10.1016/j.atmosenv.2015.12.044>, 2016.
- Kirkby, J., Curtius, J., Almeida, J., Dunne, E., Duplissy, J., Ehrhart, S., Franchin, A., Gagne, S., Ickes, L., Kurten, A., Kupc, A., Metzger, A., Riccobono, F., Rondo, L., Schobesberger, S., Tsagkogeorgas, G., Wimmer, D., Amorim, A., Bianchi, F., Breitenlechner, M., David, A., Dommen, J., Downard, A., Ehn, M., Flagan, R. C., Haider, S., Hansel, A., Hauser, D., Jud, W., Junninen, H., Kreissl, F., Kvashin, A., Laaksonen, A., Lehtipalo, K., Lima, J., Lovejoy, E. R., Makhmutov, V., Mathot, S., Mikkilä, J., Minginette, P., Mogo, S., Nieminen, T., Onnela, A., Pereira, P., Petaja, T., Schnitzhofer, R., Seinfeld, J. H., Sipila, M., Stozhkov, Y., Stratmann, F., Tome, A., Vanhanen, J., Viisanen, Y., Vrtala, A., Wagner, P. E., Walther, H., Weingartner, E., Wex, H., Winkler, P. M., Carslaw, K. S., Worsnop, D. R., Baltensperger, U., and Kulmala, M.: Role of sulphuric acid, ammonia and galactic cosmic rays in atmospheric aerosol nucleation, *Nature*, 476, 429-433, <http://www.nature.com/nature/journal/v476/n7361/abs/nature10343.html#supplementary-information>, 2011.

Kroll, J. H., and Seinfeld, J. H.: Chemistry of secondary organic aerosol: Formation and evolution of low-volatility organics in the atmosphere, *Atmos. Environ.*, 42, 3593-3624, 2008.

Li, D., Xue, L., Wen, L., Wang, X., Chen, T., Mellouki, A., Chen, J., and Wang, W.: Characteristics and sources of nitrous acid in an urban atmosphere of northern China: Results from 1-yr continuous observations, *Atmos. Environ.*, 182, 296-306, <https://doi.org/10.1016/j.atmosenv.2018.03.033>, 2018.

Liang, Y., Zha, Q., Wang, W., Cui, L., Lui, K. H., Ho, K. F., Wang, Z., Lee, S.-c., and Wang, T.: Revisiting nitrous acid (HONO) emission from on-road vehicles: A tunnel study with a mixed fleet, *J. Air Waste Manage. Assoc.*, 67, 797-805, 10.1080/10962247.2017.1293573, 2017.

Liggio, J., Li, S.-M., Hayden, K., Taha, Y. M., Stroud, C., Darlington, A., Drollette, B. D., Gordon, M., Lee, P., Liu, P., Leithead, A., Moussa, S. G., Wang, D., O'Brien, J., Mittermeier, R. L., Brook, J. R., Lu, G., Staebler, R. M., Han, Y., Tokarek, T. W., Osthoff, H. D., Makar, P. A., Zhang, J., L. Plata, D., and Gentner, D. R.: Oil sands operations as a large source of secondary organic aerosols, *Nature*, 534, 91-94, 10.1038/nature17646 <http://www.nature.com/nature/journal/vaop/ncurrent/abs/nature17646.html#supplementary-information>, 2016.

Liu, Y., Lu, K., Ma, Y., Yang, X., Zhang, W., Wu, Y., Peng, J., Shuai, S., Hu, M., and Zhang, Y.: Direct emission of nitrous acid (HONO) from gasoline cars in China determined by vehicle chassis dynamometer experiments, *Atmos. Environ.*, 169, 89-96, 10.1016/j.atmosenv.2017.07.019, 2017.

Liu, Y. H., Lu, K. D., Li, X., Dong, H. B., Tan, Z. F., Wang, H. C., Zou, Q., Wu, Y. S., Zeng, L. M., Hu, M., Min, K. E., Kecorius, S., Wiedensohler, A., and Zhang, Y. H.: A Comprehensive Model Test of the HONO Sources Constrained to Field Measurements at Rural North China Plain, *Environ. Sci. Technol.*, 53, 3517-3525, 10.1021/acs.est.8b06367, 2019.

Meng, F., Qin, M., Tang, K., Duan, J., Fang, W., Liang, S., Ye, K., Xie, P., Sun, Y., Xie, C., Ye, C., Fu, P., Liu, J., and Liu, W.: High resolution vertical distribution and sources of HONO and NO₂ in the nocturnal boundary layer in urban Beijing, China, *Atmos. Chem. Phys. Discuss.*, 2019, 1-34, 10.5194/acp-2019-613, 2019.

Rohrer, F., Bohn, B., Brauers, T., Bruning, D., Johnen, F. J., Wahner, A., and Kleffmann, J.: Characterisation of the photolytic HONO-source in the atmosphere simulation chamber SAPHIR, *Atmos. Chem. Phys.*, 5, 2189-2201, 10.5194/acp-5-2189-2005, 2005.

Sun, P., Nie, W., Chi, X., Xie, Y., Huang, X., Xu, Z., Qi, X., Xu, Z., Wang, L., Wang, T., Zhang, Q., and Ding, A.: Two years of online measurement of fine particulate nitrate in the western Yangtze River Delta: influences of thermodynamics and N₂O₅ hydrolysis, *Atmos. Chem. Phys.*, 18, 17177-17190, 10.5194/acp-18-17177-2018, 2018.

Tan, Z., Fuchs, H., Lu, K., Hofzumahaus, A., Bohn, B., Broch, S., Dong, H., Gomm, S., Häsel, R., He, L., Holland, F., Li, X., Liu, Y., Lu, S., Rohrer, F., Shao, M., Wang, B., Wang, M., Wu, Y., Zeng, L., Zhang, Y., Wahner, A., and Zhang, Y.: Radical chemistry at a rural site (Wangdu) in the North China Plain: observation and model calculations of OH, HO₂ and RO₂ radicals, *Atmos. Chem. Phys.*, 17, 663-690, 10.5194/acp-17-663-2017, 2017.

Tan, Z., Rohrer, F., Lu, K., Ma, X., Bohn, B., Broch, S., Dong, H., Fuchs, H., Gkatzelis, G. I., Hofzumahaus, A., Holland, F., Li, X., Liu, Y., Liu, Y., Novelli, A., Shao, M., Wang, H., Wu, Y., Zeng, L., Hu, M., Kiendler-Scharr, A., Wahner, A., and Zhang, Y.: Wintertime photochemistry in Beijing: observations of RO_x radical concentrations in the North China Plain during the BEST-ONE campaign, *Atmos. Chem. Phys.*, 18, 12391-12411, 10.5194/acp-18-12391-2018, 2018.

Tan, Z. F., Lu, K. D., Jiang, M. Q., Su, R., Wang, H. L., Lou, S. R., Fu, Q. Y., Zhai, C. Z., Tan, Q. W., Yue, D. L., Chen, D. H., Wang, Z. S., Xie, S. D., Zeng, L. M., and Zhang, Y. H.: Daytime atmospheric oxidation capacity in four Chinese megacities during the photochemically polluted season: a case study based on box model simulation, *Atmos. Chem. Phys.*, 19, 3493-3513, 10.5194/acp-19-3493-2019, 2019.

Tang, Y., An, J., Wang, F., Li, Y., Qu, Y., Chen, Y., and Lin, J.: Impacts of an unknown daytime HONO source on the mixing ratio and budget of HONO, and hydroxyl, hydroperoxyl, and organic peroxy radicals, in the coastal regions of China, *Atmos. Chem. Phys.*, 15, 9381-9398, 10.5194/acp-15-9381-2015, 2015.

Tian, M., Liu, Y., Yang, F. M., Zhang, L. M., Peng, C., Chen, Y., Shi, G. M., Wang, H. B., Luo, B., Jiang, C. T., Li, B., Takeda, N., and Koizumi, K.: Increasing importance of nitrate formation for heavy aerosol pollution in two megacities in Sichuan Basin, southwest China, *Environ. Pollut.*, 250, 898-905, 10.1016/j.envpol.2019.04.098, 2019.

Wang, G., Zhang, R., Gomez, M. E., Yang, L., Zamora, M. L., Hu, M., Lin, Y., Peng, J., Guoc, S., Meng, J., Li, J., Cheng, C., Hu, T., Ren, Y., Wang, Y., Gao, J., Cao, J., An, Z., Zhou, W., Li, G., Wang, J., Tian, P., Marrero-Ortiz, W., Secrest, J., Du, Z., Zheng, J., Shang, D., Zeng, L., Shao, M., Wang, W., Huang, Y., Wang, Y., Zhu, Y., Li, Y., Hu, J., Pan, B., Cai, L., Cheng, Y., Ji, Y., Zhang, F., Rosenfeld, D., Liss, P. S., Duce, R. A., Kolb, C. E., and Molina, M. J.: Persistent sulfate formation from London Fog to Chinese haze, *Proc. Natl. Acad. Sci. USA*, 113, 13630-13635, 2016.

Wang, H. C., Lu, K. D., Chen, X. R., Zhu, Q. D., Wu, Z. J., Wu, Y. S., and Sun, K.: Fast particulate nitrate formation via N₂O₅ uptake aloft in winter in Beijing, *Atmos. Chem. Phys.*, 18, 10483-10495, 10.5194/acp-18-10483-2018, 2018.

Wen, L., Xue, L., Wang, X., Xu, C., Chen, T., Yang, L., Wang, T., Zhang, Q., and Wang, W.: Summertime fine particulate nitrate pollution in the North China Plain: increasing trends, formation mechanisms and implications for control policy, *Atmos. Chem. Phys.*, 18, 11261-11275, 10.5194/acp-18-11261-2018, 2018.

Xing, L., Wu, J., Elser, M., Tong, S., Liu, S., Li, X., Liu, L., Cao, J., Zhou, J., El-Haddad, I., Huang, R., Ge, M., Tie, X., Prévôt, A. S. H., and Li, G.: Wintertime secondary organic aerosol formation in Beijing–Tianjin–Hebei (BTH): contributions of HONO sources and heterogeneous reactions, *Atmos. Chem. Phys.*, 19, 2343-2359, 10.5194/acp-19-2343-2019, 2019.

Xu, Z., Wang, T., Wu, J., Xue, L., Chan, J., Zha, Q., Zhou, S., Louie, P. K. K., and Luk, C. W. Y.: Nitrous acid (HONO) in a polluted subtropical atmosphere: Seasonal variability, direct vehicle emissions and heterogeneous production at ground surface, *Atmos. Environ.*, 106, 100-109, 10.1016/j.atmosenv.2015.01.061, 2015.

Yadav, A. K., Raman, S., and Niyogi, D. D. S.: A note on the estimation of eddy diffusivity and dissipation length in low winds over a tropical urban terrain, *Pure and Applied Geophysics*, 160, 395-404, 10.1007/s00024-003-8785-4, 2003.

Yang, D., Zhang, S., Niu, T., Wang, Y., Xu, H., Zhang, K. M., and Wu, Y.: High-resolution mapping of vehicle emissions of atmospheric pollutants based on large-scale, real-world traffic datasets, *Atmos. Chem. Phys.*, 2019, 8831-8843, 10.5194/acp-2019-32, 2019.

Yang, Q., Su, H., Li, X., Cheng, Y., Lu, K., Cheng, P., Gu, J., Guo, S., Hu, M., Zeng, L., Zhu, T., and Zhang, Y.: Daytime HONO formation in the suburban area of the megacity Beijing, China, *Science China-Chemistry*, 57, 1032-1042, 10.1007/s11426-013-5044-0, 2014.

Zhang, J., An, J., Qu, Y., Liu, X., and Chen, Y.: Impacts of potential HONO sources on the concentrations of oxidants and secondary organic aerosols in the Beijing–Tianjin–Hebei region of China, *Sci. Total Environ.*, 647, 836-852, <https://doi.org/10.1016/j.scitotenv.2018.08.030>, 2019a.

Zhang, J. W., Chen, J. M., Xue, C. Y., Chen, H., Zhang, Q., Liu, X. G., Mu, Y. J., Guo, Y. T., Wang, D. Y., Chen, Y., Li, J. L., Qu, Y., and An, J. L.: Impacts of six potential HONO sources on HO_x budgets and SOA formation during a wintertime heavy haze period in the North China Plain, *Sci. Total Environ.*, 681, 110-123, 10.1016/j.scitotenv.2019.05.100, 2019b.

Zhang, L., Wang, T., Zhang, Q., Zheng, J., Xu, Z., and Lv, M.: Potential sources of nitrous acid (HONO) and their impacts on ozone: A WRF-Chem study in a polluted subtropical region, *Journal of Geophysical Research-*

Atmospheres, 121, 3645-3662, 10.1002/2015jd024468, 2016.

Zhang, W., Tong, S., Ge, M., An, J., Shi, Z., Hou, S., Xia, K., Qu, Y., Zhang, H., Chu, B., Sun, Y., and He, H.: Variations and sources of nitrous acid (HONO) during a severe pollution episode in Beijing in winter 2016, *The Science of the total environment*, 648, 253-262, 10.1016/j.scitotenv.2018.08.133, 2019c.

1 **The promotion effect of nitrous acid on aerosol formation in**
2 **wintertime Beijing: possible contribution of traffic-related**
3 **emission**

4

5 Yongchun Liu^{1*}, Yusheng Zhang¹, Chaofan Lian^{2,6}, Chao Yan³, Zeming Feng¹, Feixue
6 Zheng¹, Xiaolong Fan¹, Yan Chen^{2,6}, Weigang Wang^{2,6*}, Biwu Chu^{3,4}, Yonghong Wang³,
7 Jing Cai³, Wei Du³, Kaspar R. Daellenbach³, Juha Kangasluoma^{1,3}, Federico Bianchi^{1,3},
8 Joni Kujansuu^{1,3}, Tuukka Petäjä³, Xuefei Wang⁶, Bo Hu⁵, Yuesi Wang⁵, Maofa Ge²,
9 Hong He⁴ and Markku Kulmala^{1,3*}

10

11 1. Aerosol and Haze Laboratory, Advanced Innovation Center for Soft Matter Science and
12 Engineering, Beijing University of Chemical Technology, Beijing, 100029, China

13 2. State Key Laboratory for Structural Chemistry of Unstable and Stable Species, Beijing
14 National Laboratory for Molecular Sciences, Institute of Chemistry, Chinese Academy of
15 Sciences, Beijing 100190, China

16 3. Institute for Atmospheric and Earth System Research/Physics, Faculty of Science, University
17 of Helsinki, P.O. Box 64, FI-00014, Finland

18 4. State Key Joint Laboratory of Environment Simulation and Pollution Control, Research
19 Center for Eco-Environmental Sciences, Chinese Academy of Sciences, Beijing, 100085, China

20 5. State Key Laboratory of Atmospheric Boundary Layer Physics and Atmospheric Chemistry,
21 Institute of Atmospheric Physics, Chinese Academy of Sciences, Beijing, 100029, China

22 6. University of Chinese Academy of Sciences, Beijing 100049, PR China

23 *Correspondence to:* liuyc@buct.edu.cn, wangwg@iccas.ac.cn or markku.kulmala@helsinki.fi

24

25 **Abstract**

26 Secondary aerosol is a major component of PM_{2.5}, yet its formation mechanism in the
27 ambient atmosphere is still an open question. Based on field measurements in
28 downtown Beijing, we show that the photolysis of nitrous acid (HONO) could promote
29 the formation of organic and nitrate aerosol in wintertime Beijing as evidenced by the
30 growth of the mass concentration of organic and nitrate aerosols linearly increasing as
31 a function of consumed HONO from early morning to noon. The increased nitrate also
32 lead to the formation of particulate matter ammonium by enhancing the neutralization
33 of nitric acid by ammonia. We further illustrate that over 50 % of the ambient HONO
34 during pollution events in wintertime Beijing might be related to traffic-related
35 emission including direct emission and formation via the reaction between OH and
36 vehicle-emitted NO. Overall, our results highlight that the traffic-related HONO plays
37 an important role in the oxidative capacity and in turn, contribute to the haze formation
38 in winter Beijing. Mitigation of HONO and NO_x emission from the vehicles might be
39 an effective way to reduce secondary aerosol mass formation and severe haze events in
40 wintertime Beijing.

41

42 **1. Introduction**

43 China is one of the most suffering countries from the pollution of fine particulate matter
44 with diameter less than or equal to 2.5 μm ($\text{PM}_{2.5}$) (Lelieveld et al., 2015). Although
45 the regional air quality has been continuously improving since the central government
46 of China issued the Clean Air Act in 2013 (Vu et al., 2019), $\text{PM}_{2.5}$ concentration is still
47 significantly higher than that in developed countries (Fu et al., 2014;An et al., 2019).
48 Nowadays, a consensus has been reached that haze events are driven by local emissions
49 (An et al., 2019), regional transport (Zheng et al., 2015b) and secondary formation
50 (Huang et al., 2014;He et al., 2018) of pollutants under unfavorable meteorological
51 conditions (stagnant atmosphere and high relative humidity) (Zhu et al., 2018;Liu et al.,
52 2017c). A feedback loop between meteorological parameters and haze formation has
53 also been found playing an important role in the evolution of haze events (Zhang et al.,
54 2018).

55 Secondary aerosol can contribute up to ~70 % to the aerosol mass concentration on
56 polluted days (Huang et al., 2014). Several reaction pathways have been proposed in
57 the atmospheric chemistry community, such as sulfate formation via heterogeneous
58 oxidation of SO_2 promoted by H_2O_2 and/or NO_2 on mineral dust (Huang et al., 2015;He
59 et al., 2014), aqueous oxidation of SO_2 promoted by NO_2 in the presence or absence of
60 NH_3 in particle-bound water film (He et al., 2014;Wang et al., 2016), catalytic
61 conversion of SO_2 to sulfate by black carbon (Zhang et al., 2020), nitrate formation via
62 efficient hydrolysis of N_2O_5 on aerosol surfaces (Wang et al., 2017c;Wang et al.,
63 2019;Kulmala, 2018;Li et al., 2017), and the haze formation initiated by new particle

64 formation and growth (Guo et al., 2014;Guo et al., 2020). During the past years, strict
65 control of coal combustion has successfully reduced the SO₂ concentration, resulting in
66 a reduction of sulfate (SO₄²⁻) component in PM_{2.5}; in stark contrast, the contributions
67 from organic and nitrate become increasingly more significant in China (Lang et al.,
68 2017).

69 The formation of secondary organic aerosol (SOA) starts from the gas-phase
70 oxidation of volatile organic compounds (VOCs) leading to various oxidized low-
71 volatility and semi-volatile products (Bianchi et al., 2019), followed by their
72 partitioning into the particle phase (Hallquist et al., 2009). Similarly, the formation of
73 nitrate aerosol in the daytime is largely due to the partitioning of gaseous nitric acid,
74 which is formed via the oxidation of NO₂ by OH (Seinfeld and Pandis, 2006;Wang et
75 al., 2019). It is traditionally believed that the wintertime atmospheric oxidation capacity
76 is weak due to the weak solar radiation, which limits the formation of SOA and nitrate
77 (Sun et al., 2013). However, it is very recently shown that the peak OH concentration
78 on polluted days in winter Beijing varies from 2×10⁶ to 6×10⁶ molecules cm⁻³, which
79 is 6-10 times higher than what is predicted by the global model (Tan et al., 2018). This
80 discrepancy can be largely reduced after accounting for other OH production processes
81 in model simulations, which shows that the photolysis of nitrous acid (HONO)
82 dominates the initiation of HO_x (OH and HO₂) and RO_x (RO and RO₂) radical chain in
83 wintertime Beijing (Tan et al., 2018), and some other cities (Ren et al., 2006;Stutz et
84 al., 2013).

85 The HONO concentration has been measured with a wide rang from 0.18 to 9.71

86 ppbv at different locations, such as Beijing (Zhang et al., 2019d;Hu et al.,
87 2002;Hendrick et al., 2014;Wang et al., 2017b), Shanghai (Wang et al., 2013;Zhang et
88 al., 2019b), Guangdong (Hu et al., 2002;Su et al., 2008a), Hongkong (Xu et al., 2015),
89 Shandong (Li et al., 2018), Xi'an (Huang et al., 2017b) and so on in China since 2000.
90 More recently, modelling studies have suggested that nitrous acid (HONO) could
91 enhance secondary aerosols formation in Beijing-Tianjin-Hebei (BTH) region (Zhang
92 et al., 2019c), Pearl-River-Delta (PRD) region of China (Zhang et al., 2019a;Xing et al.,
93 2019) and Houston (Czader et al., 2015). These results imply that the role of HONO in
94 haze chemistry might be crucial in wintertime Beijing, while the direct evidence from
95 observation has not been reported, yet. On the other hand, the HONO budget has been
96 investigated via modelling studies (Liu et al., 2019c;Zhang et al., 2019c) and
97 photostationary state calculations (Wang et al., 2017b;Li et al., 2018;Huang et al.,
98 2017b;Lee et al., 2016;Oswald et al., 2015;Zhang et al., 2019d) at different locations.
99 At the present time, the study of the HONO budget is still far from closed, which would
100 require a significant effort on both the accurate measurement of HONO and the
101 determination of related kinetic parameters for its production pathways (Liu et al.,
102 2019c). For example, photo-enhanced conversion of NO₂ (Su et al., 2008b) and
103 photolysis of particulate nitrate were found to be the two major mechanisms with large
104 potential of HONO formation during noontime, but the associated uncertainty may
105 reduce their importance (Liu et al., 2019c). The heterogeneous reactions of NO₂ on
106 ground/aerosol surfaces were proposed to be an important HONO source during
107 nighttime (Wang et al., 2017b;Zhang et al., 2019c) and daytime in Beijing-Tianjin-

108 Hebei (BTH) (Zhang et al., 2019c), but it was unimportant compared with the unknown
109 sources and the homogeneous reaction between NO and OH in Ji'an (Li et al., 2018) or
110 compared with the traffic emission on haze days in Beijing (Zhang et al., 2019d). The
111 traffic emission was found to be an important HONO source during nighttime and a
112 minor daytime HONO source in BTH (Zhang et al., 2019c). However, it was proposed
113 that direct emission of HONO from vehicles should contribute about 51.1 % (Meng et
114 al., 2019) and 52 % of HONO source on haze days in Beijing (Zhang et al., 2019d).
115 These results mean that more studies are still required on the HONO budget. In
116 particular, it is meaningful to analyze the HONO budget in polluted events for
117 understanding the possible influence of HONO sources on secondary pollutants
118 formation.

119 In this work, we carried out comprehensive measurements at a newly constructed
120 observation station (Aerosol and Haze Laboratory, Beijing University of Chemical
121 Technology, AHL/BUCT Station) located in the western campus of Beijing University
122 of Chemical Technology in downtown Beijing. We show observational evidence that
123 HONO has a prominent promotion effect on the secondary aerosol mass formation in
124 winter. Traffic-related emission seems to be a vital contributor to ambient HONO
125 during the pollution events in winter in Beijing.

126 **2. Materials and methods**

127 **2.1 Field measurements.** Field measurements were performed at AHL/BUCT Station
128 (Lat. 39°56'31" and Lon. 116°17'52") from February 1 to June 30, 2018. The
129 observation station is on a rooftop of the main building, which is 550 m from the 3rd

130 ring road in the East, 130 m from the Zizhuyuan road in the North and 565 m from the
131 Nandianchang road in the West (Figure S1). The station is surrounded by both traffic
132 and residential emissions, thus, is a typical urban observation site.

133 Ambient air was sampled from the roof of the main building with five floors (~18
134 m above the surface). A PM_{2.5} inlet (URG) was used to cut off the particles with
135 diameter larger than 2.5 μm before going to a Nafion dryer (MD-700-24, Perma Pure).
136 Then a Time-of-Flight Aerosol Chemical Speciation Monitor equipped a PM_{2.5}
137 aerodynamic lens (ToF-ACSM, Aerodyne) and an Aethalometer (AE33, Magee
138 Scientific) were connected to the manifold of aerosol sampling tube. The Reynolds
139 number in the aerosol sampling tube was 800 with the total flow rate of 16.7 lpm and
140 the residence time of 6.5 s. The details about ToF-ACSM measurement was described
141 in the Supplement information. Ambient air was drawn from the roof using a Teflon
142 sampling tube (BMET-S, Beijing Saak-Mar Environmental Instrument Ltd.) with the
143 residence time <10 s for gas phase pollutants measurements. Trace gases including NO_x,
144 SO₂, CO and O₃ were measured with the corresponding analyzer (Thermo Scientific,
145 42i, 43i, 48i and 49i). Volatile organic compounds (VOCs) was measured using an
146 online Single Photon Ionization Time-of-flight Mass Spectrometer (SPI-ToF-MS
147 3000R, Hexin Mass Spectrometry) with unit mass resolution (UMR). The principle and
148 the configuration of the instrument has been described in detail elsewhere (Gao et al.,
149 2013) and the Supplement information. HONO concentration was measured using a
150 home-made Long Path Absorption Photometer (LOPAP) (Tong et al., 2016). The details
151 are described in the Supplement information. Particle size and number concentration

152 from 1 nm to 10 μm were measured with Scanning Mobility Particle Sizer (SMPS 3936,
153 TSI), particle size magnifier (PSM, Airmodus) and Neutral Cluster and Air Ion
154 Spectrometer (NIAS, Aired Ltd.). Meteorological parameters including temperature,
155 pressure, relative humidity (RH), wind speed and direction were measured using a
156 weather station (AWS310, Vaisala). Visibility and planetary boundary layer (PBL)
157 height were measured using a visibility sensor (PWD22, Vaisala) and a ceilometer
158 (CL51, Vaisala), respectively

159 **2.2 HONO budget calculation.** Multiple sources of ambient HONO have been
160 identified, such as emission from soil (E_{soil}) (Oswald et al., 2015; Meusel et al., 2018)
161 and vehicle exhaust (E_{vehicle}) (Trinh et al., 2017), production through homogeneous
162 reaction between NO and OH ($P_{\text{NO-OH}}$) in the atmosphere, photolysis of nitrate (P_{nitrate})
163 (Bao et al., 2018), nitrous acid (P_{HNO_3}) and nitrophenol ($P_{\text{nitrophenol}}$) (Sangwan and
164 Zhu, 2018), heterogeneous reaction of NO_2 on aerosol surface (P_{aerosol}) (Liu et al., 2015)
165 and ground surface (P_{ground}) (Liu et al., 2019c; Li et al., 2018; Wang et al., 2017b).
166 However, the photolysis of HNO_3 and nitrophenol were excluded in this work because
167 they were believed as minor sources (Lee et al., 2016) and their concentrations were
168 unavailable during our observation. The removal pathways of HONO including
169 photolysis ($L_{\text{photolysis}}$), the homogeneous reaction with OH radical ($L_{\text{HONO-OH}}$) and dry
170 deposition ($L_{\text{deposition}}$) (Liu et al., 2019c) were considered.

171 The HONO budget could be calculated by,

$$172 \frac{dc_{\text{HONO}}}{dt} = E_{\text{HONO}} + P_{\text{HONO}} - L_{\text{HONO}} + T_{\text{vertical}} + T_{\text{horizontal}} \quad (1)$$

173 where $\frac{dc_{\text{HONO}}}{dt}$ is the observed change rate of HONO mixing ratios (ppbv h^{-1}); E_{HONO}

174 represents the emission rate of HONO from different sources (ppbv h⁻¹); P_{HONO} is the
 175 in-situ production rate of HONO in the troposphere (ppbv h⁻¹); L_{HONO} is the loss rate of
 176 HONO (ppbv h⁻¹) (Li et al., 2018); $T_{vertical}$ and $T_{horizontal}$ are the vertical and horizontal
 177 transport (Soergel et al., 2011), which can mimic source or sink terms depending on the
 178 HONO mixing ratios of the advected air relative to that of the measurement site and
 179 height (Soergel et al., 2011).

180 The emission rate (E_{HONO} , ppbv h⁻¹) was calculated based on the emission flux
 181 ($F_{HONO}=EI_{HONO}/A$, g m⁻² s⁻¹) and PBL height (H , m) according to the following equation,

$$182 \quad E_{HONO} = \frac{\alpha \cdot F_{HONO}}{H} \quad (2)$$

183 where, EI_{HONO} , is the emission inventory of HONO (g s⁻¹), A is the urban area of Beijing
 184 (m²), α is the conversion factor ($\alpha = \frac{1 \times 10^9 \cdot 3600 \cdot R \cdot T}{M \cdot P} = \frac{2.99 \times 10^{13} \cdot T}{M \cdot P}$), M is the molecular
 185 weight (g mol⁻¹), T is the temperature (K) and P is the atmospheric pressure (Pa).

186 The production rates of HONO (P_{HONO} , ppbv h⁻¹) in the troposphere was calculated
 187 by,

$$188 \quad P_{HONO} = 3600 \cdot k_1 \cdot c_{precursor} \quad (3)$$

189 where, k_1 is the quasi first-order reaction rate constant (s⁻¹), $c_{precursor}$ is the concentration
 190 of precursor (ppbv). For homogeneous reaction between NO and OH,

$$191 \quad k_1 = k_2 \cdot c_{OH} \quad (4)$$

192 where, k_2 is the second-order reaction rate constant (7.2×10^{-12} cm³ molecule⁻¹ s⁻¹) (Li et
 193 al., 2012), c_{OH} is the OH concentration (molecules cm⁻³). For heterogeneous reaction,

$$194 \quad k_1 = \frac{\gamma \cdot A_s \cdot \omega}{4} \cdot Y_{HONO} \quad (5)$$

195 where, A_s is the surface area concentration of the reactive surface (m² m⁻³), ω is the

196 molecular mean speed (m s^{-1}), γ is the uptake coefficient of the precursor, Y_{HONO} is the
197 yield of HONO. For ground surface, the surface area concentration is

$$198 \quad A_s = \frac{\delta}{H} \quad (6)$$

199 where δ is the surface roughness, which is calculated according to the mean project area,
200 perimeter and height of the buildings in Beijing.

$$201 \quad \delta = \frac{f_{\text{building}} \cdot (A_{\text{projected}} + h \cdot P_{\text{building}})}{A_{\text{projected}}} + f_{\text{blank}} \quad (7)$$

202 where f_{building} (0.31) and f_{blank} (0.69) are the fraction of the projected area ($A_{\text{projected}}$) of
203 buildings and blank space, respectively; P_{building} and h are the perimeter and the height
204 of the building, respectively. The f_{building} and P_{building} are measured from ~1000 buildings
205 randomly selected on the Google Map using ImageJ software. The mean height (44.5
206 m) of the building in Beijing is linearly extrapolated from the literature data based on
207 remote measurement using Light Detection and Ranging (LiDAR) sensor from 2004 to
208 2008 (Cheng et al., 2011). The δ in Beijing is calculated to be 3.85, which is slightly
209 higher than the value (2.2) used by Li et al. (2018).

210 As for photolysis reaction, the first-order reaction rate was

$$211 \quad k_1 = J \quad (8)$$

212 where, J is the photolysis rate to produce HONO (s^{-1}).

213 The loss rates of HONO by photolysis ($L_{\text{photolysis}}$), homogeneous reaction with
214 OH radicals ($L_{\text{HONO-OH}}$) and dry deposition ($L_{\text{deposition}}$) (Liu et al., 2019c) were calculated
215 according to the following equations.

$$216 \quad L_{\text{photolysis}} = 3600 \cdot J_{\text{HONO}} \cdot c_{\text{HONO}} \quad (9)$$

$$217 \quad L_{\text{HONO-OH}} = 3600 \cdot k_{\text{HONO-OH}} \cdot c_{\text{OH}} \cdot c_{\text{HONO}} \quad (10)$$

218 $L_{deposition} = \frac{3600 \cdot v_d \cdot c_{HONO}}{H}$ (11)

219 where, J_{HONO} is the photolysis rate of HONO (s^{-1}), $k_{HONO-OH}$ is the second-order reaction
 220 rate constant between HONO and OH ($6 \times 10^{-12} \text{ cm}^3 \text{ molecule}^{-1} \text{ s}^{-1}$) (Atkinson et al.,
 221 2004), and v_d is the dry deposition rate of HONO (0.001 m s^{-1}) (Han et al., 2017).

222 Vertical transport by advection ($T_{vertical}$), which is an important sink of HONO in
 223 the night (Gall et al., 2016; Meng et al., 2019), can be calculated according to equation
 224 (12).

225 $T_{vertical} = -K_h(z, t) \frac{\partial c(z, t)}{\partial z} \frac{1}{h}$ (12)

226 where $K_h(z, t)$ is the eddy diffusivity of heat ($\text{m}^2 \text{ s}^{-1}$) at height z (m) and time t , h is the
 227 height of the second layer (18 m in this study) (Gall et al., 2016). On the other hand,
 228 both the vertical and horizontal transport can be estimate according to Eq. (13),

229 $T_{vertical} = k_{dilution}(c_{HONO} - c_{HONO,background})$ (13)

230 where $k_{dilution}$ is a dilution rate (0.23 h^{-1} , including both vertical and horizontal transport)
 231 (Dillon et al., 2002), c_{HONO} and $c_{HONO,background}$ is the HONO concentration at the
 232 observation site and background site, respectively (Dillon et al., 2002).

233 In addition, even though all the current known sources had been considered in
 234 models, the modelled daytime HONO concentrations were still lower than the observed
 235 concentration (Tang et al., 2015; Michoud et al., 2014). Therefore, the HONO
 236 concentration could be described in equation (14).

237 $\frac{dc_{HONO}}{dt} = E_{soil} + E_{vehicle} + P_{NO-OH} + P_{nitrate} + P_{aerosol} + P_{ground} + P_{unknown} -$
 238 $L_{photolysis} - L_{HONO-OH} - L_{deposition} + T_{vertical} + L_{horizontal}$ (14)

239 **3. Results and discussion**

240 **3.1 Overview of the air pollution.** The mass concentration of non-refractory PM_{2.5}
241 (NR-PM_{2.5}) and HONO along with metrological parameters are shown in Fig. 1. The
242 time series of other pollutants (SO₂, CO, O₃, benzene, toluene and black carbon) are
243 shown in Fig. S2 in the Supplement information.

244 Similar to previous measurements (Guo et al., 2014;Wang et al., 2016), the air
245 pollution events showed a periodic cycle of 3-5 days during the observation, as
246 indicated by the concentration of NR-PM_{2.5} (Fig. 1A), gaseous pollutants and the
247 visibility. During the observation period, 20-60% of hourly PM_{2.5} concentration was
248 higher than 75 µg m⁻³ (the criterion for pollution according to the national air quality
249 standards) in each month (Fig. S3A). Both the frequency of severe polluted episodes
250 and the mean mass concentration of PM_{2.5} and NR-PM_{2.5} were obviously higher in
251 March than that in the rest months (Fig. 1 and S3). This can be explained by both the
252 intensive emission during the heating season as evidenced by the high concentration of
253 primary pollutants including CO, SO₂ and BC (Table S1) and the stagnant
254 meteorological conditions supported by the low wind speed (<2 m s⁻¹) and the low
255 planetary boundary layer (PBL) height, in particular, in March (Fig. S4A).

256 OA and nitrate dominated the NR-PM_{2.5}, while their relative contribution varied
257 significantly during the observation (Fig. 1B and Table S1). This is similar to the
258 previously reported NR-PM_{1.0} composition (Sun et al., 2015). The monthly mean
259 fraction of OA varied from 45.9±10.2 % to 52.6±18.7 %, which was accompanied by a
260 slight increase of sulfate from 16.0±9.1 % to 18.2±8.0 % (Fig. S4D). At the same time,
261 the monthly mean fraction of nitrate and chloride decreased from 26.7±8.8 % to

262 16.7±12.8 % and from 7.7±6.1 % to 0.3±0.2 %, respectively. Ammonium showed a
263 peak value (14.2±2.8 %) in March, then slightly decreased to 12.2±5.2 %. The intensive
264 emission of chloride from coal combustion during heating season (Cho et al., 2008) and
265 firework burning (Zhang et al., 2017), which was transported from Tangshan during
266 Chinese New Year (Fig. S5A and B), led to high fraction of chloride in February and
267 March. The decrease in nitrate and ammonium fractions from February to June should
268 be related to **the increase in temperature** (Fig. S2) which was in favor of NH₄NO₃
269 decomposition (Wang et al., 2015). Besides the reduction of the contribution from other
270 components, secondary formation due to increased UV light (Fig. S4C) might also
271 favor the increased OA fraction (Huang et al., 2014). This means that chemical
272 transformation in March should still be vigorous although the UV light intensity in
273 March is lower than in summer (Fig. S4C). It also implies other factors may compensate
274 the weak UV light intensity in March.

275 HONO, which has been recognized as the important precursor of **primary** OH
276 radical (Ren et al., 2006; Alicke et al., 2003), ranged from 0.05 to 10.32 ppbv from
277 February 1 to June 30, 2018 (Fig. 1C) with the mean value of 1.26±1.06 ppbv. In winter
278 (February and March), HONO concentration was 1.15±1.10 ppbv and comparable to
279 the previous results (1.05±0.89 ppbv) measured in the winter of Beijing (Wang et al.,
280 2017b; Hou et al., 2016), while it was slightly lower than that from April to June
281 (1.35±1.11 ppbv) in this work and those measured in the summer of Shanghai (2.31
282 ppbv, in May) (Cui et al., 2018) and Guangzhou (2.8 ppbv, in July) (Qin et al., 2009).
283 The mean HONO concentration in March (1.53±1.25 ppbv) was higher than that in

284 February and April (Fig. S3D), while was slightly higher or close to that in May and
285 June. Chamber studies have found that HONO is responsible for the initiation of
286 photomog reactions (Rohrer et al., 2005). It is reasonable to postulate that HONO
287 probably play an important **role** in the secondary chemistry of particle formation in
288 March.

289 **3.2 Promotion effect of HONO photolysis on aerosol formation in winter.** Oxidation
290 of precursors by OH radicals is the main mechanism regarding to secondary aerosol
291 formation in the troposphere. After partially ruling out the possible influence of PBL
292 variation by normalizing the concentrations of all pollutants to CO (Cheng et al., 2016)
293 **or BC (Liggio et al., 2016)**, we found all secondary species including sulfate, nitrate
294 and ammonium show obvious daytime peaks from 7:00 am to 6:00 pm (Figure S5C)
295 (Cheng et al., 2016). The similar trends were observed after the concentrations of
296 pollutants were normalized to BC (not shown). This suggests they might connect with
297 photochemistry.

298 Photolysis of H₂O₂, HCHO, O₃ and HONO, and **the reaction between NO and HO₂**
299 are known as sources of OH radical in the atmosphere (Alicke et al., 2003; Volkamer et
300 al., 2010; Tan et al., 2018; Tang et al., 2015). In this work, the concentration of H₂O₂,
301 HCHO and **HO₂** are unavailable. Thus, their contributions to OH production were not
302 discussed here. However, it has been well recognized that the photolysis of HONO is
303 the **dominant** source of OH in the dawn and dusk period (Holland et al., 2003), even
304 contributes up to 60% of daytime OH source in winter (Spataro et al., 2013; Rohrer et
305 al., 2005). **In addition, it has been confirmed that HONO dominates the primary OH**

306 source at various locations (Tan et al., 2018; Liu et al., 2019c; Tan et al., 2017; Aumont
307 et al., 2003). Therefore, it is meaningful to discuss the contribution of HONO to
308 secondary aerosol formation through OH production. We simply compared the OH
309 production via photolysis of HONO ($P_{\text{OH-HONO}}=J_{\text{HONO}}\times C_{\text{HONO}}$) and O₃ ($P_{\text{OH-}}$
310 $\text{O}_3=J_{\text{O}_3}\times C_{\text{O}_3}$) in Fig. 2 when the PM_{2.5} concentration was larger than 50 μg m⁻³ and the
311 RH was less than 90 % to understand the chemistry in pollution events. Under these
312 conditions, local chemistry should be more important as 75 % of the wind speed was
313 less than 1.0 m s⁻¹ (Fig. S6). The details about the J_{HONO} and J_{O_3} calculation were
314 shown in the Supplement information and their time series were shown in Fig. S7. On
315 polluted days in winter, the daytime $P_{\text{OH-HONO}}$ was always significantly higher than the
316 $P_{\text{OH-O}_3}$ in winter and the maximal $P_{\text{OH-HONO}}$ and $P_{\text{OH-O}_3}$ were $1.73\pm 0.86 \times 10^7$ molecules
317 cm⁻³ s⁻¹ (2.43 ± 1.21 ppb h⁻¹) and $1.03\pm 1.06 \times 10^7$ molecules cm⁻³ s⁻¹ (1.45 ± 1.49 ppb h⁻
318 ¹), respectively (Fig. 2A). Owing to the high HONO concentration accumulated
319 throughout the night, the maximal $P_{\text{OH-HONO}}$ in winter was as about 2-6 times of that
320 was observed in the wintertime of Colorado, USA (~ 0.59 ppb h⁻¹) (Kim et al., 2014),
321 New York, USA (~ 0.40 ppb h⁻¹) (Kanaya et al., 2007) and Nanjing, China (0.90 ± 0.27
322 ppb h⁻¹) (Liu et al., 2019b). In the period from April to June, the daily maxima of $P_{\text{OH-}}$
323 HONO and $P_{\text{OH-O}_3}$ were $2.48\pm 1.42 \times 10^7$ molecules cm⁻³ s⁻¹ (3.48 ± 1.99 ppb h⁻¹) and
324 $6.51\pm 4.17 \times 10^7$ molecules cm⁻³ s⁻¹ (9.15 ± 5.86 ppb h⁻¹), respectively. These results
325 mean that the photolysis of HONO should play an important role in the initiation of the
326 daytime HO_x and RO_x chemistry on polluted days in winter, while photolysis of O₃
327 becomes more important from April to June. This is consistent with the previous

328 findings that HONO photolysis dominates the primary OH source in winter of BTH
329 (Xing et al., 2019; Tan et al., 2018), Colorado and New York City (Ren et al., 2006; Kim
330 et al., 2014), while photolysis of O₃ and HCHO related reactions usually dominated
331 primary OH production in summer (Alicke et al., 2003).

332 Oxidation of trace gas pollutants, in particular VOCs, by OH is their main removal
333 pathway in the troposphere (Atkinson and Arey, 2003), subsequently, contribute to
334 secondary aerosol formation (Kroll and Seinfeld, 2008). A very recent work has found
335 that oxidation of VOCs from local traffic emission is still efficient even under pollution
336 conditions (Guo et al., 2020). We partially ascribe this to the high HONO concentration
337 in winter Beijing. To confirm this assumption, 12 episodes in winter were chosen (Fig.
338 1) to uncover the connection between aerosol formation and HONO photolysis. The 1st,
339 3rd and 5th episodes were clean days and the other 9 episodes were typical haze events
340 with duration above 2 days. The features of these episodes were summarized in Table
341 S2. Fig. 2C shows the CO-normalized daytime profiles of OA and HONO in the 7th and
342 12th episodes as two examples. In all selected cases, HONO exhibited quick reduction
343 due to the photolysis after sunrise, and simultaneously, OA concentration started to
344 increase. This is similar to the evolution of the concentration of pollutants in a typical
345 smog chamber experiment. We further show the formation of OA ($\Delta C_{OA}/C_{CO}$) as a
346 function of the consumed HONO ($-\Delta C_{HONO}/C_{CO}$) in Fig. 2D. Except for the 4th episode
347 that was highly affected by firework emission during the Spring Festival, $\Delta C_{OA}/C_{CO}$
348 showed a linear dependence on $-\Delta C_{HONO}/C_{CO}$ in winter, and the correlation coefficient
349 was 0.75. As the meteorological condition was stagnant during these cases as indicated

350 by the low wind speed ($< 1.0 \text{ m s}^{-1}$, Fig. S5D), it was reasonable to ascribe the increase
351 of OA concentration to local secondary formation initiated by OH radical and
352 photolysis of HONO should play an important role in initiation the HO_x and RO_x
353 chemistry. This kind of correlation could not be seen for the pollution events from April
354 to June because the primary OH production was no longer dominated by HONO
355 photolysis as indicated by Fig. 2D. It should be noted that oxidation of biogenic alkenes
356 by O_3 might also contribute to OA formation. However, anthropogenic VOCs instead
357 of biogenic VOCs dominated the wintertime VOCs in Beijing (Liu et al., 2017a).
358 Although vehicles can emit isoprene (Zou et al., 2019), the contribution of isoprene to
359 the observed increase of OA concentration should be unimportant due to the low
360 concentration of isoprene in winter (Zou et al., 2019). Therefore, it is reasonable to
361 conclude that the increase of OA concentration in daytime might be mainly resulted
362 from oxidation of VOCs by OH.

363 Similar to OA, $\Delta C_{\text{nitrate}}/C_{\text{CO}}$ in winter also showed good linear correlation with -
364 $\Delta C_{\text{HONO}}/C_{\text{CO}}$ ($R=0.67$, Fig. S5E), suggesting that the increase of particle-phase nitrate
365 in the daytime should also be promoted by OH radical from HONO photolysis.
366 Interestingly, $\Delta C_{\text{ammonium}}/\text{CO}$ also showed a good correlation with $-\Delta C_{\text{HONO}}/C_{\text{CO}}$
367 ($R=0.61$, Fig. S5E), although particle-phase ammonium should not be directly related
368 to oxidation of NH_3 by OH. We explained the increased ammonium as the result of
369 enhanced neutralization of HNO_3 by NH_3 (Wang et al., 2018; Wen et al., 2018; Sun et
370 al., 2018) because NH_4^+ was adequate to neutralize both sulfate and nitrate as shown in
371 Fig.S8. This was consistent with the recent work which observed the important role of

372 photochemical reactions in daytime nitrate formation, while hydrolysis of N_2O_5 mainly
373 contributed to nighttime nitrate (Tian et al., 2019). Although a recent work has found
374 that daytime hydrolysis of N_2O_5 on hygroscopic aerosols is also an important source of
375 daytime nitrate in winter Beijing (Wang et al., 2017a), the linearly correlation between
376 $\Delta C_{\text{nitrate}}/C_{\text{CO}}$ and $\Delta C_{\text{HONO}}/C_{\text{CO}}$ at least implies that the promotion effect of HONO on
377 nitrate formation could not be excluded. On the other hand, the correlation between
378 $\Delta C_{\text{sulfate}}/C_{\text{CO}}$ and $-\Delta C_{\text{HONO}}/C_{\text{CO}}$ was much weaker ($R=0.26$), suggesting a weak
379 connection between particle-phase sulfate and gas-phase H_2SO_4 . This was also
380 consistent with the previous understanding that heterogeneous reactions of SO_2 were
381 the **dominant** pathway for sulfate formation (Zheng et al., 2015a;He et al., 2018;Zhang
382 et al., 2020). Overall, this work well supported the recent modeling results that HONO
383 could obviously promote the aerosol production in winter (Zhang et al., 2019a;Zhang
384 et al., 2019c;Xing et al., 2019;An et al., 2013) from the point of view of observation.

385 **3.3 HONO budget in polluted events.** To understand the possible sources of HONO
386 in polluted events in winter, the HONO budget was calculated for the events when the
387 $PM_{2.5}$ concentration was larger than $50 \mu\text{g m}^{-3}$ and the RH was less than 90 % according
388 to the method described in Section 2.2.

389 **Vehicle emission.** The E_{vehicle} was calculated **according to Eq. (2)** using the relative
390 emission rate of HONO to NO_x and the emission inventory of NO_x from vehicles. Firstly,
391 the ratio of HONO/ NO_x was calculated according to the method reported by Xu et al.
392 (Xu et al., 2015) and Li et al. (Li et al., 2018) from the fresh nighttime plumes which
393 were strictly satisfy the following criteria: 1) $NO_x > 45$ ppb (highest 25% of NO_x data);

394 2) $\Delta\text{NO}/\Delta\text{NO}_x > 0.8$, with good correlation between NO and NO_x ($R > 0.9$, $P < 0.05$);
395 3) Good correlation between HONO and NO_x ($R^2 > 0.65$, $P < 0.05$); and 4) Dataset from
396 5:00 am to 8:00 am. The mean emission ratio of HONO to NO_x was $1.8 \pm 0.5\%$ based
397 on 5 fresh vehicle exhaust plumes during our observation (Table S3). This value is
398 higher than that in Hongkong ($1.2 \pm 0.4\%$) (Xu et al., 2015), Beijing (1.3%) (Zhang et
399 al., 2019d) and Jinan ($0.53 \pm 0.20\%$) (Li et al., 2018) using the same method, while is
400 comparable with the result measured in tunnel experiments (2.1%) carried out in
401 Beijing (Yang et al., 2014). Secondly, low HONO concentration should be accompanied
402 with high NO_x and high ratio of $\Delta\text{NO}/\Delta\text{NO}_x$ if direct emission from vehicles was the
403 major source of HONO and the source from secondary formation was negligible in the
404 urban atmosphere. Therefore, we further estimated the HONO/ NO_x ratio using a low
405 limit correlation method (Li et al., 2012). In the 2D space of HONO versus NO_x (Fig.
406 S8), the lowest margin with $\Delta\text{NO}/\Delta\text{NO}_x$ larger than 0.8 were chosen for linear
407 correlation. The ratio of $\Delta\text{HONO}/\Delta\text{NO}_x$ is $1.17 \pm 0.05\%$. This value is lower than that
408 estimated through empirical method discussed above, while is very close to that
409 measured in Hongkong ($1.2 \pm 0.4\%$) (Xu et al., 2015) and ($1.23 \pm 0.35\%$) (Liang et al.,
410 2017), Guangzhou (1.0%) (Li et al., 2012) and Beijing (1.3% and 1.41%) (Zhang et al.,
411 2019d; Meng et al., 2019). Finally, several studies have measured the direct emission of
412 HONO from vehicle exhaust. The HONO/ NO_x was 0.18% from gasoline cars through
413 chassis dynamometer tests in China (Liu et al., 2017d), while it was 0-0.95% for
414 gasoline vehicles and 0.16-1.0% for diesel vehicles measured under real-world driving
415 test cycles in Japan (Trinh et al., 2017). Thus, three levels of vehicle emission factor

416 were considered. $1.17\pm 0.05\%$ was taken as the middle value which was very close to
417 the mean emission ratio (1.21) for all of these reported values in China (Li et al.,
418 2018; Xu et al., 2015; Yang et al., 2014; Liu et al., 2017d; Gall et al., 2016; Meng et al.,
419 2019), while 0.18% (Liu et al., 2017d) and 1.8 % were the lower limit and the upper
420 limit, respectively.

421 The E_{vehicle} was calculated using the hourly NO_x emission inventory from vehicles
422 in Beijing (Yang et al., 2019) after converted to emission flux of HONO ($F_{\text{HONO}}=F_{\text{NO}_x}\times$
423 HONO/NO_x) and the PBL height as described in Section 2.2. Thus, the calculated
424 emission rate reflected the diurnal variation of both the emission inventory and the PBL
425 height. The calculated hourly middle value of E_{vehicle} using the HONO/NO_x of 1.17%
426 was from 0.085 ± 0.038 to 0.34 ± 0.15 ppbv h^{-1} , which was slightly higher than the
427 daytime emission rate of HONO in Xi'an (Huang et al., 2017b). This is reasonable
428 when the vehicle population in Beijing is taken into consideration. The lower limit of
429 E_{vehicle} was $0.013\pm 0.006-0.053\pm 0.023$ ppbv h^{-1} , which was close to the estimated
430 emission rate of HONO in Jinan (Li et al., 2018). The upper limit was in the range of
431 $0.13\pm 0.06-0.53\pm 0.23$ ppbv h^{-1} .

432 **Soil emission.** The emission flux of HONO from soil depends on the water content, the
433 nitrogen nutrient content and the temperature of soil (Oswald et al., 2013). Oswald et
434 al. (2013) measured the emission flux of HONO from 17 soil samples, including
435 eucalyptus forest, tropical rain forest, coniferous forest, pasture, woody savannah,
436 grassland, stone desert, maize field, wheat field, jujube field an cotton field etc. Tropical
437 rain forest, coniferous forest and grassland are the typical plants in downtown Beijing

438 (Huang et al., 2017a). At the same time, their emission fluxes of HONO are comparable
 439 (Oswald et al., 2013). Thus, we used the emission flux from grassland to calculate the
 440 emission rate of HONO from soil in Beijing because the temperature and water holding
 441 content dependent emission flux of HONO was available for grassland soil. Three
 442 levels of water content including 25-35%, 35-45% and 45-55% were considered. The
 443 temperature dependence of F_{HONO} was calculated using the mean value of the F_{HONO}
 444 with different water content, while the low limit and upper limit of F_{HONO} were
 445 calculated using the emission flux from 45-55% of water content and 25-35% of water
 446 content, respectively. The lower limit, the middle value and the upper limit of the E_{soil}
 447 are $0.0032 \pm 0.0027 - 0.013 \pm 0.014$, $0.0046 \pm 0.0039 - 0.020 \pm 0.20$ and $0.0057 \pm 0.0047 -$
 448 0.025 ± 0.024 ppbv h⁻¹, respectively, calculated according to Eq. (2).

449 **Homogeneous reaction between NO and OH.** Direct measurement of OH
 450 concentration was unavailable in this work, while several methods were used to
 451 estimate the ambient OH concentration. In winter in Beijing, it has been found that the
 452 OH concentration is linearly correlated with J_{O1D} , that's, $c_{\text{OH}} = J_{\text{O1D}} \times 2 \times 10^{11}$ molecules
 453 cm⁻³ (Tan et al., 2019). However, Tan et al. (2018) reported a larger conversion factor
 454 (4.33×10^{11} molecules cm⁻³). Li et al. (2018) estimated the OH radical concentration
 455 considering both photolysis rate and NO₂ concentration, namely,

$$456 \quad c_{\text{OH}} = \frac{4.1 \times 10^9 \times (J_{\text{O1D}})^{0.83} \times (J_{\text{NO}_2})^{0.19} \times (140c_{\text{NO}_2} + 1)}{0.41c_{\text{NO}_2}^2 + 1.7c_{\text{NO}_2} + 1} \quad (15)$$

457 Overall, the estimated OH concentrations according to Eq. (15) were comparable with
 458 that estimated by Tan et al. (2019) (Fig. S10C). The method for the photolysis rates
 459 calculation were shown in the SI and the time series of the photolysis rates were shown

460 in Fig. S7. On polluted days, high concentration of NO₂ resulted into lower OH
 461 concentrations estimated using the Eq. (15). Therefore, the corresponding $P_{\text{NO-OH}}$ was
 462 taken as the low limit for homogeneous reaction between NO and HONO because
 463 polluted events were discussed in this work, while $P_{\text{NO-OH}}$ calculated using the OH
 464 concentration ($J_{\text{O1D}} \times 4.33 \times 10^{11}$ molecules cm⁻³) (Tan et al., 2018) was taken as the upper
 465 limit and $P_{\text{NO-OH}}$ calculated using the OH concentration ($J_{\text{O1D}} \times 2 \times 10^{11}$ molecules cm⁻³)
 466 (Tan et al., 2019) was the middle value. In the night, OH concentration usually varied
 467 from 1.0×10^5 molecules cm⁻³ (Li et al., 2012; Tan et al., 2018) in winter to 5×10^5
 468 molecules cm⁻³ in summer (Tan et al., 2017). The nighttime OH concentration was
 469 estimated linearly correlated with the product of nighttime O₃ concentration and alkenes
 470 concentration, namely,

$$471 \quad c_{\text{OH},\text{night}} = 1 \times 10^5 + 4 \times 10^5 \times \frac{(c_{\text{O}_3} \times c_{\text{alkenes}})_{\text{night}} - (c_{\text{O}_3} \times c_{\text{alkenes}})_{\text{night},\text{min}}}{(c_{\text{O}_3} \times c_{\text{alkenes}})_{\text{night},\text{max}} - (c_{\text{O}_3} \times c_{\text{alkenes}})_{\text{night},\text{min}}} \quad (16)$$

472 The time series of OH concentration calculated using different methods was shown in
 473 Fig. S11. Thus, the lower limit, the middle value and the upper limit of $P_{\text{NO-OH}}$ were
 474 0.007 ± 0.019 - 0.43 ± 0.26 , 0.026 ± 0.053 - 0.99 ± 0.79 and 0.028 ± 0.053 - 2.14 ± 1.71 ppbv h⁻¹,
 475 respectively, calculated according to Eqs. (3) and (4). The calculated middle value of
 476 $P_{\text{NO-OH}}$ (with mean daytime value of 0.49 ± 0.35 ppb h⁻¹) was comparable with these
 477 estimated values by Li et al. (2018) (0.4 ppb h⁻¹) and Huang et al. (2017b) (0.28 ppb h⁻¹).
 478 It should be noted that measured NO concentration was used to calculate the $P_{\text{NO-OH}}$.
 479 Besides vehicle emission, power plant and industries also contribute NO emission. 40 %
 480 of NO_x was from vehicle emission according to the emission inventory of NO_x in
 481 Beijing (He et al., 2002).

482 It should be noted that OH concentration was estimated based on J_{O1D} (Tan et al.,
483 2019; Tan et al., 2018) or J_{O1D} and J_{NO_2} (Li et al., 2018). As discussed in Section 3.2,
484 HONO was an important primary OH source in the daytime. Unfortunately, it could not
485 be parameterized for calculating OH concentration because the measured or modelled
486 OH concentration was unavailable in this work. This might underestimate the early
487 daytime OH concentration, subsequently, the contribution of homogeneous reaction of
488 NO with OH to HONO source. This need to be further investigated in the future.

489 **Photolysis of nitrate.** A recent work reported the photolysis rate of nitrate (J_{nitrate}) in
490 ambient $\text{PM}_{2.5}$ at a solar zenith angle of 0° (Bao et al., 2018). The J_{nitrate} varied from
491 1.22×10^{-5} to $4.84 \times 10^{-4} \text{ s}^{-1}$ with the mean value of $8.24 \times 10^{-5} \text{ s}^{-1}$. These values were
492 further normalized according to the zenith angle and UV light at our observation station
493 to calculate the low limit, the upper limit and the middle J_{nitrate} . The time series of the
494 measured nitrate concentration and the middle value of J_{nitrate} were shown in Fig. 1 and
495 Fig. S7, respectively. Therefore, the corresponding daytime lower limit, the middle
496 value and the upper limit of HONO from photolysis of nitrate were 0.0011 ± 0.0021 -
497 0.096 ± 0.092 , 0.0072 ± 0.0021 - 0.66 ± 0.092 and 0.042 ± 0.082 - $3.86 \pm 0.008 \text{ ppbv h}^{-1}$,
498 respectively, calculated in the light of Eqs. (3) and (8).

499 **Heterogeneous reactions of NO_2 on aerosol and ground surface.** The production of
500 HONO from heterogeneous reactions of NO_2 on aerosol surface was calculated
501 according to Eqs. (3) and (5). The aerosol surface concentration was measured with a
502 SMPS. The uptake coefficient (γ) of NO_2 on different particles varied from 5×10^{-9} to
503 9.6×10^{-6} (Ndour et al., 2009; Underwood et al., 2001; Underwood et al., 1999), while it

504 was recommended to be 1.2×10^{-8} (Crowley et al., 2010), which was used to calculate
505 the P_{aerosol} in the base case. It has been found that the γ highly depends on the relative
506 humidity (RH). The low limit bound of P_{aerosol} was calculated based on the RH
507 dependent uptake coefficient of NO_2 on kaolinite ($\gamma_{\text{NO}_2} = 4.47 \times 10^{39} / (1.75 \times 10^{46} + 1.93$
508 $\times 10^{45} \text{RH})$), while the upper limit of P_{aerosol} was calculated according to the RH
509 dependent γ on hematite ($\gamma_{\text{NO}_2} = 4.46 \times 10^{39} / (6.73 \times 10^{44} + 3.48 \times 10^{44} \text{RH})$) (Liu et al.,
510 2015). Heterogeneous reaction of NO_2 on black carbon (BC) was also considered in the
511 night. The surface area concentration of BC was calculated according to its specific
512 area ($87 \text{ m}^2 \text{ g}^{-1}$) (Su et al., 2018) and the measured mass concentration. The γ_{NO_2} on BC
513 is 1.17×10^{-5} , with a HONO yield of 0.8 (Han et al., 2013). The light enhanced uptake γ
514 of NO_2 (1.9×10^{-6}) on mineral dust was further parameterized (Ndour et al., 2008) after
515 normalized to the solar radiation intensity in Beijing.

516 The contribution of heterogeneous reaction of NO_2 on ground surface was
517 calculated similar to that on mineral dust. The same kinetics for heterogeneous reaction
518 of NO_2 on aerosol surface were used to calculate the nighttime contribution of ground
519 surface. A recent work observed a significant enhancement of NO_2 and HONO
520 formation by UV light on the real urban grime (Liu et al., 2019a). Thus, RH dependent
521 kinetic data measured on urban grime ($\gamma_{\text{NO}_2} = 7.4 \times 10^{-7} + 5.5 \times 10^{-8} \text{RH}$) was used to
522 calculate the daytime upper limit for heterogeneous uptake of NO_2 on the ground
523 surface. The A_s of aerosols varied from 1×10^{-4} to $4.8 \times 10^{-3} \text{ m}^{-1}$ with a mean value of
524 $1.4 \pm 0.5 \times 10^{-3} \text{ m}^{-1}$ during pollution events. This value is comparable with that used in
525 modeling studies (Zhang et al., 2016; Aumont et al., 2003). The A_s of ground surface

526 which was calculated according to Eq. (6) and (7) varied from 1.5×10^{-3} to $3.85 \times 10^{-2} \text{ m}^{-1}$
527 1 with a mean value of $1.3 \pm 0.9 \times 10^{-2} \text{ m}^{-1}$ during pollution events. The surface roughness
528 was 3.85 calculated according to Eq. (7). The Y_{HONO} was set to 0.5 because of the
529 hydrolysis reaction of NO_2 (Liu et al., 2015), while it was 0.8 for light enhanced
530 reaction (Liu et al., 2019a; Ndour et al., 2008) and on BC (Han et al., 2013).

531 The lower limit, the middle value and the upper limit of P_{aerosol} were 0.038 ± 0.030 -
532 0.087 ± 0.072 , 0.038 ± 0.030 - 0.088 ± 0.072 and 0.041 ± 0.032 - 0.092 ± 0.073 ppbv h^{-1} ,
533 respectively. The corresponding values were 0.00027 ± 0.00017 - 0.0020 ± 0.0012 ,
534 0.0014 ± 0.00095 - 0.0089 ± 0.006 and 0.0025 ± 0.0023 - 0.060 ± 0.032 ppbv h^{-1} for P_{ground} .
535 Although the A_s of ground surface was higher than that of aerosol, the larger γ_{NO_2}
536 (1.17×10^{-5}) on soot particles than that on other aerosols and ground surface led to a
537 larger production rate of HONO in this work. The P_{aerosol} calculated in this work was
538 on the same orders as soil emission, while it was lower than the P_{aerosol} estimated by
539 Huang et al. (Huang et al., 2017b) because different calculation methods have been
540 used. In their work, the production rate of HONO was estimated based on the
541 conversion rate (Huang et al., 2017b), whilst it was calculated based on the measured
542 aerosol surface area concentration and uptake coefficient of NO_2 on different particles
543 in this work.

544 It should be pointed out that HONO production from heterogeneous reaction of
545 NO_2 on both aerosol and ground surface greatly depend on the $\gamma_{\text{NO}_2, \text{BET}}$ and A_s . The A_s
546 of aerosols was comparable with the modeling input. However, the small nighttime $\gamma_{\text{NO}_2, \text{BET}}$
547 (10^{-8} - 10^{-7}) on dust were used in this work rather than the $\gamma_{\text{NO}_2, \text{BET}}$ (1×10^{-6}) used in

548 modelling studies (Zhang et al., 2016; Aumont et al., 2003; Gall et al., 2016). This leads
549 to a lower production rate of HONO from heterogeneous reaction of NO₂ on aerosols.
550 As for heterogeneous reaction of NO₂ on ground surface, besides the small $\gamma_{\text{NO}_2, \text{BET}}$
551 used in this work, the A_s of ground surface (0.0015 to 0.0385 m⁻¹) calculated using the
552 surface roughness and PBL height was also significantly lower than the fixed value of
553 0.3 m⁻¹ in modeling studies that might overestimate the contribution of HONO
554 production from heterogeneous reaction of NO₂ on ground surface. It should be noted
555 that the initial uptake coefficient (γ_{ini}) was parameterized in this work. This will
556 overestimate the contribution of heterogeneous reaction of NO₂ to HONO source
557 because the steady-state uptake coefficient is usually one order of magnitude lower than
558 γ_{ini} (Han et al., 2013; Liu et al., 2015). These results mean that heterogeneous reaction
559 might not be a major HONO source. This is consistent with a recent work that found
560 heterogeneous reaction being unimportant when compared with traffic emission during
561 haze events in winter in Beijing (Zhang et al., 2019d).

562 **Sinks of HONO.** The loss rates of HONO by photolysis ($L_{\text{photolysis}}$), homogeneous
563 reaction with OH radicals ($L_{\text{HONO-OH}}$) and dry deposition were calculated according to
564 Eqs. (9)-(11). The daytime J_{HONO} varied from 1.71×10^{-5} to 1.13×10^{-3} s⁻¹ on polluted
565 days in winter, while it was in the range of 5.89×10^{-5} to 1.53×10^{-3} s⁻¹ from April to June.
566 These values are comparable to modelling results (3.9×10^{-5} - 1.8×10^{-3} s⁻¹) (Gall et al.,
567 2016). The daytime $L_{\text{photolysis}}$ were in the range of 0.03-5.23 ppb h⁻¹ and 0.25-7.10 ppb
568 h⁻¹ in winter and the rest months, respectively. It was the major sink of HONO in the
569 daytime. The $L_{\text{HONO-OH}}$ varied from 0.0049 to 0.069 ppbv h⁻¹ in winter using the $k_{\text{HONO-OH}}$.

570 OH of $6 \times 10^{-12} \text{ cm}^3 \text{ molecule}^{-1} \text{ s}^{-1}$ (Atkinson et al., 2004) and the middle value of OH
571 concentrations. It was from 0.0050 to 0.085 ppbv h^{-1} from April to June. The $L_{\text{deposition}}$
572 was in the range of 0.004-0.056 ppbv h^{-1} in winter and 0.004-0.030 ppbv h^{-1} from April
573 to June, calculated according to Eq. (11).

574 As pointed in Section 2.2, vertical transport by advection is an important nocturnal
575 sink of HONO (Gall et al., 2016). In this work, the vertical distribution of HONO
576 concentration is unavailable. Recently, Meng et al. (2019) measured the vertical
577 distribution of HONO in Beijing in December, 2016. The concentration of HONO
578 showed nearly flat profiles from ground level to 240 m in pollution events after sunset,
579 while negative profiles of HONO were observed in pollution events during night (Meng
580 et al., 2019). The nighttime concentration gradient was $0.0047 \pm 0.0025 \text{ ppb m}^{-1}$ derived
581 from the nighttime dataset (Meng et al., 2019). In the daytime, we assume a zero
582 concentration gradient. On the other hand, the eddy diffusivity of heat in urban
583 environment was measured in New Delhi, Indian (Yadav et al., 2003). Using their
584 dataset with the wind speed lower than 2.0 m s^{-1} , we derived the relationship between
585 the K_h and the wind speed (WS) ($K_h = 0.9389 \times \text{WS} - 0.3374 \text{ m}^2 \text{ s}^{-1}$). The nighttime T_{vertical}
586 changed from 0.15 to 0.37 ppbv h^{-1} in winter, while it was from 0.12 to 0.68 ppbv h^{-1}
587 according to Eq. (12) from April to June. Because the wind speed was usually lower
588 than 1.0 m s^{-1} in pollution events (Fig. S6), horizontal transport should have little
589 influence on the daytime sources or sinks of HONO because of the short lifetime of
590 HONO (Spataro and Ianniello, 2014). In the night, 79 % of the wind speed was lower
591 than 1.0 m s^{-1} in winter, thus the air masses from suburban areas should have influence

592 on the sources and sinks of HONO in Beijing. If the HONO concentration at
593 background was zero, the vertical and horizontal transport rate of HONO varied from
594 0.17 to 0.61 ppbv h⁻¹ which is calculated in the light of Eq. (13) on haze days in winter
595 and from 0.15 to 0.74 ppbv h⁻¹ in pollution events from April to June. These values
596 were higher than that calculated according to Eq. (12). Because the background HONO
597 concentration was unavailable, we only considered the nighttime transport calculated
598 according to Eq. (12) in the following section.

599 **Comparison among different HONO sources.** Fig. 3 summarizes the diurnal patterns
600 of each sources with different parameterizations during the pollution events from
601 February to March. The black dots and lines mean the middle values, while the shadow
602 indicates the corresponding lower bound and upper bound. In the nighttime, vehicle
603 and soil emission, and homogeneous reaction between NO and OH were the important
604 sources of HONO. In the daytime, however, photolysis of nitrate and homogeneous
605 reaction between NO and OH dominated the sources of HONO. Heterogeneous
606 reactions of NO₂ on aerosol surface and ground surfaces were not the major HONO
607 source during night unlike the modelled results (Zhang et al., 2016; Aumont et al., 2003).

608 Fig. 4A-F shows the HONO budget estimated using the middle values among these
609 parameters during the polluted events. The mean production rate of HONO varied in
610 the range of 0.25 - 1.81 ppbv h⁻¹ from these identified sources, while the corresponding
611 loss rate was from 0.21 to 2.34 ppbv h⁻¹ during the polluted events in winter. The main
612 loss of HONO was the photolysis during the daytime (1.74± 0.44 ppbv h⁻¹), whereas it
613 was vertical transport in the nighttime (0.28±0.08 ppbv h⁻¹). Direct emission from

614 vehicles exhaust was the largest nighttime source of HONO (0.23 ± 0.06 ppbv h^{-1}),
615 followed by heterogeneous reactions of NO_2 on the ground surface (0.07 ± 0.01 ppbv h^{-1}),
616 homogeneous reaction between NO and OH (0.04 ± 0.01 ppbv h^{-1}), emission from
617 soil (0.014 ± 0.005 ppbv h^{-1}), and heterogeneous reactions of NO_2 on aerosol surface
618 (0.006 ± 0.002 ppbv h^{-1}). P_{NO-OH} and $P_{nitrate}$ dominated the daytime HONO production,
619 with daytime mean values of 0.49 ± 0.35 ppbv h^{-1} and 0.34 ± 0.23 ppbv h^{-1} , respectively.
620 As shown in Fig. 4, these six sources still underestimated the daytime sources of HONO.
621 The $P_{unknown}$ was 0.20 ± 0.24 ppbv h^{-1} in February and March, while it was 0.50 ± 0.24
622 ppbv h^{-1} from April to June.

623 The $E_{vehicle}$ contributed $57.0\pm 10.0\%$ and $51.5\pm 20.1\%$ to the nighttime HONO
624 sources from February to March and the rest months, respectively, even when the
625 $P_{unknown}$ was taken into consideration. The relative contribution of daytime $E_{vehicle}$
626 decreased to $15.2\pm 15.4\%$ in winter and $9.7\pm 7.8\%$ from April to June. Thus, the daily
627 mean fraction of the $E_{vehicle}$ was $39.6\pm 24.3\%$ and $34.0\pm 24.3\%$ from February to March
628 and from April to June, respectively. This means that the $E_{vehicle}$ dominates the nighttime
629 HONO source during the polluted events in Beijing, which is consistent with the
630 previous result that vehicle emission was the major nighttime or haze day HONO source
631 (51.1% - 52%) in Beijing (Zhang et al., 2019c; Meng et al., 2019). As pointed out in
632 Section 3.3, $E_{vehicle}$ was calculated based on the NO_x inventory from vehicle sector. On
633 the other hand, NO is prone to be quickly converted to NO_2 and NO_z (including HONO,
634 HNO_3 , N_2O_5 , PAN and organonitrate etc) by O_3 , HO_2 , RO_2 and OH in the atmosphere.
635 It is reasonable to assume that local traffic emission dominates the ambient NO source

636 in the urban environment. Thus, homogeneous reaction between NO and OH in the
637 atmosphere could also be related to vehicle exhaust. As shown in Fig.3, although the
638 diurnal curve of $P_{\text{NO-OH}}$ coincided well with that of OH concentration (Fig. S10), which
639 means the $P_{\text{NO-OH}}$ should be mainly determined by OH concentration, the $P_{\text{NO-OH}}$ should
640 still reflect the indirect contribution of traffic related emission to HONO source because
641 the ambient NO concentration was used to calculate the $P_{\text{NO-OH}}$. Traffic-related HONO
642 sources ($E_{\text{vehicles}} + P_{\text{NO-OH}}$) might contribute $57.8 \pm 15.8\%$ and $48.6 \pm 15.9\%$ to the daily
643 HONO source in winter and the rest months, respectively. Even if 40 % of NO_x was
644 from vehicle exhaust in Beijing (He et al., 2002), traffic-related source ($E_{\text{vehicles}} +$
645 $0.4P_{\text{NO-OH}}$) might still contribute $46.9 \pm 20.5\%$ in winter and $39.9 \pm 20.5\%$ from April to
646 June to the corresponding daily HONO source. The contribution of traffic-related
647 source was still an important daytime source of HONO ($43.9 \pm 10.6\%$ for $E_{\text{vehicles}} + P_{\text{NO-OH}}$
648 OH, and $26.7 \pm 12.4\%$ for $E_{\text{vehicles}} + 0.4P_{\text{NO-OH}}$) on polluted days in winter.

649 As shown in Fig. 3, uncertainties existed when calculating each HONO source. To
650 further understand the role of traffic emission, we also estimated the lower limit of the
651 traffic-related contribution as follows: 1) the lower limit of E_{vehicle} was obtained by
652 using the lowest reported emission ratio of HONO/ NO_x from vehicles (0.18%) (Liu et
653 al., 2017d) rather than 1.17%, which was the empirical value calculated based on the
654 field measurement in Fig. S7; 2) the lower limit for homogeneous reaction between NO
655 and OH radical was calculated according to the method by Li et al. (2018); 3) the upper
656 limit of the emission rate from soil was estimated using the emission flux of HONO
657 with low water content (Oswald et al., 2013); 4) the upper limit of HONO production

658 rate from heterogeneous reaction of NO₂ on the aerosol was calculated using the large
659 RH-dependent uptake coefficient of NO₂ on hematite (Liu et al., 2015) rather the value
660 recommended by Crowley et al. (Crowley et al., 2010); 5) the upper limit for
661 heterogeneous reaction on ground surface was calculated using the RH-dependent
662 kinetic data measured on urban grime (Liu et al., 2019a). As shown in Fig. 5, traffic-
663 related source ($E_{\text{vehicles}} + P_{\text{NO-OH}}$) contributed 25.7 ± 15.8 % to the **daily HONO sources**
664 **in winter** if all NO was assumed to be dominated by local traffic emission, while it was
665 14.5 ± 15.8 % when 40 % of NO was considered as local traffic emission (He et al.,
666 2002). Under this circumstance, the daytime P_{unknown} of HONO in winter increased to
667 0.83 ± 0.36 ppbv h⁻¹, which was corresponding to 58.1 ± 8.6 % of the HONO source. This
668 means these assumptions might underestimate the contribution of the HONO sources.
669 In addition, P_{ground} , P_{aerosol} and P_{nitrate} could be also partially related to traffic emission
670 of NO_x (Lee et al., 2016; Tan et al., 2017). These results mean that the contribution of
671 traffic-related emission might be larger than our estimation in this work. Therefore, our
672 work at least suggests that traffic related emission should be a very important HONO
673 source in winter Beijing although more work is required based on comprehensive
674 modelling studies.

675 **4. Conclusions and atmospheric implications.**

676 In this work, the promotion effect of HONO on aerosol mass formation in polluted
677 events was observed based on the good correlation between the growth of OA and
678 nitrate mass concentration and the consumed HONO from early morning to noon during
679 the polluted days in winter. This promotion effect could be related to OH production

680 from photolysis of HONO on aerosol formation followed by oxidation process of the
681 corresponding precursors. Our observation supports well the recent modelling studies
682 that HONO may significantly promote secondary aerosol mass formation (Zhang et al.,
683 2019a;Zhang et al., 2019c;Xing et al., 2019;An et al., 2013). Based on **budget analysis**
684 calculations, traffic-related sources (direction emission and conversion of NO from
685 vehicle emission) was found to be an important contributor to HONO source during
686 polluted days in winter in Beijing. This means that HONO from the traffic-related
687 sources can have an important role in aerosol mass formation in the atmosphere.

688 Vehicle population in China is increasing very quickly (Liu et al., 2017b;Wang et
689 al., 2011). Thus, the negative influences of the vehicle emission on air quality will
690 increase especially in populous metropolitan areas (Yang et al., 2019;Guo et al., 2020),
691 such as Beijing and Shanghai, if targeted pollution control technologies are not applied.
692 It has been estimated that the vehicles emission accounted for over 40% of total urban
693 NO_x emissions in Beijing (He et al., 2002). In the atmosphere, NO_x involves very
694 complicated reaction network, from which finally leads to aerosol mass formation and
695 production of ozone in VOC limited environment. At the same time, reactions of NO_x
696 also leads to some reactive NO_z species (Seinfeld and Pandis, 2006). In particular,
697 HONO is an important precursor of OH, which governs the conversion of primary
698 pollutants to secondary pollutants in the atmosphere. Besides **indirect production** of
699 HONO from NO, the vehicles also directly emits HONO as discussed in this work.
700 Even if the low limit of emission factor was used to calculating the HONO source from
701 the vehicles, the traffic-related emission can still be an important source of HONO in

702 winter Beijing. Therefore, this work implies that mitigation of HONO and NO_x
703 emission from vehicles might be an effective way to reduce secondary aerosol mass
704 formation and can have a positive effect on severe haze events in wintertime Beijing.

705 It should be pointed out that we only considered O₃ and HONO when discussing
706 the sources of OH. Other sources such as HO₂ (and RO₂) with NO, ozonolysis of
707 alkenes and photolysis of OVOCs might also contribute to OH radicals in the
708 atmosphere (Tan et al., 2018). In the future it will be vital to comprehensively analyze
709 OH sources and to quantify the role of HONO in secondary aerosol mass formation
710 although photolysis of HONO is the major OH source in winter. On the other hand, as
711 discussed in Section 3.3, uncertainties about the HONO budget might originate from
712 the emission factors, OH concentration, and reaction kinetics and so on. **The source of**
713 **HONO from vehicles was calculated based on the emission inventories, which should**
714 **have a significant bias (Squires et al., 2020). For example, the emission flux of NO_x**
715 **calculated using the emission inventory from Yang et al. (2019) is as 2.4±0.5 times as**
716 **the reported emission flux reported by Squires et al. (2020).** To take the next step, it is
717 required to measure the emission factors from vehicle exhaust under real road
718 conditions in the future. When calculating the OH concentration, the factor between
719 OH concentration and $J_{\text{O}1\text{D}}$ might vary over locations and seasons due to different
720 NO_x/VOCs ratio (Holland et al., 2003). Direct measurements of OH concentration
721 would be helpful for decreasing the uncertainty of both OH sources and HONO budget
722 analysis. Finally, it is necessary to quantify the contribution of traffic-related source of
723 HONO on secondary aerosol formation based on modelling studies in the future.

724

725 *Data availability.* The experimental data are available upon request to the
726 corresponding authors.

727

728 *Supplement.* The supplement related to this article is available online at:

729

730 *Competing interests.* The authors declare that they have no conflict of
731 interest.

732

733 **Author information**

734 *Author contributions.* YL, WW and MK designed the experiments. YL wrote the paper
735 and performed HONO budget analysis. YZ, CL, WW, YC, MG and XW carried out
736 HONO measurement. ZF, FZ, JC, WD and KD did aerosol composition measurements.
737 BC and JK did particle size measurements. YW, BH and YW analyzed meteorological
738 data analysis. CY, FB, JK, TP, HH, MG and MK revised the manuscript.

739

740 **Acknowledgements:**

741 This research was financially supported by the National Natural Science Foundation of
742 China (41877306), the Ministry of Science and Technology of the People's Republic of
743 China (2019YFC0214701), Academy of Finland via Center of Excellence in
744 Atmospheric Sciences (272041, 316114, and 315203) and European Research Council
745 vShandong Universityia ATM-GTP 266 (742206), the Strategic Priority Research

746 Program of Chinese Academy of Sciences and Beijing University of Chemical
747 Technology.

748

749 **References:**

750 Aliche, B., Geyer, A., Hofzumahaus, A., Holland, F., Konrad, S., Patz, H. W., Schafer, J., Stutz, J., Volz-
751 Thomas, A., and Platt, U.: OH formation by HONO photolysis during the BERLIOZ experiment, *J.*
752 *Geophys. Res.-Atmos.*, 108, 17, 10.1029/2001jd000579, 2003.

753 An, J., Li, Y., Chen, Y., Li, J., Qu, Y., and Tang, Y.: Enhancements of major aerosol components due to
754 additional HONO sources in the North China Plain and implications for visibility and haze, *Adv. Atmos.*
755 *Sci.*, 30, 57-66, 10.1007/s00376-012-2016-9, 2013.

756 An, Z., Huang, R.-J., Zhang, R., Tie, X., Li, G., Cao, J., Zhou, W., Shi, Z., Han, Y., Gu, Z., and Ji, Y.:
757 Severe haze in northern China: A synergy of anthropogenic emissions and atmospheric processes, *Proc.*
758 *Natl. Acad. Sci. USA*, 116, 8657-8666, 10.1073/pnas.1900125116, 2019.

759 Atkinson, R., and Arey, J.: Atmospheric Degradation of Volatile Organic Compounds, *Chem. Rev.*, 103,
760 4605-4638, doi: 10.1021/cr0206420, 2003.

761 Atkinson, R., Baulch, D. L., Cox, R. A., Crowley, J. N., Hampson, R. F., Hynes, R. G., Jenkin, M. E.,
762 Rossi, M. J., and Troe, J.: Evaluated kinetic and photochemical data for atmospheric chemistry: Volume
763 I - gas phase reactions of Ox, HOx, NOx and SOx species, *Atmos. Chem. Phys.*, 4, 1461-1738,
764 10.5194/acp-4-1461-2004, 2004.

765 Aumont, B., Chervier, F., and Laval, S.: Contribution of HONO sources to the NOx/HOx/O3 chemistry
766 in the polluted boundary layer, *Atmos. Environ.*, 37, 487-498, [https://doi.org/10.1016/S1352-](https://doi.org/10.1016/S1352-2310(02)00920-2)
767 [2310\(02\)00920-2](https://doi.org/10.1016/S1352-2310(02)00920-2), 2003.

768 Bao, F., Li, M., Zhang, Y., Chen, C., and Zhao, J.: Photochemical Aging of Beijing Urban PM2.5: HONO
769 Production, *Environ. Sci. Technol.*, 52, 6309-6316, 10.1021/acs.est.8b00538, 2018.

770 Bianchi, F., Kurtén, T., Riva, M., Mohr, C., Rissanen, M. P., Roldin, P., Berndt, T., Crouse, J. D.,
771 Wennberg, P. O., Mentel, T. F., Wildt, J., Junninen, H., Jokinen, T., Kulmala, M., Worsnop, D. R.,
772 Thornton, J. A., Donahue, N., Kjaergaard, H. G., and Ehn, M.: Highly Oxygenated Organic Molecules
773 (HOM) from Gas-Phase Autoxidation Involving Peroxy Radicals: A Key Contributor to Atmospheric
774 Aerosol, *Chem. Rev.*, 119, 3472-3509, 10.1021/acs.chemrev.8b00395, 2019.

775 Cheng, F., Wang, C., Wang, J., Tang, F., and Xi, X.: Trend analysis of building height and total floor
776 space in Beijing, China using ICESat/GLAS data, *Int. J. Remote Sens.*, 32, 8823-8835, 2011.

777 Cheng, Y., Zheng, G., Wei, C., Mu, Q., Zheng, B., Wang, Z., Gao, M., Zhang, Q., He, K., Carmichael,
778 G., Poschl, U., and Su, H.: Reactive nitrogen chemistry in aerosol water as a source of sulfate during
779 haze events in China, *Sci. Adv.*, 2, 10.1126/sciadv.1601530, 2016.

780 Cho, M.-H., Niles, A., uili Huang, Inglese, J., Austin, C. P., Riss, T., and Xia, M.: A bioluminescent
781 cytotoxicity assay for assessment of membrane integrity using a proteolytic biomarker, *Toxicol. In Vitro.*,
782 22, 1099-1106, 2008.

783 Crowley, J. N., Ammann, M., Cox, R. A., Hynes, R. G., Jenkin, M. E., Mellouki, A., Rossi, M. J., Troe,
784 J., and Wallington, T. J.: Evaluated kinetic and photochemical data for atmospheric chemistry: Volume
785 V – heterogeneous reactions on solid substrates, *Atmos. Chem. Phys.*, 10, 9059-9223, doi: 10.5194/acp-

786 10-9059-2010, 2010.

787 Cui, L., Li, R., Zhang, Y., Meng, Y., Fu, H., and Chen, J.: An observational study of nitrous acid (HONO)
788 in Shanghai, China: The aerosol impact on HONO formation during the haze episodes, *Sci. Total*
789 *Environ.*, 630, 1057-1070, 10.1016/j.scitotenv.2018.02.063, 2018.

790 Czader, B. H., Choi, Y., Li, X., Alvarez, S., and Lefer, B.: Impact of updated traffic emissions on HONO
791 mixing ratios simulated for urban site in Houston, Texas, *Atmos. Chem. Phys.*, 15, 1253-1263,
792 10.5194/acp-15-1253-2015, 2015.

793 Dillon, M. B., Lamanna, M. S., Schade, G. W., Goldstein, A. H., and Cohen, R. C.: Chemical evolution
794 of the Sacramento urban plume: Transport and oxidation, *J. Geophys. Res.- Atmos.*, 107, ACH 3-1-ACH
795 3-15, 10.1029/2001jd000969, 2002.

796 Fu, G. Q., Xu, W. Y., Yang, R. F., Li, J. B., and Zhao, C. S.: The distribution and trends of fog and haze
797 in the North China Plain over the past 30 years, *Atmos. Chem. Phys.*, 14, 11949-11958, 10.5194/acp-14-
798 11949-2014, 2014.

799 Gall, E. T., Griffin, R. J., Steiner, A. L., Dibb, J., Scheuer, E., Gong, L., Rutter, A. P., Cevik, B. K., Kim,
800 S., Lefer, B., and Flynn, J.: Evaluation of nitrous acid sources and sinks in urban outflow, *Atmos.*
801 *Environ.*, 127, 272-282, <https://doi.org/10.1016/j.atmosenv.2015.12.044>, 2016.

802 Gao, W., Tan, G., Hong, Y., Li, M., Nian, H., Guo, C., Huang, Z., Fu, Z., Dong, J., Xu, X., Cheng, P., and
803 Zhou, Z.: Development of portable single photon ionization time-of-flight mass spectrometer combined
804 with membrane inlet, *Int. J. Mass Spectrom.*, 334, 8-12, <https://doi.org/10.1016/j.ijms.2012.09.003>, 2013.

805 Guo, S., Hu, M., Zamora, M. L., Peng, J., Shang, D., Zheng, J., Du, Z., Wu, Z., Shao, M., Zeng, L.,
806 Molina, M. J., and Zhang, R.: Elucidating severe urban haze formation in China, *Proc. Natl. Acad. Sci.*
807 *USA*, 111, 17373-17378, 10.1073/pnas.1419604111, 2014.

808 Guo, S., Hu, M., Peng, J., Wu, Z., Zamora, M. L., Shang, D., Du, Z., Zheng, J., Fang, X., Tang, R., Wu,
809 Y., Zeng, L., Shuai, S., Zhang, W., Wang, Y., Ji, Y., Li, Y., Zhang, A. L., Wang, W., Zhang, F., Zhao, J.,
810 Gong, X., Wang, C., Molina, M. J., and Zhang, R.: Remarkable nucleation and growth of ultrafine
811 particles from vehicular exhaust, *Proc. Natl. Acad. Sci. USA*, 117 3427-3432, 10.1073/pnas.1916366117,
812 2020.

813 Hallquist, M., Wenger, J. C., Baltensperger, U., Rudich, Y., Simpson, D., Claeys, M., Dommen, J.,
814 Donahue, N. M., George, C., Goldstein, A. H., Hamilton, J. F., Herrmann, H., Hoffmann, T., Iinuma, Y.,
815 Jang, M., Jenkin, M. E., Jimenez, J. L., Kiendler-Scharr, A., Maenhaut, W., McFiggans, G., Mentel, T.
816 F., Monod, A., Prévôt, A. S. H., Seinfeld, J. H., Surratt, J. D., Szmigielski, R., and Wildt, J.: The formation,
817 properties and impact of secondary organic aerosol: current and emerging issues, *Atmos. Chem. Phys.*,
818 9, 5155-5236, 10.5194/acp-9-5155-2009, 2009.

819 Han, C., Liu, Y., and He, H.: Role of Organic Carbon in Heterogeneous Reaction of NO₂ with Soot,
820 *Environ. Sci Technol.*, 47, 3174-3181, 10.1021/es304468n, 2013.

821 Han, X., Zhang, M. G., Skorokhod, A., and Kou, X. X.: Modeling dry deposition of reactive nitrogen in
822 China with RAMS-CMAQ, *Atmos. Environ.*, 166, 47-61, 10.1016/j.atmosenv.2017.07.015, 2017.

823 He, H., Wang, Y., Ma, Q., Ma, J., Chu, B., Ji, D., Tang, G., Liu, C., Zhang, H., and Hao, J.: Mineral dust
824 and NO_x promote the conversion of SO₂ to sulfate in heavy pollution days, *Sci. Rep.*, 4,
825 10.1038/srep04172, 2014.

826 He, K., Huo, H., and Zhang, Q.: Urban air pollution in China: current status, characteristics, and progress,
827 *Annu. Rev. Energ. Env.*, 27, 397-431, 2002.

828 He, P. Z., Alexander, B., Geng, L., Chi, X. Y., Fan, S. D., Zhan, H. C., Kang, H., Zheng, G. J., Cheng, Y.
829 F., Su, H., Liu, C., and Xie, Z. Q.: Isotopic constraints on heterogeneous sulfate production in Beijing

830 haze, *Atmos. Chem. Phys.*, 18, 5515-5528, 10.5194/acp-18-5515-2018, 2018.

831 Hendrick, F., Muller, J. F., Clemer, K., Wang, P., De Maziere, M., Fayt, C., Gielen, C., Hermans, C., Ma,
832 J. Z., Pinardi, G., Stavrou, T., Vlemmix, T., and Van Roozendaal, M.: Four years of ground-based
833 MAX-DOAS observations of HONO and NO₂ in the Beijing area, *Atmos. Chem. Phys.*, 14, 765-781,
834 10.5194/acp-14-765-2014, 2014.

835 Holland, F., Hofzumahaus, A., Schafer, R., Kraus, A., and Patz, H. W.: Measurements of OH and HO₂
836 radical concentrations and photolysis frequencies during BERLIOZ, *J. Geophys. Res.-Atmos.*, 108, 22,
837 10.1029/2001jd001393, 2003.

838 Hou, S., Tong, S., Ge, M., and An, J.: Comparison of atmospheric nitrous acid during severe haze and
839 clean periods in Beijing, China, *Atmos. Environ.*, 124, 199-206,
840 <https://doi.org/10.1016/j.atmosenv.2015.06.023>, 2016.

841 Hu, M., Zhou, F., Shao, K., Zhang, Y., Tang, X., and Slanina, J.: Diurnal variations of aerosol chemical
842 compositions and related gaseous pollutants in Beijing and Guangzhou, *J. Environ. Sci. Health, Part A*,
843 37, 479-488, 10.1081/ESE-120003229, 2002.

844 Huang, H., Chen, Y., Clinton, N., Wang, J., Wang, X., Liu, C., Gong, P., Yang, J., Bai, Y., Zheng, Y., and
845 Zhu, Z.: Mapping major land cover dynamics in Beijing using all Landsat images in Google Earth Engine,
846 *Remote Sens. Environ.*, 202, 166-176, <https://doi.org/10.1016/j.rse.2017.02.021>, 2017a.

847 Huang, L., Zhao, Y., Li, H., and Chen, Z.: Kinetics of Heterogeneous Reaction of Sulfur Dioxide on
848 Authentic Mineral Dust: Effects of Relative Humidity and Hydrogen Peroxide, *Environ. Sci. Technol.*,
849 49, 10797-10805, 10.1021/acs.est.5b03930, 2015.

850 Huang, R.-J., Zhang, Y., Bozzetti, C., Ho, K.-F., Cao, J.-J., Han, Y., Daellenbach, K. R., Slowik, J. G.,
851 Platt, S. M., Canonaco, F., Zotter, P., Wolf, R., Pieber, S. M., Brun, E. A., Crippa, M., Ciarelli, G.,
852 Piazzalunga, A., Schwikowski, M., Abbazade, G., Schnelle-Kreis, J., Zimmermann, R., An, Z., Szidat,
853 S., Baltensperger, U., Haddad, I. E., and Prevot, A. S. H.: High secondary aerosol contribution to
854 particulate pollution during haze events in China, *Nature*, 514(7521), 218-222, 10.1038/nature13774,
855 2014.

856 Huang, R.-J., Yang, L., Cao, J., Wang, Q., Tie, X., Ho, K.-F., Shen, Z., Zhang, R., Li, G., Zhu, C., Zhang,
857 N., Dai, W., Zhou, J., Liu, S., Chen, Y., Chen, J., and O'Dowd, C. D.: Concentration and sources of
858 atmospheric nitrous acid (HONO) at an urban site in Western China, *Sci. Total Environ.*, 593, 165-172,
859 10.1016/j.scitotenv.2017.02.166, 2017b.

860 Kanaya, Y., Cao, R., Akimoto, H., Fukuda, M., Komazaki, Y., Yokouchi, Y., Koike, M., Tanimoto, H.,
861 Takegawa, N., and Kondo, a. Y.: Urban photochemistry in central Tokyo: 1. Observed and modeled OH
862 and HO₂ radical concentrations during the winter and summer of 2004, *J. Geophys. Res.- Atmos.*, 112,
863 10.1029/2007JD008670, 2007.

864 Kim, S., VandenBoer, T. C., Young, C. J., Riedel, T. P., Thornton, J. A., Swarthout, B., Sive, B., Lerner,
865 B., Gilman, J. B., Warneke, C., Roberts, J. M., Guenther, A., Wagner, N. L., Dubé, W. P., Williams, E.,
866 and Brown, S. S.: The primary and recycling sources of OH during the NACHTT-2011 campaign: HONO
867 as an important OH primary source in the wintertime, *J. Geophys. Res.- Atmos.*, 119, 6886-6896,
868 doi:10.1002/2013JD019784, 2014.

869 Kroll, J. H., and Seinfeld, J. H.: Chemistry of secondary organic aerosol: Formation and evolution of
870 low-volatility organics in the atmosphere, *Atmos. Environ.*, 42, 3593-3624, 2008.

871 Kulmala, M.: Build a global Earth observatory, *Nature*, 553, 21-23, 10.1038/d41586-017-08967-y, 2018.

872 Lang, J., Zhang, Y., Zhou, Y., Cheng, S., Chen, D., Guo, X., Chen, S., Li, X., Xing, X., and Wang, H.:
873 Trends of PM_{2.5} and Chemical Composition in Beijing, 2000-2015, *Aerosol Air Qual. Res.*, 17, 412-

874 425, 10.4209/aaqr.2016.07.0307, 2017.

875 Lee, J. D., Whalley, L. K., Heard, D. E., Stone, D., Dunmore, R. E., Hamilton, J. F., Young, D. E., Allan,
876 J. D., Laufs, S., and Kleffmann, J.: Detailed budget analysis of HONO in central London reveals a
877 missing daytime source, *Atmos. Chem. Phys.*, 16, 2747-2764, 10.5194/acp-16-2747-2016, 2016.

878 Lelieveld, J., Evans, J. S., Fnais, M., Giannadaki, D., and Pozzer, A.: The contribution of outdoor air
879 pollution sources to premature mortality on a global scale, *Nature*, 525, 367-371, 10.1038/nature15371,
880 2015.

881 Li, D., Xue, L., Wen, L., Wang, X., Chen, T., Mellouki, A., Chen, J., and Wang, W.: Characteristics and
882 sources of nitrous acid in an urban atmosphere of northern China: Results from 1-yr continuous
883 observations, *Atmos. Environ.*, 182, 296-306, <https://doi.org/10.1016/j.atmosenv.2018.03.033>, 2018.

884 Li, X., Brauers, T., H'aseler, R., Bohn, B., Fuchs, H., Hofzumahaus, A., Holland, F., Lou, S., Lu, K. D.,
885 Rohrer, F., Hu, M., Zeng, L. M., Zhang, Y. H., Garland, R. M., Su, H., Nowak, A., Wiedensohler, A.,
886 Takegawa, N., Shao, M., and Wahner, A.: Exploring the atmospheric chemistry of nitrous acid (HONO)
887 at a rural site in Southern China, *Atmos. Chem. Phys.*, 12, 1497-1513, 2012.

888 Li, Z. Q., Guo, J. P., Ding, A. J., Liao, H., Liu, J. J., Sun, Y. L., Wang, T. J., Xue, H. W., Zhang, H. S.,
889 and Zhu, B.: Aerosol and boundary-layer interactions and impact on air quality, *Natl. Sci. Rev.*, 4, 810-
890 833, 10.1093/nsr/nwx117, 2017.

891 Liang, Y., Zha, Q., Wang, W., Cui, L., Lui, K. H., Ho, K. F., Wang, Z., Lee, S.-c., and Wang, T.: Revisiting
892 nitrous acid (HONO) emission from on-road vehicles: A tunnel study with a mixed fleet, *J. Air Waste
893 Manage. Assoc.*, 67, 797-805, 10.1080/10962247.2017.1293573, 2017.

894 Liggio, J., Li, S.-M., Hayden, K., Taha, Y. M., Stroud, C., Darlington, A., Drollette, B. D., Gordon, M.,
895 Lee, P., Liu, P., Leithead, A., Moussa, S. G., Wang, D., O'Brien, J., Mittermeier, R. L., Brook, J. R., Lu,
896 G., Staebler, R. M., Han, Y., Tokarek, T. W., Osthoff, H. D., Makar, P. A., Zhang, J., L. Plata, D., and
897 Gentner, D. R.: Oil sands operations as a large source of secondary organic aerosols, *Nature*, 534, 91-94,
898 10.1038/nature17646, 2016.

899 Liu, C., Ma, Z., Mu, Y., Liu, J., Zhang, C., Zhang, Y., Liu, P., and Zhang, H.: The levels, variation
900 characteristics, and sources of atmospheric non-methane hydrocarbon compounds during wintertime in
901 Beijing, China, *Atmos. Chem. Phys.*, 17, 10633-10649, 10.5194/acp-17-10633-2017, 2017a.

902 Liu, F., Beirle, S., Zhang, Q., van der A, R. J., Zheng, B., Tong, D., and He, K.: NO_x emission trends
903 over Chinese cities estimated from OMI observations during 2005 to 2015, *Atmos. Chem. Phys.*, 17,
904 9261-9275, 10.5194/acp-17-9261-2017, 2017b.

905 Liu, J., Li, S., Mekic, M., Jiang, H., Zhou, W., Loisel, G., Song, W., Wang, X., and Gligorovski, S.:
906 Photoenhanced Uptake of NO₂ and HONO Formation on Real Urban Grime, *Environ. Sci. Technol. Lett.*,
907 6, 413-417, 10.1021/acs.estlett.9b00308, 2019a.

908 Liu, T., Gong, S., He, J., Yu, M., Wang, Q., Li, H., Liu, W., Zhang, J., Li, L., Wang, X., Li, S., Lu, Y., Du,
909 H., Wang, Y., Zhou, C., Liu, H., and Zhao, Q.: Attributions of meteorological and emission factors to the
910 2015 winter severe haze pollution episodes in China's Jing-Jin-Ji area, *Atmos. Chem. Phys.*, 17, 2971-
911 2980, 10.5194/acp-17-2971-2017, 2017c.

912 Liu, Y., Han, C., Ma, J., Bao, X., and He, H.: Influence of relative humidity on heterogeneous kinetics of
913 NO₂ on kaolin and hematite, *Phys. Chem. Chem. Phys.*, 17, 19424-19431, doi: 10.1039/C5CP02223A,
914 2015.

915 Liu, Y., Lu, K., Ma, Y., Yang, X., Zhang, W., Wu, Y., Peng, J., Shuai, S., Hu, M., and Zhang, Y.: Direct
916 emission of nitrous acid (HONO) from gasoline cars in China determined by vehicle chassis
917 dynamometer experiments, *Atmos. Environ.*, 169, 89-96, 10.1016/j.atmosenv.2017.07.019, 2017d.

918 Liu, Y., Nie, W., Xu, Z., Wang, T., Wang, R., Li, Y., Wang, L., Chi, X., and Ding, A.: Contributions of
919 different sources to nitrous acid (HONO) at the SORPES station in eastern China: results from one-year
920 continuous observation, *Atmos. Chem. Phys. Discuss.*, 2019, 1-47, 10.5194/acp-2019-219, 2019b.

921 Liu, Y. H., Lu, K. D., Li, X., Dong, H. B., Tan, Z. F., Wang, H. C., Zou, Q., Wu, Y. S., Zeng, L. M., Hu,
922 M., Min, K. E., Kecorius, S., Wiedensohler, A., and Zhang, Y. H.: A Comprehensive Model Test of the
923 HONO Sources Constrained to Field Measurements at Rural North China Plain, *Environ. Sci. Technol.*,
924 53, 3517-3525, 10.1021/acs.est.8b06367, 2019c.

925 Meng, F., Qin, M., Tang, K., Duan, J., Fang, W., Liang, S., Ye, K., Xie, P., Sun, Y., Xie, C., Ye, C., Fu,
926 P., Liu, J., and Liu, W.: High resolution vertical distribution and sources of HONO and NO₂ in the
927 nocturnal boundary layer in urban Beijing, China, *Atmos. Chem. Phys. Discuss.*, 2019, 1-34,
928 10.5194/acp-2019-613, 2019.

929 Meusel, H., Tamm, A., Kuhn, U., Wu, D., Leifke, A. L., Fiedler, S., Ruckteschler, N., Yordanova, P.,
930 Lang-Yona, N., Poehlker, M., Lelieveld, J., Hoffmann, T., Poeschl, U., Su, H., Weber, B., and Cheng, Y.:
931 Emission of nitrous acid from soil and biological soil crusts represents an important source of HONO in
932 the remote atmosphere in Cyprus, *Atmos. Chem. Phys.*, 18, 799-813, 10.5194/acp-18-799-2018, 2018.

933 Michoud, V., Colomb, A., Borbon, A., Miet, K., Beekmann, M., Camredon, M., Aumont, B., Perrier, S.,
934 Zapf, P., Siour, G., Ait-Helal, W., Afif, C., Kukui, A., Furger, M., Dupont, J. C., Haeffelin, M., and
935 Doussin, J. F.: Study of the unknown HONO daytime source at a European suburban site during the
936 MEGAPOLI summer and winter field campaigns, *Atmos. Chem. Phys.*, 14, 2805-2822, 10.5194/acp-14-
937 2805-2014, 2014.

938 Ndour, M., D'Anna, B., George, C., Ka, O., Balkanski, Y., K., J., S., and K., A., M.: Photoenhanced
939 uptake of NO₂ on mineral dust: Laboratory experiments and model simulations, *Geophys. Res. Lett.*, 35,
940 L05812. doi:05810.01029/02007GL032006, 2008.

941 Ndour, M., Nicolas, M., D'Anna, B., Ka, O., and George, C.: Photoreactivity of NO₂ on mineral dusts
942 originating from different locations of the Sahara desert, *Phys. Chem. Chem. Phys.*, 11, 1312-1319, 2009.

943 Oswald, R., Behrendt, T., Ermel, M., Wu, D., Su, H., Cheng, Y., Breuninger, C., Moravek, A., Mougín,
944 E., Delon, C., Loubet, B., Pommerening-Röser, A., Sörgel, M., Pöschl, U., Hoffmann, T., Andreae, M.
945 O., Meixner, F. X., and Trebs, I.: HONO Emissions from Soil Bacteria as a Major Source of Atmospheric
946 Reactive Nitrogen, *Science*, 341, 1233-1235, 10.1126/science.1242266, 2013.

947 Oswald, R., Ermel, M., Hens, K., Novelli, A., Ouwersloot, H. G., Paasonen, P., Petäjä, T., Sipilä, M.,
948 Keronen, P., Bäck, J., Königstedt, R., Hosaynali Beygi, Z., Fischer, H., Bohn, B., Kubistin, D., Harder,
949 H., Martinez, M., Williams, J., Hoffmann, T., Trebs, I., and Sörgel, M.: A comparison of HONO budgets
950 for two measurement heights at a field station within the boreal forest in Finland, *Atmos. Chem. Phys.*,
951 15, 799-813, 10.5194/acp-15-799-2015, 2015.

952 Qin, M., Xie, P., Su, H., Gu, J., Peng, F., Li, S., Zeng, L., Liu, J., Liu, W., and Zhang, Y.: An observational
953 study of the HONO-NO₂ coupling at an urban site in Guangzhou City, South China, *Atmos. Environ.*,
954 43, 5731-5742, 10.1016/j.atmosenv.2009.08.017, 2009.

955 Ren, X., Brune, W. H., Mao, J., Mitchell, M. J., Leshner, R. L., Simpas, J. B., Metcalf, A. R., Schwab, J.
956 J., Cai, C., Li, Y., Demerjian, K. L., Felton, H. D., Boynton, G., Adams, A., Perry, J., He, Y., Zhou, X.,
957 and Hou, J.: Behavior of OH and HO₂ in the winter atmosphere in New York City, *Atmos. Environ.*, 40,
958 252-263, <https://doi.org/10.1016/j.atmosenv.2005.11.073>, 2006.

959 Rohrer, F., Bohn, B., Brauers, T., Bruning, D., Johnen, F. J., Wahner, A., and Kleffmann, J.:
960 Characterisation of the photolytic HONO-source in the atmosphere simulation chamber SAPHIR, *Atmos.*
961 *Chem. Phys.*, 5, 2189-2201, 10.5194/acp-5-2189-2005, 2005.

962 Sangwan, M., and Zhu, L.: Role of Methyl-2-nitrophenol Photolysis as a Potential Source of OH Radicals
963 in the Polluted Atmosphere: Implications from Laboratory Investigation, *J. Phys. Chem. A*, 122, 1861-
964 1872, 10.1021/acs.jpca.7b11235, 2018.

965 Seinfeld, J. H., and Pandis, S. N.: Atmospheric chemistry and physics: From air pollution to climate
966 change, Second ed., John Wiley and Sons, New Jersey, 2006.

967 Soergel, M., Regelin, E., Bozem, H., Diesch, J. M., Drewnick, F., Fischer, H., Harder, H., Held, A.,
968 Hosaynali-Beygi, Z., Martinez, M., and Zetzsch, C.: Quantification of the unknown HONO daytime
969 source and its relation to NO₂, *Atmos. Chem. Phys.*, 11, 10433-10447, 10.5194/acp-11-10433-2011,
970 2011.

971 Spataro, F., Ianniello, A., Esposito, G., Allegrini, I., Zhu, T., and Hu, M.: Occurrence of atmospheric
972 nitrous acid in the urban area of Beijing (China), *Sci. Total Environ.*, 447, 210-224,
973 <https://doi.org/10.1016/j.scitotenv.2012.12.065>, 2013.

974 Spataro, F., and Ianniello, A.: Sources of atmospheric nitrous acid: State of the science, current research
975 needs, and future prospects, *J. Air Waste Manage. Assoc.*, 64, 1232-1250,
976 10.1080/10962247.2014.952846, 2014.

977 Squires, F. A., Nemitz, E., Langford, B., Wild, O., Drysdale, W. S., Acton, W. J. F., Fu, P., Grimmond, C.
978 S. B., Hamilton, J. F., Hewitt, C. N., Hollaway, M., Kotthaus, S., Lee, J., Metzger, S., Pingingtha-Durden,
979 N., Shaw, M., Vaughan, A. R., Wang, X., Wu, R., Zhang, Q., and Zhang, Y.: Measurements of traffic
980 dominated pollutant emissions in a Chinese megacity, *Atmos. Chem. Phys. Discuss.*, 2020, 1-33,
981 10.5194/acp-2019-1105, 2020.

982 Stutz, J., Wong, K. W., and Tsai, C.: Field Observations of Daytime HONO Chemistry and Its Impact on
983 the OH Radical Budget, in: *Disposal of Dangerous Chemicals in Urban Areas and Mega Cities*,
984 Dordrecht, 2013, 1-14.

985 Su, H., Cheng, Y. F., Cheng, P., Zhang, Y. H., Dong, S., Zeng, L. M., Wang, X., Slanina, J., Shao, M.,
986 and Wiedensohler, A.: Observation of nighttime nitrous acid (HONO) formation at a non-urban site
987 during PRIDE-PRD2004 in China, *Atmos. Environ.*, 42, 6219-6232, 10.1016/j.atmosenv.2008.04.006,
988 2008a.

989 Su, H., Cheng, Y. F., Shao, M., Gao, D. F., Yu, Z. Y., Zeng, L. M., Slanina, J., Zhang, Y. H., and
990 Wiedensohler, A.: Nitrous acid (HONO) and its daytime sources at a rural site during the 2004 PRIDE-
991 PRD experiment in China, *J. Geophys. Res.-Atmos.*, 113, 10.1029/2007jd009060, 2008b.

992 Su, P. H., Kuo, D. T. F., Shih, Y. H., and Chen, C. Y.: Sorption of organic compounds to two diesel soot
993 black carbons in water evaluated by liquid chromatography and polyparameter linear solvation energy
994 relationship, *Water Res.*, 144, 709-718, 10.1016/j.watres.2018.07.064, 2018.

995 Sun, P., Nie, W., Chi, X., Xie, Y., Huang, X., Xu, Z., Qi, X., Xu, Z., Wang, L., Wang, T., Zhang, Q., and
996 Ding, A.: Two years of online measurement of fine particulate nitrate in the western Yangtze River Delta:
997 influences of thermodynamics and N₂O₅ hydrolysis, *Atmos. Chem. Phys.*, 18, 17177-17190,
998 10.5194/acp-18-17177-2018, 2018.

999 Sun, Y. L., Wang, Z. F., Fu, P. Q., Yang, T., Jiang, Q., Dong, H. B., Li, J., and Jia, J. J.: Aerosol
1000 composition, sources and processes during wintertime in Beijing, China, *Atmos. Chem. Phys.*, 13, 4577-
1001 4592, 10.5194/acp-13-4577-2013, 2013.

1002 Sun, Y. L., Wang, Z. F., Du, W., Zhang, Q., Wang, Q. Q., Fu, P. Q., Pan, X. L., Li, J., Jayne, J., and
1003 Worsnop, D. R.: Long-term real-time measurements of aerosol particle composition in Beijing, China:
1004 seasonal variations, meteorological effects, and source analysis, *Atmos. Chem. Phys.*, 15, 10149-10165,
1005 10.5194/acp-15-10149-2015, 2015.

1006 Tan, Z., Fuchs, H., Lu, K., Hofzumahaus, A., Bohn, B., Broch, S., Dong, H., Gomm, S., Häsel, R., He,
1007 L., Holland, F., Li, X., Liu, Y., Lu, S., Rohrer, F., Shao, M., Wang, B., Wang, M., Wu, Y., Zeng, L., Zhang,
1008 Y., Wahner, A., and Zhang, Y.: Radical chemistry at a rural site (Wangdu) in the North China Plain:
1009 observation and model calculations of OH, HO₂ and RO₂ radicals, *Atmos. Chem. Phys.*, 17, 663-690,
1010 10.5194/acp-17-663-2017, 2017.

1011 Tan, Z., Rohrer, F., Lu, K., Ma, X., Bohn, B., Broch, S., Dong, H., Fuchs, H., Gkatzelis, G. I.,
1012 Hofzumahaus, A., Holland, F., Li, X., Liu, Y., Liu, Y., Novelli, A., Shao, M., Wang, H., Wu, Y., Zeng, L.,
1013 Hu, M., Kiendler-Scharr, A., Wahner, A., and Zhang, Y.: Wintertime photochemistry in Beijing:
1014 observations of RO_x radical concentrations in the North China Plain during the BEST-ONE campaign,
1015 *Atmos. Chem. Phys.*, 18, 12391-12411, 10.5194/acp-18-12391-2018, 2018.

1016 Tan, Z. F., Lu, K. D., Jiang, M. Q., Su, R., Wang, H. L., Lou, S. R., Fu, Q. Y., Zhai, C. Z., Tan, Q. W.,
1017 Yue, D. L., Chen, D. H., Wang, Z. S., Xie, S. D., Zeng, L. M., and Zhang, Y. H.: Daytime atmospheric
1018 oxidation capacity in four Chinese megacities during the photochemically polluted season: a case study
1019 based on box model simulation, *Atmos. Chem. Phys.*, 19, 3493-3513, 10.5194/acp-19-3493-2019, 2019.

1020 Tang, Y., An, J., Wang, F., Li, Y., Qu, Y., Chen, Y., and Lin, J.: Impacts of an unknown daytime HONO
1021 source on the mixing ratio and budget of HONO, and hydroxyl, hydroperoxyl, and organic peroxy
1022 radicals, in the coastal regions of China, *Atmos. Chem. Phys.*, 15, 9381-9398, 10.5194/acp-15-9381-
1023 2015, 2015.

1024 Tian, M., Liu, Y., Yang, F. M., Zhang, L. M., Peng, C., Chen, Y., Shi, G. M., Wang, H. B., Luo, B., Jiang,
1025 C. T., Li, B., Takeda, N., and Koizumi, K.: Increasing importance of nitrate formation for heavy aerosol
1026 pollution in two megacities in Sichuan Basin, southwest China, *Environ. Pollut.*, 250, 898-905,
1027 10.1016/j.envpol.2019.04.098, 2019.

1028 Tong, S., Hou, S., Zhang, Y., Chu, B., Liu, Y., He, H., Zhao, P., and Ge, M.: Exploring the nitrous acid
1029 (HONO) formation mechanism in winter Beijing: direct emissions and heterogeneous production in
1030 urban and suburban areas, *Faraday Discuss.*, 189, 213-230, 10.1039/c5fd00163c, 2016.

1031 Trinh, H. T., Imanishi, K., Morikawa, T., Hagino, H., and Takenaka, N.: Gaseous nitrous acid (HONO)
1032 and nitrogen oxides (NO_x) emission from gasoline and diesel vehicles under real-world driving test
1033 cycles, *J. Air Waste Manage. Assoc.*, 67, 412-420, 10.1080/10962247.2016.1240726, 2017.

1034 Underwood, G. M., Miller, T. M., and Grassian, V. H.: Transmission FT-IR and Knudsen Cell Study of
1035 the Heterogeneous Reactivity of Gaseous Nitrogen Dioxide on Mineral Oxide Particles, *J. Phys. Chem.*
1036 *A*, 103 6184-6190, 1999.

1037 Underwood, G. M., Song, C. H., Phadnis, M., Carmichael, G. R., and Grassian, V. H.: Heterogeneous
1038 reactions of NO₂ and HNO₃ on oxides and mineral dust: A combined laboratory and modeling study, *J.*
1039 *Geophys. Res.- Atmos.*, 106, 18055-18066, 10.1029/2000jd900552, 2001.

1040 Volkamer, R., Sheehy, P., Molina, L. T., and Molina, M. J.: Oxidative capacity of the Mexico City
1041 atmosphere – Part I: A radical source perspective, *Atmos. Chem. Phys.*, 10, 6969-6991, 10.5194/acp-10-
1042 6969-2010, 2010.

1043 Vu, T. V., Shi, Z., Cheng, J., Zhang, Q., He, K., Wang, S., and Harrison, R. M.: Assessing the impact of
1044 Clean Air Action Plan on Air Quality Trends in Beijing Megacity using a machine learning technique,
1045 *Atmos. Chem. Phys. Discuss.*, 2019, 1-18, 10.5194/acp-2019-173, 2019.

1046 Wang, G., Zhang, R., Gomez, M. E., Yang, L., Zamora, M. L., Hu, M., Lin, Y., Peng, J., Guoc, S., Meng,
1047 J., Li, J., Cheng, C., Hu, T., Ren, Y., Wang, Y., Gao, J., Cao, J., An, Z., Zhou, W., Li, G., Wang, J., Tian,
1048 P., Marrero-Ortiz, W., Secrest, J., Du, Z., Zheng, J., Shang, D., Zeng, L., Shao, M., Wang, W., Huang, Y.,
1049 Wang, Y., Zhu, Y., Li, Y., Hu, J., Pan, B., Cai, L., Cheng, Y., Ji, Y., Zhang, F., Rosenfeld, D., Liss, P. S.,

1050 Duce, R. A., Kolb, C. E., and Molina, M. J.: Persistent sulfate formation from London Fog to Chinese
1051 haze, *Proc. Natl. Acad. Sci. USA*, 113, 13630-13635, 2016.

1052 Wang, H., Lu, K., Chen, X., Zhu, Q., Chen, Q., Guo, S., Jiang, M., Li, X., Shang, D., Tan, Z., Wu, Y.,
1053 Wu, Z., Zou, Q., Zheng, Y., Zeng, L., Zhu, T., Hu, M., and Zhang, Y.: High N₂O₅ Concentrations
1054 Observed in Urban Beijing: Implications of a Large Nitrate Formation Pathway, *Environ. Sci. Technol.*
1055 *Lett.*, 4, 416-420, 10.1021/acs.estlett.7b00341, 2017a.

1056 Wang, H. C., Lu, K. D., Chen, X. R., Zhu, Q. D., Wu, Z. J., Wu, Y. S., and Sun, K.: Fast particulate nitrate
1057 formation via N₂O₅ uptake aloft in winter in Beijing, *Atmos. Chem. Phys.*, 18, 10483-10495,
1058 10.5194/acp-18-10483-2018, 2018.

1059 Wang, J., Zhang, X., Guo, J., Wang, Z., and Zhang, M.: Observation of nitrous acid (HONO) in Beijing,
1060 China: Seasonal variation, nocturnal formation and daytime budget, *Sci. Total Environ.*, 587, 350-359,
1061 10.1016/j.scitotenv.2017.02.159, 2017b.

1062 Wang, S., Zhou, R., Zhao, H., Wang, Z., Chen, L., and Zhou, B.: Long-term observation of atmospheric
1063 nitrous acid (HONO) and its implication to local NO₂ levels in Shanghai, China, *Atmos. Environ.*, 77,
1064 718-724, 10.1016/j.atmosenv.2013.05.071, 2013.

1065 Wang, S., Nan, J., Shi, C., Fu, Q., Gao, S., Wang, D., Cui, H., Saiz-Lopez, A., and Zhou, B.: Atmospheric
1066 ammonia and its impacts on regional air quality over the megacity of Shanghai, China, *Sci. Rep.*, 5,
1067 15842-15842, 10.1038/srep15842, 2015.

1068 Wang, Y. L., Song, W., Yang, W., Sun, X. C., Tong, Y. D., Wang, X. M., Liu, C. Q., Bai, Z. P., and Liu,
1069 X. Y.: Influences of Atmospheric Pollution on the Contributions of Major Oxidation Pathways to PM_{2.5}
1070 Nitrate Formation in Beijing, *J. Geophys. Res.-Atmos.*, 124, 4174-4185, 10.1029/2019jd030284, 2019.

1071 Wang, Y. S., Teter, J., and Sperling, D.: China's soaring vehicle population: Even greater than forecasted?,
1072 *Energy Policy*, 39, 3296-3306, 10.1016/j.enpol.2011.03.020, 2011.

1073 Wang, Z., Wang, W., Tham, Y. J., Li, Q., Wang, H., Wen, L., Wang, X., and Wang, T.: Fast heterogeneous
1074 N₂O₅ uptake and ClNO₂ production in power plant and industrial plumes observed in the nocturnal
1075 residual layer over the North China Plain, *Atmos. Chem. Phys.*, 17, 12361-12378, 10.5194/acp-17-
1076 12361-2017, 2017c.

1077 Wen, L., Xue, L., Wang, X., Xu, C., Chen, T., Yang, L., Wang, T., Zhang, Q., and Wang, W.: Summertime
1078 fine particulate nitrate pollution in the North China Plain: increasing trends, formation mechanisms and
1079 implications for control policy, *Atmos. Chem. Phys.*, 18, 11261-11275, 10.5194/acp-18-11261-2018,
1080 2018.

1081 Xing, L., Wu, J., Elser, M., Tong, S., Liu, S., Li, X., Liu, L., Cao, J., Zhou, J., El-Haddad, I., Huang, R.,
1082 Ge, M., Tie, X., Prévôt, A. S. H., and Li, G.: Wintertime secondary organic aerosol formation in Beijing–
1083 Tianjin–Hebei (BTH): contributions of HONO sources and heterogeneous reactions, *Atmos. Chem.*
1084 *Phys.*, 19, 2343-2359, 10.5194/acp-19-2343-2019, 2019.

1085 Xu, Z., Wang, T., Wu, J., Xue, L., Chan, J., Zha, Q., Zhou, S., Louie, P. K. K., and Luk, C. W. Y.: Nitrous
1086 acid (HONO) in a polluted subtropical atmosphere: Seasonal variability, direct vehicle emissions and
1087 heterogeneous production at ground surface, *Atmos. Environ.*, 106, 100-109,
1088 10.1016/j.atmosenv.2015.01.061, 2015.

1089 Yadav, A. K., Raman, S., and Niyogi, D. D. S.: A note on the estimation of eddy diffusivity and
1090 dissipation length in low winds over a tropical urban terrain, *Pure and Applied Geophysics*, 160, 395-
1091 404, 10.1007/s00024-003-8785-4, 2003.

1092 Yang, D., Zhang, S., Niu, T., Wang, Y., Xu, H., Zhang, K. M., and Wu, Y.: High-resolution mapping of
1093 vehicle emissions of atmospheric pollutants based on large-scale, real-world traffic datasets, *Atmos.*

1094 Chem. Phys., 2019, 8831–8843, 10.5194/acp-2019-32, 2019.

1095 Yang, Q., Su, H., Li, X., Cheng, Y., Lu, K., Cheng, P., Gu, J., Guo, S., Hu, M., Zeng, L., Zhu, T., and
1096 Zhang, Y.: Daytime HONO formation in the suburban area of the megacity Beijing, China, *Sci. China-*
1097 *Chem.*, 57, 1032-1042, 10.1007/s11426-013-5044-0, 2014.

1098 Zhang, F., Wang, Y., Peng, J., Chen, L., Sun, Y., Duan, L., Ge, X., Li, Y., Zhao, J., Liu, C., Zhang, X.,
1099 Zhang, G., Pan, Y., Wang, Y., Zhang, A. L., Ji, Y., Wang, G., Hu, M., Molina, M. J., and Zhang, R.: An
1100 unexpected catalyst dominates formation and radiative forcing of regional haze, *Proc. Natl. Acad. Sci.*
1101 *USA*, 117, 10.1073/pnas.1919343117, 2020.

1102 Zhang, J., An, J., Qu, Y., Liu, X., and Chen, Y.: Impacts of potential HONO sources on the concentrations
1103 of oxidants and secondary organic aerosols in the Beijing-Tianjin-Hebei region of China, *Sci. Total*
1104 *Environ.*, 647, 836-852, <https://doi.org/10.1016/j.scitotenv.2018.08.030>, 2019a.

1105 Zhang, J., Chen, J., Xue, C., Chen, H., Zhang, Q., Liu, X., Mu, Y., Guo, Y., Wang, D., Chen, Y., Li, J.,
1106 Qu, Y., and An, J.: Impacts of six potential HONO sources on HOx budgets and SOA formation during
1107 a wintertime heavy haze period in the North China Plain, *Sci. Total Environ.*, 681, 110-123,
1108 <https://doi.org/10.1016/j.scitotenv.2019.05.100>, 2019b.

1109 Zhang, J. M., Yang, L. X., Chen, J. M., Mellouki, A., Jiang, P., Gao, Y., Li, Y. Y., Yang, Y. M., and Wang,
1110 W. X.: Influence of fireworks displays on the chemical characteristics of PM_{2.5} in rural and suburban
1111 areas in Central and East China, *Sci. Total Environ.*, 578, 476-484, 10.1016/j.scitotenv.2016.10.212,
1112 2017.

1113 Zhang, J. W., Chen, J. M., Xue, C. Y., Chen, H., Zhang, Q., Liu, X. G., Mu, Y. J., Guo, Y. T., Wang, D.
1114 Y., Chen, Y., Li, J. L., Qu, Y., and An, J. L.: Impacts of six potential HONO sources on HOx budgets and
1115 SOA formation during a wintertime heavy haze period in the North China Plain, *Sci. Total Environ.*, 681,
1116 110-123, 10.1016/j.scitotenv.2019.05.100, 2019c.

1117 Zhang, L., Wang, T., Zhang, Q., Zheng, J., Xu, Z., and Lv, M.: Potential sources of nitrous acid (HONO)
1118 and their impacts on ozone: A WRF-Chem study in a polluted subtropical region, *J. Geophys. Res.-*
1119 *Atmos.*, 121, 3645-3662, 10.1002/2015jd024468, 2016.

1120 Zhang, W., Tong, S., Ge, M., An, J., Shi, Z., Hou, S., Xia, K., Qu, Y., Zhang, H., Chu, B., Sun, Y., and
1121 He, H.: Variations and sources of nitrous acid (HONO) during a severe pollution episode in Beijing in
1122 winter 2016, *Sci. Total Environ.*, 648, 253-262, 10.1016/j.scitotenv.2018.08.133, 2019d.

1123 Zhang, X. Y., Zhong, J. T., Wang, J. Z., Wang, Y. Q., and Liu, Y. J.: The interdecadal worsening of
1124 weather conditions affecting aerosol pollution in the Beijing area in relation to climate warming, *Atmos.*
1125 *Chem. Phys.*, 18, 5991-5999, 10.5194/acp-18-5991-2018, 2018.

1126 Zheng, B., Zhang, Q., Zhang, Y., He, K. B., Wang, K., Zheng, G. J., Duan, F. K., Ma, Y. L., and Kimoto,
1127 T.: Heterogeneous chemistry: a mechanism missing in current models to explain secondary inorganic
1128 aerosol formation during the January 2013 haze episode in North China, *Atmos. Chem. Phys.*, 15, 2031-
1129 2049, doi: 10.5194/acp-15-2031-2015, 2015a.

1130 Zheng, G. J., Duan, F. K., Su, H., Ma, Y. L., Cheng, Y., Zheng, B., Zhang, Q., Huang, T., Kimoto, T.,
1131 Chang, D., Pöschl, U., Cheng, Y. F., and He, K. B.: Exploring the severe winter haze in Beijing: the
1132 impact of synoptic weather, regional transport and heterogeneous reactions, *Atmos. Chem. Phys.*, 15,
1133 2969-2983, 10.5194/acp-15-2969-2015, 2015b.

1134 Zhu, W. H., Xu, X. D., Zheng, J., Yan, P., Wang, Y. J., and Cai, W. Y.: The characteristics of abnormal
1135 wintertime pollution events in the Jing-Jin-Ji region and its relationships with meteorological factors, *Sci.*
1136 *Total Environ.*, 626, 887-898, 10.1016/j.scitotenv.2018.01.083, 2018.

1137 Zou, Y., Deng, X. J., Deng, T., Yin, C. Q., and Li, F.: One-Year Characterization and Reactivity of

1138 Isoprene and Its Impact on Surface Ozone Formation at A Suburban Site in Guangzhou, China,
1139 Atmosphere, 10, 10.3390/atmos10040201, 2019.
1140
1141

1142 **Figure captions**

1143 Fig. 1. An overviewed measurement of non-refractory-PM_{2.5} (NR-PM_{2.5}), HONO, NO_x,
1144 PM_{2.5} and meteorological parameters from Feb. 1 to July 1, 2018. (A) the mass
1145 concentration of different components of PM_{2.5}, (B) the mass fraction of individual
1146 component, (C) HONO and NO_x concentration, (D) temperature and RH, (E) wind
1147 speed and wind direction, (F) UVB and PBL height and (G) visibility and PM_{2.5}
1148 concentration during observation. We consider the period before Apr. 1 as winter.
1149 During the winter period, 12 cases are selected and numbered, including three clean
1150 cases (1, 3, and 5, marked in yellow) and the rest 9 pollution episodes (marked in blue).

1151 **Fig. 2.** Contribution of HONO to OH production and correlation between OA and
1152 HONO concentration. Diurnal production rates of OH from photolysis of HONO and
1153 O₃ on polluted days with PM_{2.5} concentration larger than 50 μg m⁻³ and RH less than
1154 90 % (A) from Feb 1 to Mar 31, (B) from Apr 1 to Jun 30; (C) Daytime variation of
1155 OA/CO and HONO/CO concentration for the 7th and 12th episodes and (D) correlation
1156 of the daytime OA/CO increased and consumed HONO/CO.

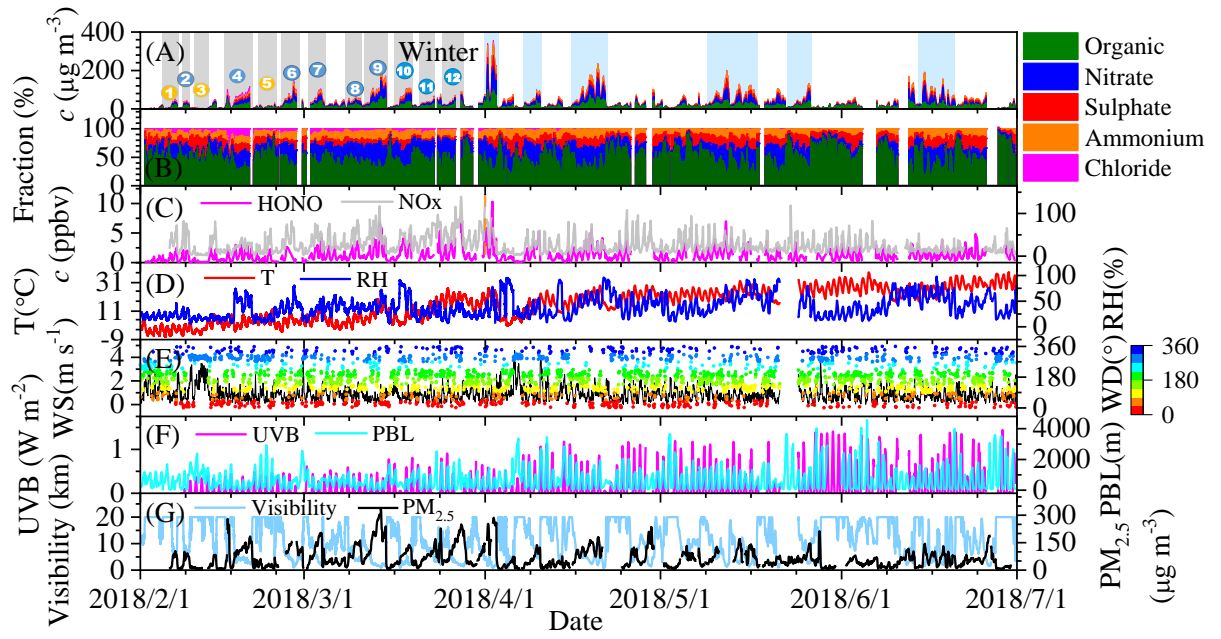
1157 **Fig. 3.** Diurnal pattern of HONO sources calculated with different parameterizations.
1158 The low bound, the middle value, and upper bound of (A) soil emission calculated
1159 based on 45-55%, 35-45% and 25-35% of water content, (B) vehicle emission with
1160 relative emission factor to NO_x of 0.18%, 1.17±0.05% and 1.8 %, (C) production from
1161 reaction between NO and OH, whose concentration estimated using Xu (Xu et al.,
1162 2015), (Tan et al., 2019)

1163 **Fig. 4.** The budget of HONO (A) and (B) Diurnal production rates of HONO, (C) and

1164 (D) loss rates of HONO, (E) and (F) relative contribution of each source on polluted
1165 days with $\text{PM}_{2.5}$ concentrations higher than $50 \mu\text{g m}^{-3}$ and RH less than 90 %. The left
1166 column shows the data from February 1 to March 31) and the right one shows the data
1167 from April 1 to June 30.

1168 **Fig. 5.** (A)-(B) Diurnal production rates and (C)-(D) diurnal loss rates of HONO; (E)-
1169 (F) relative contribution of HONO sources on polluted days with $\text{PM}_{2.5}$ concentrations
1170 higher than $50 \mu\text{g m}^{-3}$ and RH less than 90 %. The E_{vehicle} is calculated using the low
1171 limit of HONO/NO_x from vehicles (0.18%) (Liu et al., 2017d) and the $P_{\text{NO-OH}}$ is
1172 calculated using the low limit of OH concentration, while the upper limit of E_{soil} , P_{aerosol}
1173 and P_{ground} are used as described in the text.

1174 **Figures**

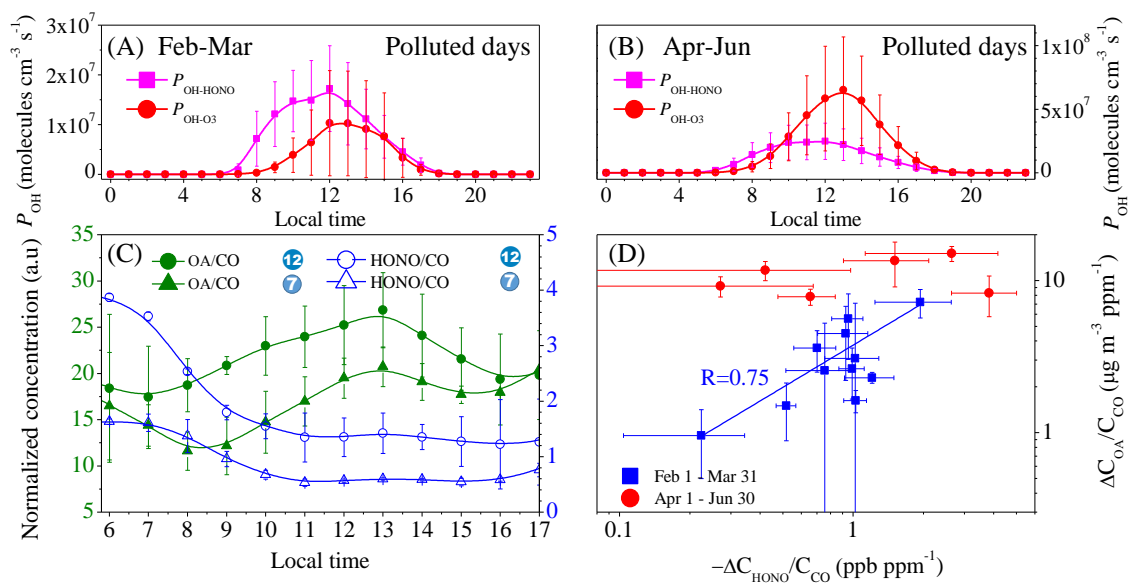


1175

1176

1177

Fig. 1.

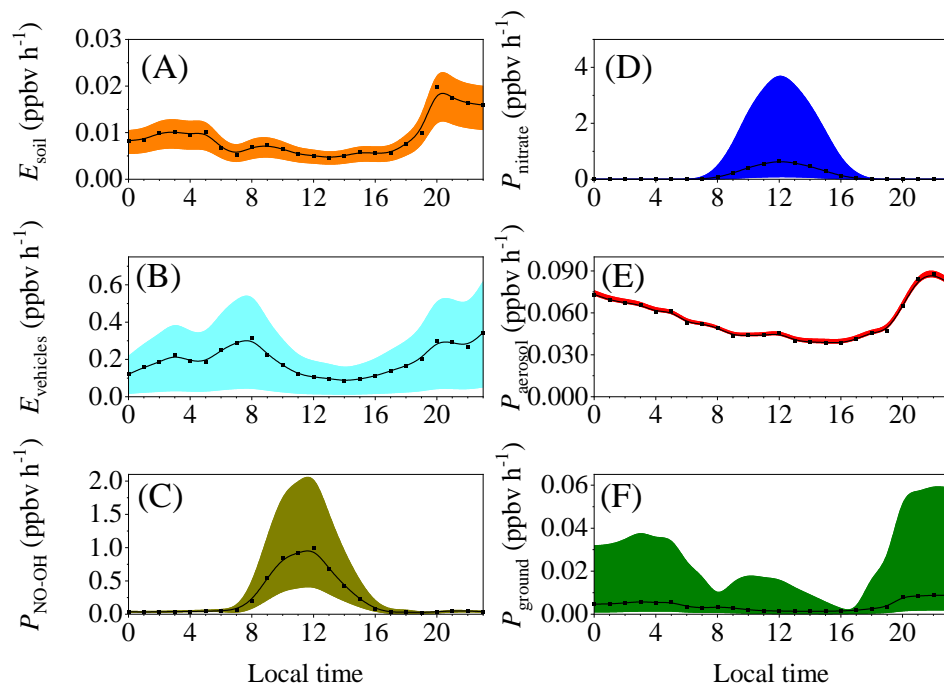


1178

1179

1180

Fig. 2.

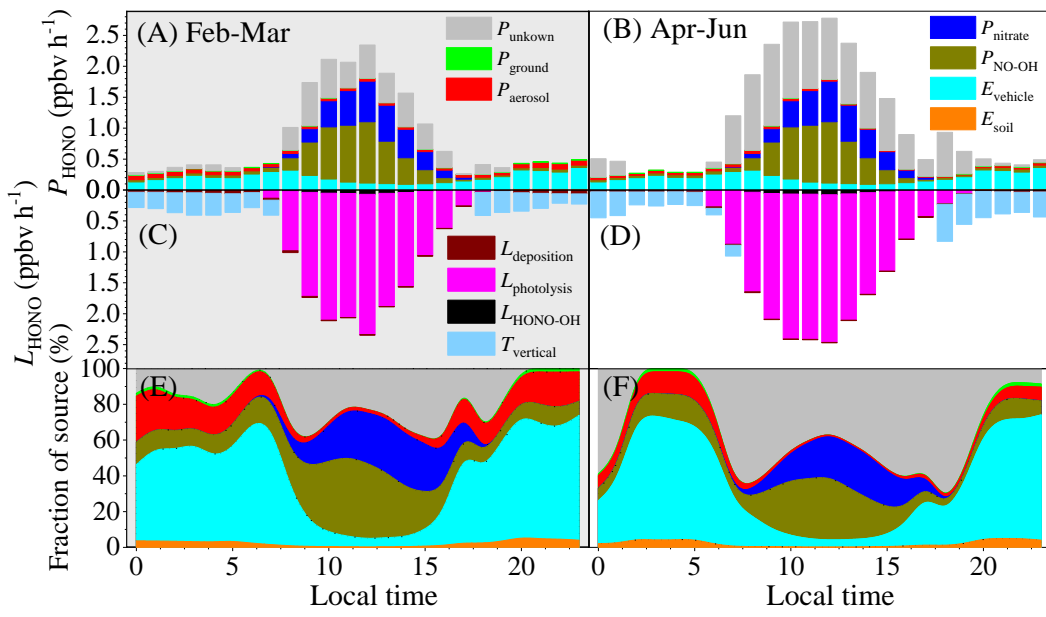


1181

1182

1183

Fig. 3

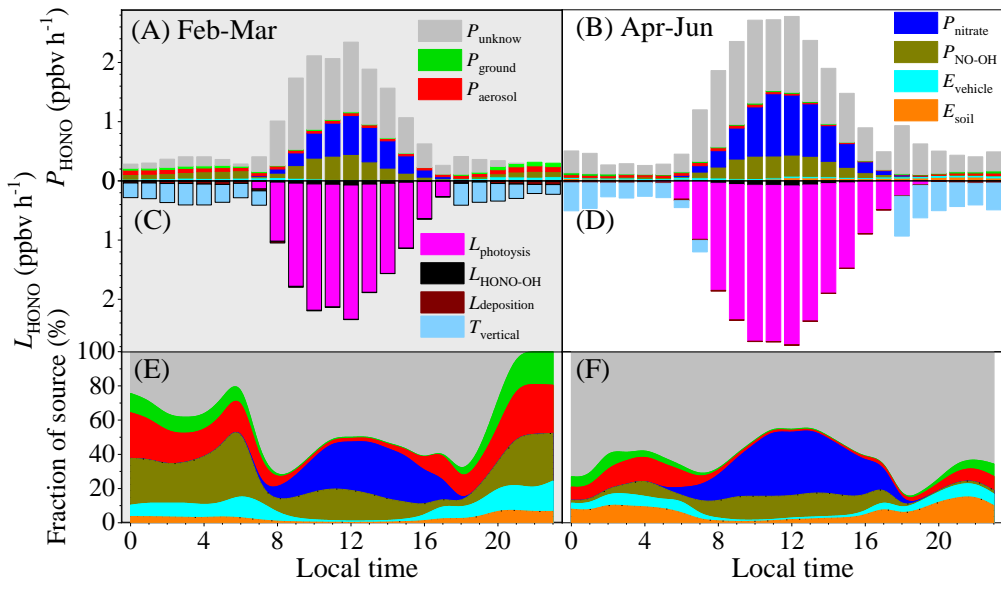


1184

1185

1186

Fig. 4.



1187

1188

Fig. 5.

1 **The promotion effect of nitrous acid on aerosol formation in**
2 **wintertime Beijing: possible contribution of traffic-related**
3 **emission**

4

5 Yongchun Liu^{1*}, Yusheng Zhang¹, Chaofan Lian^{2,6}, Chao Yan³, Zeming Feng¹, Feixue
6 Zheng¹, Xiaolong Fan¹, Yan Chen^{2,6}, Weigang Wang^{2,6*}, Biwu Chu^{3,4}, Yonghong Wang³,
7 Jing Cai³, Wei Du³, Kaspar R. Daellenbach³, Juha Kangasluoma^{1,3}, Federico Bianchi^{1,3},
8 Joni Kujansuu^{1,3}, Tuukka Petäjä³, Xuefei Wang⁶, Bo Hu⁵, Yuesi Wang⁵, Maofa Ge²,
9 Hong He⁴ and Markku Kulmala^{1,3*}

10

11 1. Aerosol and Haze Laboratory, Advanced Innovation Center for Soft Matter Science and
12 Engineering, Beijing University of Chemical Technology, Beijing, 100029, China

13 2. State Key Laboratory for Structural Chemistry of Unstable and Stable Species, Beijing
14 National Laboratory for Molecular Sciences, Institute of Chemistry, Chinese Academy of
15 Sciences, Beijing 100190, China

16 3. Institute for Atmospheric and Earth System Research/Physics, Faculty of Science, University
17 of Helsinki, P.O. Box 64, FI-00014, Finland

18 4. State Key Joint Laboratory of Environment Simulation and Pollution Control, Research
19 Center for Eco-Environmental Sciences, Chinese Academy of Sciences, Beijing, 100085, China

20 5. State Key Laboratory of Atmospheric Boundary Layer Physics and Atmospheric Chemistry,
21 Institute of Atmospheric Physics, Chinese Academy of Sciences, Beijing, 100029, China

22 6. University of Chinese Academy of Sciences, Beijing 100049, PR China

23

24

25 **Supplement information**

26 **Non-refractory PM_{2.5} (NR-PM_{2.5}) measurement.** Concentration of NR-PM_{2.5} was
27 measured with a ToF-ACSM (Aerodyne Co. Ltd., USA). The operation protocol and
28 the configuration of ToF-ACSM has been described well in previous work (Fröhlich et
29 al., 2013). Namely, PM_{2.5} particles from the inlet were focused by a PM_{2.5} aerodynamic
30 lens (Williams et al., 2013), and then vaporized by a standard vaporizer heated at 600
31 °C followed by electronic ionization (EI, 70 eV). The non-refractory components
32 including chloride, nitrate, sulfate, ammonia and organics were measured using a time-
33 of-flight mass spectrometer with unit mass resolution (UMR). The concentrations of
34 the above species were calculated based on the measured fragments signals, the signal
35 ions (SI), the fragment table, the measured ionization efficiency (IE) of nitrate and the
36 corresponding relative ionization efficiency (RIE) for sulfate, chloride, ammonia and
37 organics. IE calibration of nitrate was performed using 300 nm dry NH₄NO₃ every
38 month during this observation study.

39 **VOCs measurement.** VOCs were measured using a Single Photo Ionization Time-of-
40 flight Mass spectrometer (SPI-ToF-MS 3000R, Hexin Mass Spectrometry). 0.8 L min⁻¹
41 of filtered air was sucked from the whole sampling tube and heated to 80 °C in the
42 inlet. VOCs were selectively enriched continuously through a polydimethylsiloxane
43 (PDMS) membrane, and then ionized by VUV light (10.5 eV) with a deuterium lamp.
44 The concentration of VOCs was determined with the time-of-flight mass spectrometer
45 (ToF-MS) based upon external standard curves of PAMS and TO-15 standard gases
46 (Linde Electronics & Specialty Gases, USA). VOCs with m/z from 40 to 300 were

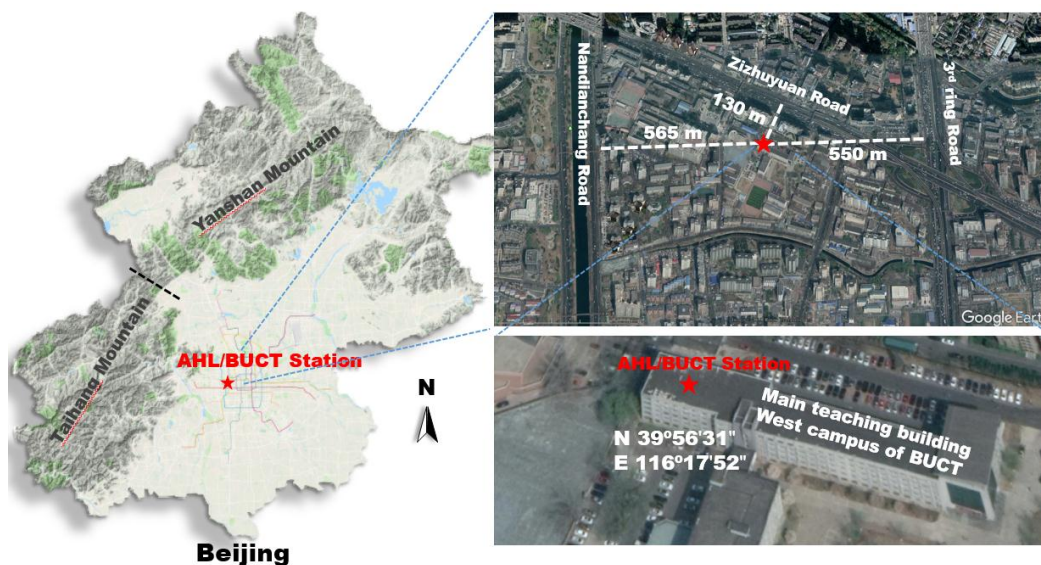
47 recorded with 3 min of time resolution, while hourly averaged concentration were
48 reported in this work. Calibration was performed every week.

49 **HONO measurement.** HONO in ambient air directly sampled from the window of the
50 laboratory was absorbed by a solution containing 0.06 mol L⁻¹ sulfnilamide in 1 mol L⁻¹
51 HCl, and then transformed into an azo dye by *N*-(1-naphthyl) ethylene-
52 diaminedihydrochloride (0.8 mmol L⁻¹). The azo dye was pumped into Teflon absorption
53 cells (Liquid Core Waveguide, LCW) and detected by a mini-spectrometer with a diode
54 array detector (Ocean Optics, SD2000). The HONO concentrations was obtained by
55 subtracting the calibrated signal of the second coil from the first coil using external
56 nitrile standard solutions. Zero point calibration was performed every day using
57 scrubbed zero air (Tong et al., 2016).

58 **Photolysis rate constants of HONO and O₃.** Photolysis rate constants of NO₂(J_{NO_2}),
59 HONO(J_{HONO}) and O₃(J_{O_3}) under clear sky conditions were calculated according to the
60 solar zenith angle and the location using a box model (FACSIMILE 4). NO₂ photolysis
61 sensor (J_{NO_2} , Metcon) was unavailable, while UVB is always available during our
62 observation study. However, it was available from Aug 17 to Sep 16, 2018. A
63 calibration function between the measured UVB light intensity and J_{NO_2} was
64 established to correct the influence the climatological O₃ column, aerosol optical depth
65 and cloud cover on surface UV light intensity from Aug 17 to Sep 16, 2008. As shown
66 in Figure S10, the model well predicted the J_{NO_2} . Then the J_{NO_2} during this campaign
67 study was predicted using the model. We further confirmed the calculated J_{NO_2} by
68 comprising the OH concentration estimated by the J_{OH} according to the equation

69 $(COH=J_{OH} \times 2 \times 10^{11} \text{ molecules cm}^{-3})$ (Tan et al., 2019) and the measured OH
70 concentration at Huairou, which is 60 km northeast from BUCT, from Jan 11 to Mar 10,
71 2016. As shown in Figure S10C, the estimated diurnal curve of OH is comparable with
72 that measured at Huairou. **Fig. S7 shows the calculated photolysis rates.**
73

74 **Supplementary figures**

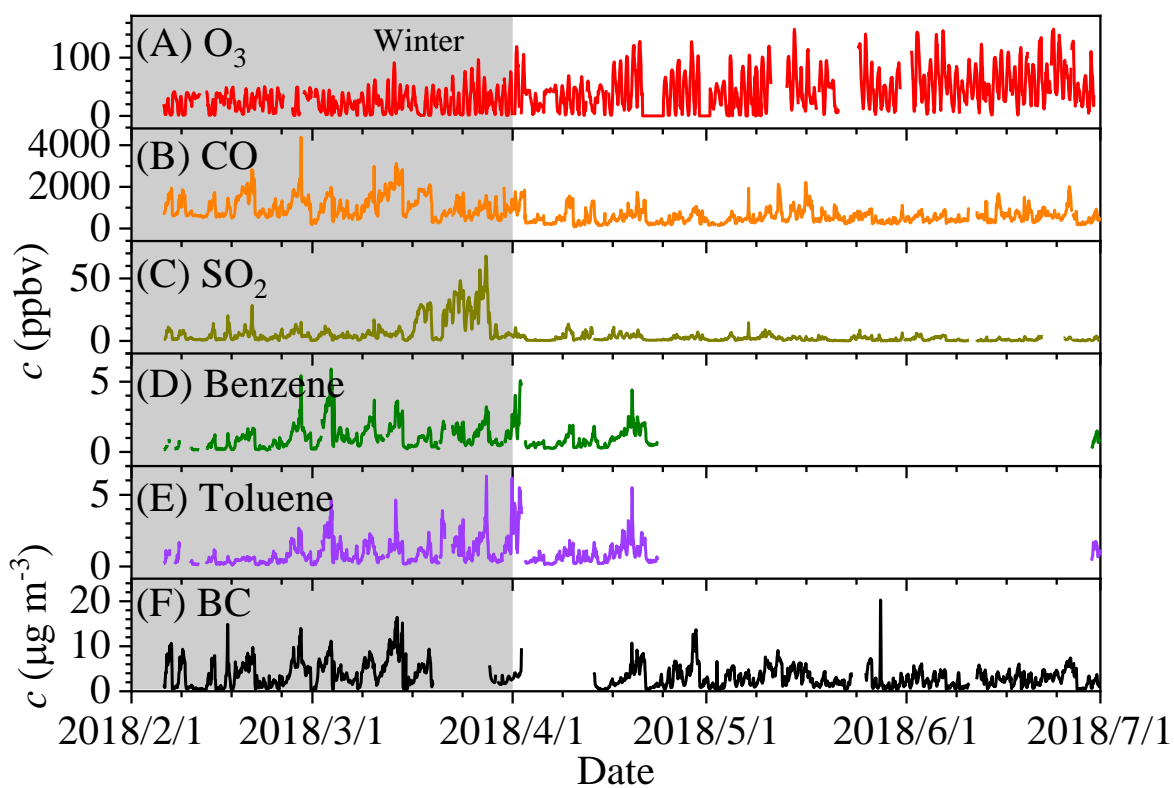


75

76 Figure S1. Location of AHL/BUCT observation station. The map was

77

made from Wemap and Google Earth.

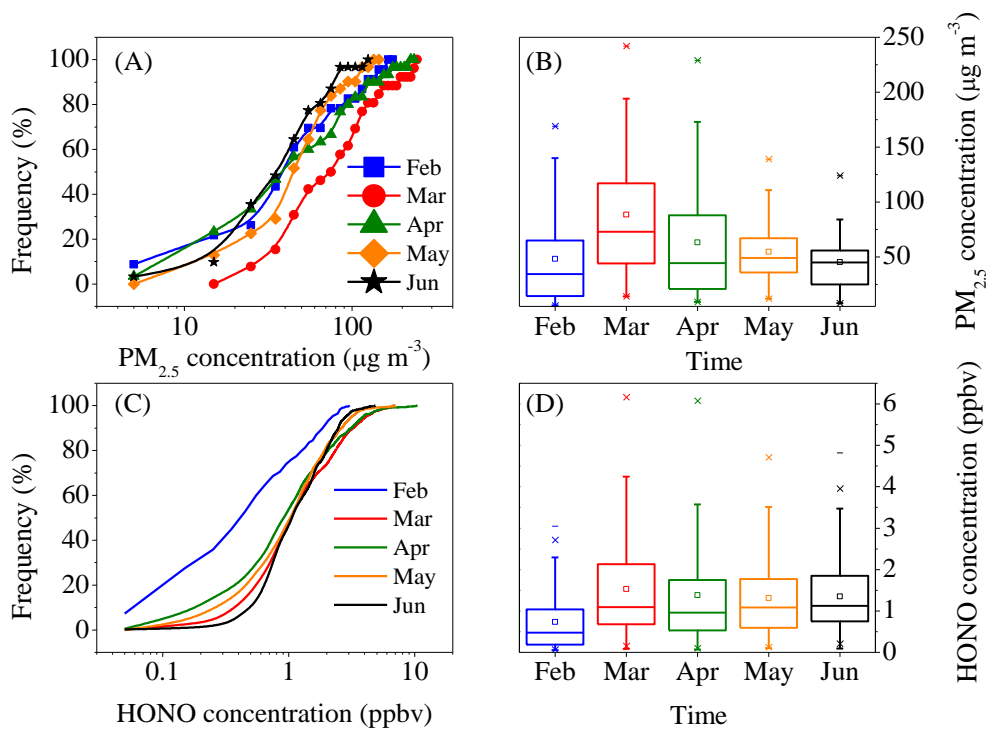


78

79 Figure S2. Hourly averaged (A)-(F) concentration of pollutants from Feb 1 to Jun 30,

80

2018.



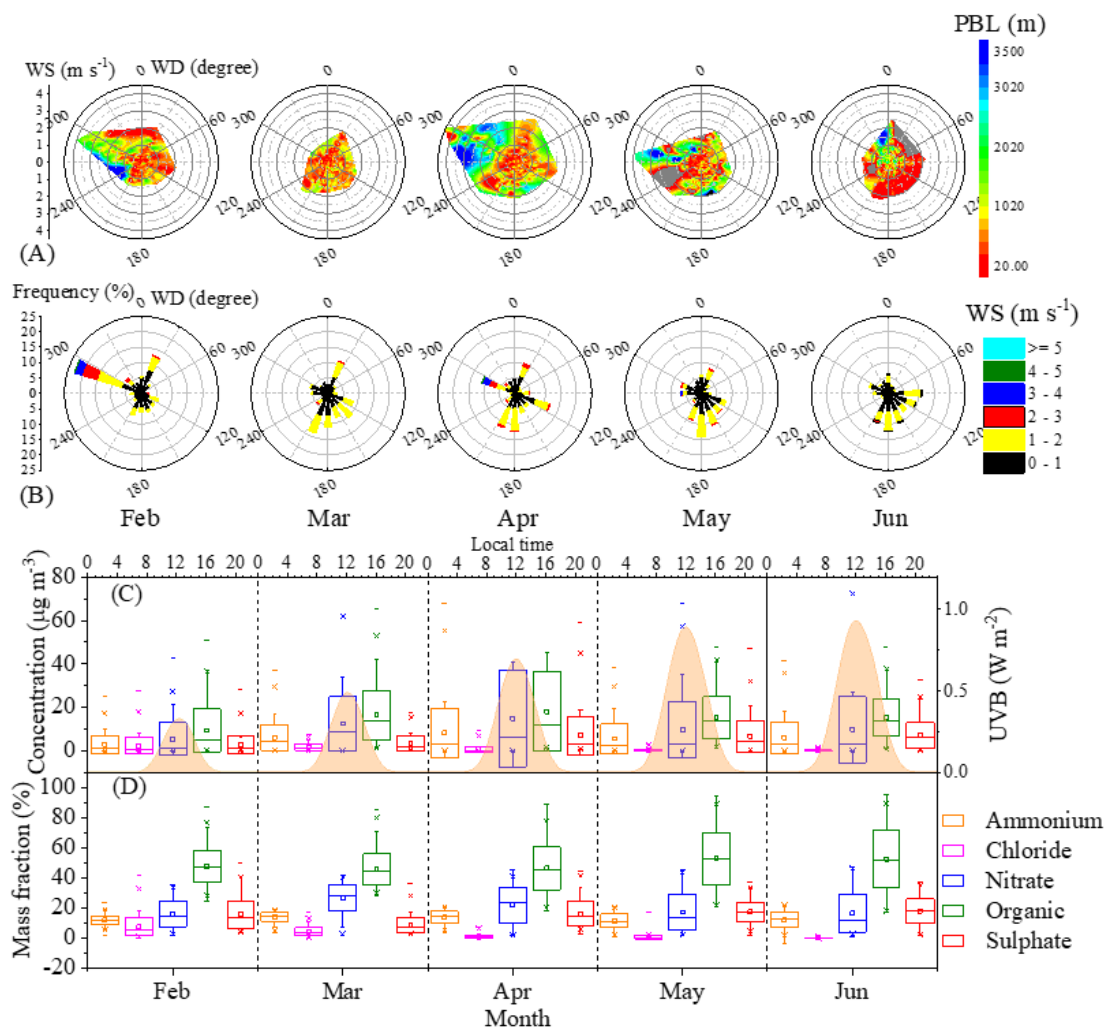
81

82

83 Figure S3. The monthly cumulative frequency of PM_{2.5} and HONO and the monthly

84 mean concentration of PM_{2.5} and HONO.

85



86

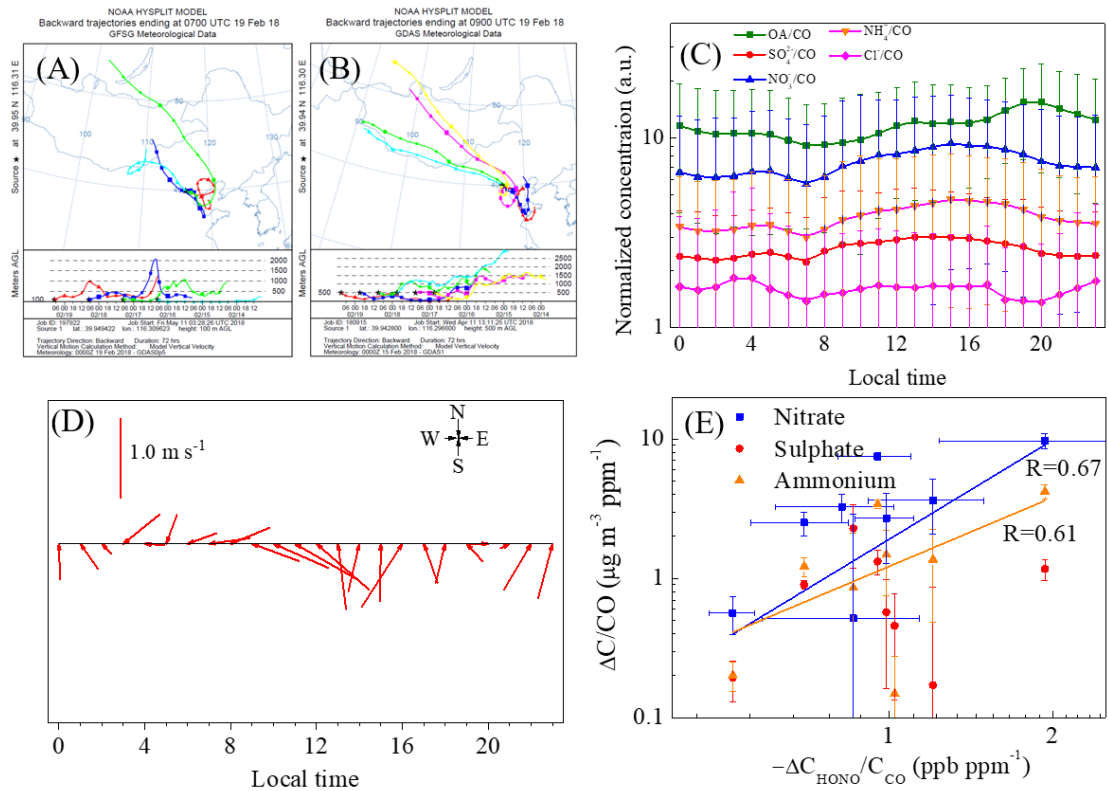
87 Figure S4. (A)-(B) monthly Windrose-PBL plots, and monthly averaged (C) UVB

88 intensity, mass concentration and (D) fraction of individual component in NR-PM_{2.5}

89 composition from Feb to Jun, 2018.

90

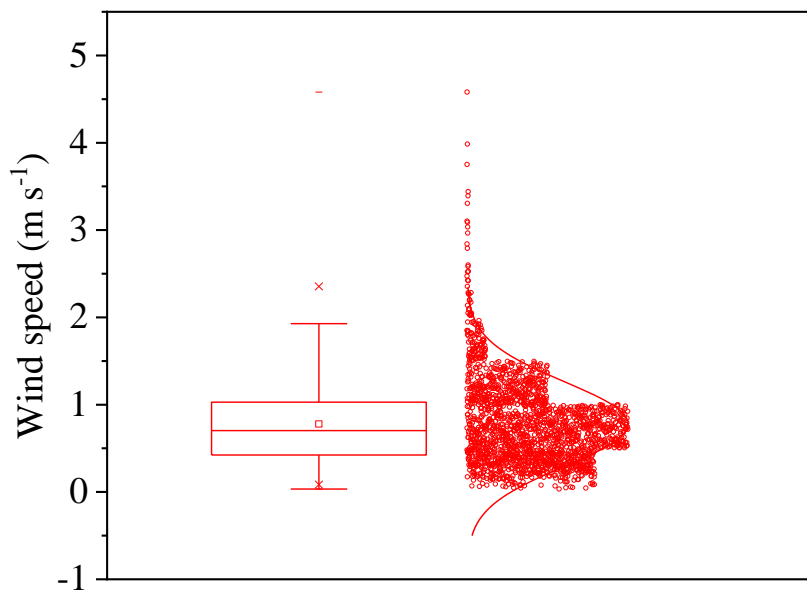
91



92

93 Figure S5. Transport of air mass during Chinese New Year based on back trajectory
 94 analysis (A) at 100 and (B) 500 m height; (C) Diurnal variation of NR-PM_{2.5} normalized
 95 to CO concentration from Feb 1 to March 31; (D) Hourly averaged wind speed variation
 96 in the 12th episode; (E) Correlation of the concentration increment of individual
 97 component and consumed HONO normalized to CO in the daytime.

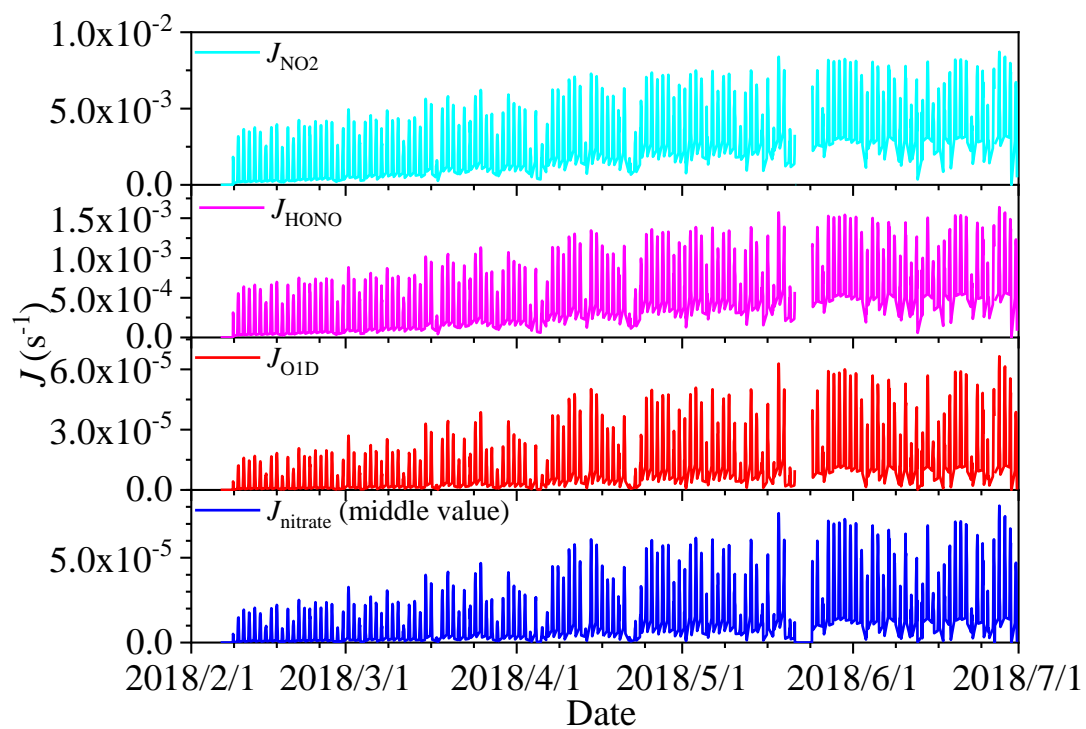
98



99

100 Figure S6. Distribution of wind speed when the $\text{PM}_{2.5}$ concentration was larger than 50

101 $\mu\text{g m}^{-3}$ and the RH was less than 90 %.



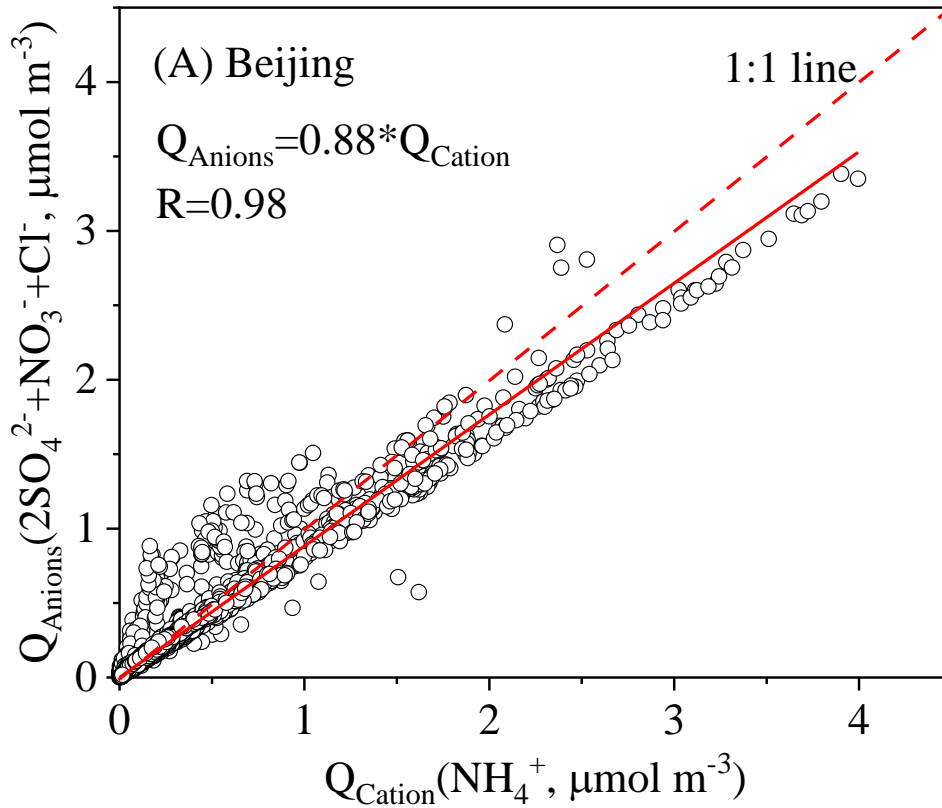
102

103 Fig. S7. The photolysis rate of NO_2 , HONO, O_3 (O1D) and nitrate (middle value)

104

from 8:00 am to 6:00 pm.

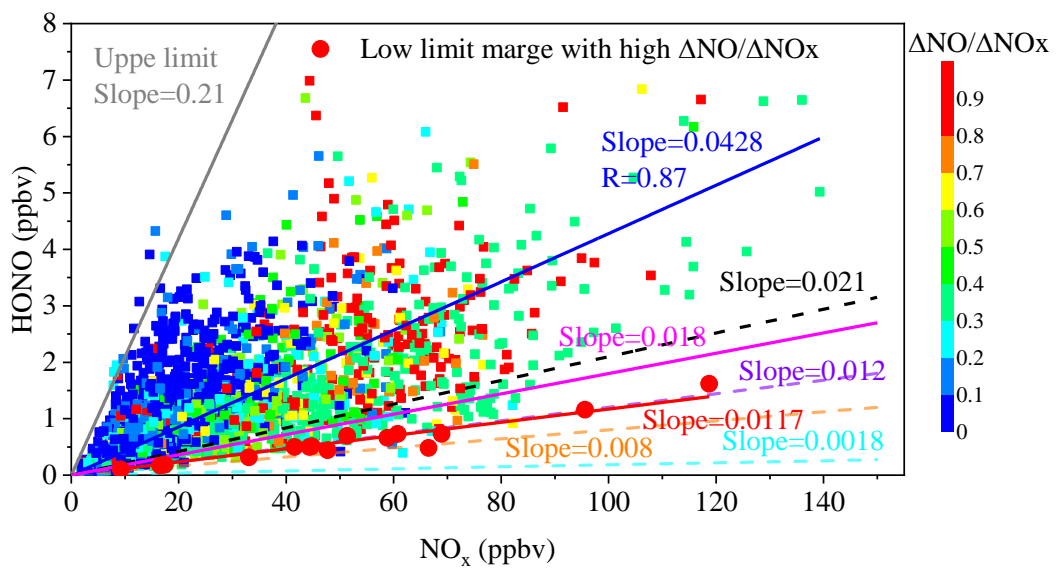
105



106

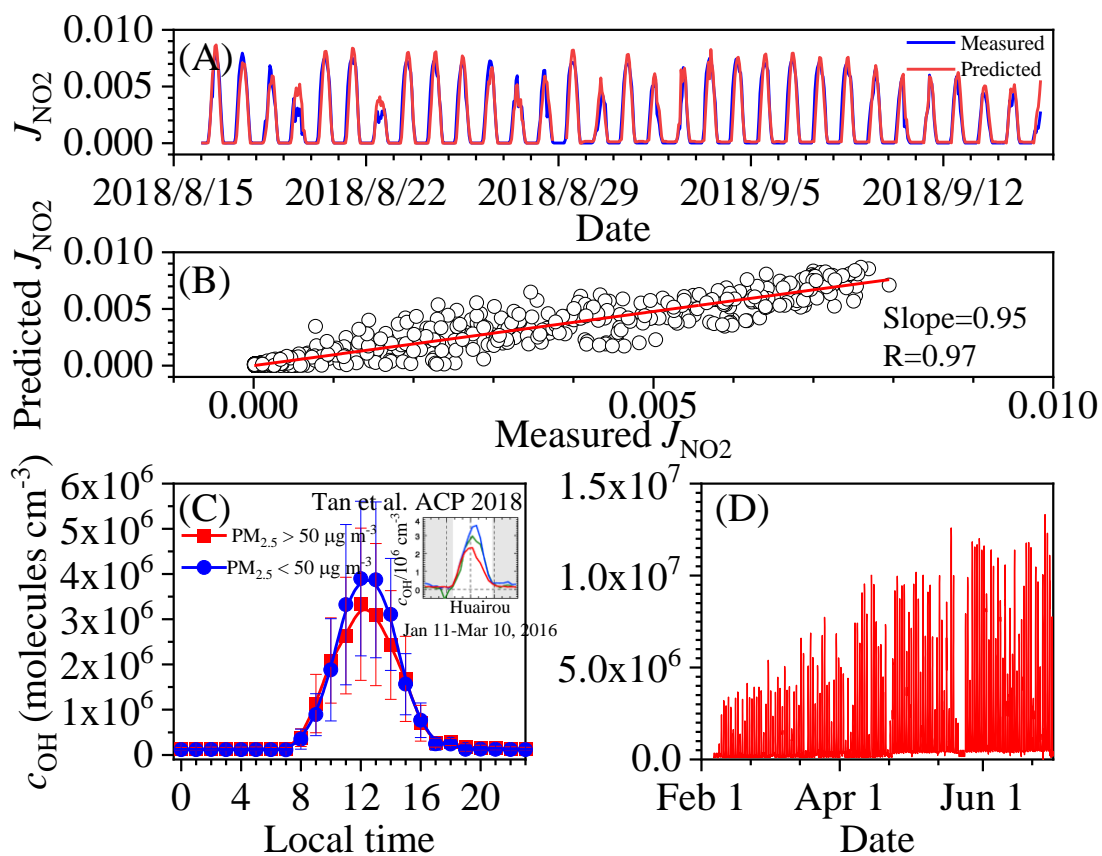
107 Figure S8. Correlation of the charge between inorganic anions and cations in non-
 108 refractory PM_{2.5} in Beijing.

109



110

111 Figure S9. Correlation of measured HONO concentration with NO_x concentration.



112

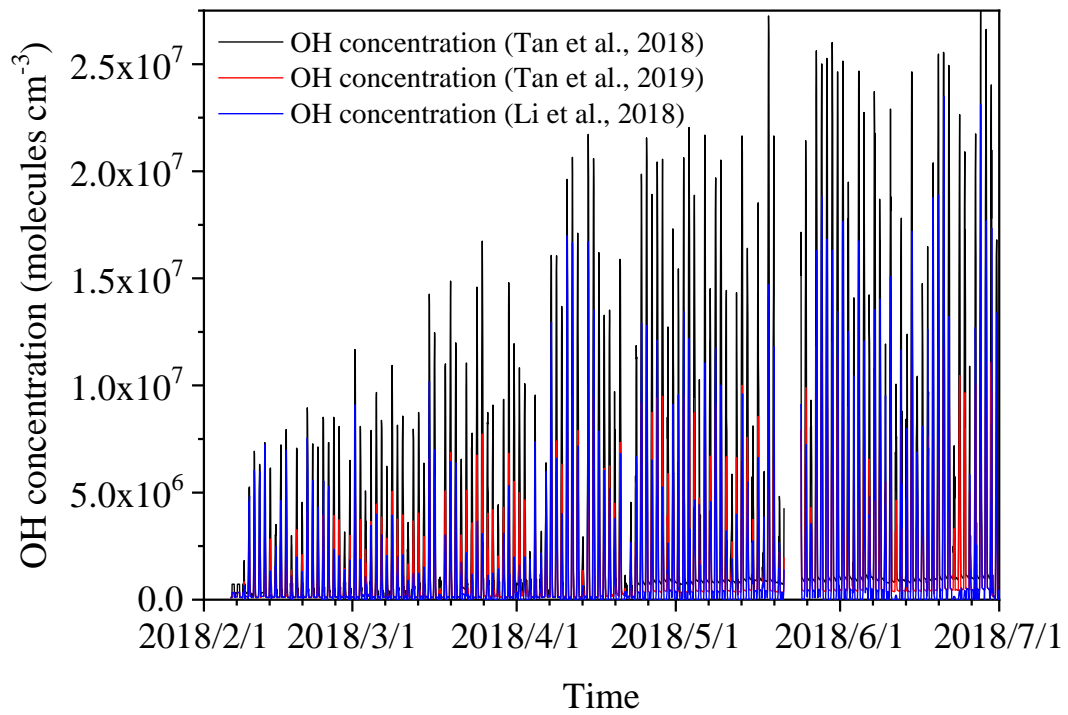
113 Figure S10. (A) Measured and predicted J_{NO_2} and (B) the correlation between measured

114 and predicted J_{NO_2} from Aug. 15 to Sep. 16; (C) calculated diurnal curve of OH

115 concentration based on $J_{\text{O}_1\text{D}}$ compared with that measured at Huairou (60 km northeast

116 from BUCT) from Jan 11 to Mar 10, 2016; (D) OH concentrations estimated using

117 $c_{\text{OH}} = J_{\text{O}_1\text{D}} \times 2 \times 10^{11}$ (Tan et al., 2019).



118
119
120

Fig. S11. Estimated OH concentration using different methods.

Supplementary tables

Table S1. ANOVA statistics analysis for the monthly mean fraction of the individual component in NR-PM_{2.5} and HONO concentration.

Component	Fraction of NR-PM _{2.5} (%) or Concentration of gaseous pollutants (ppbv)				
	Feb	Mar	Apr	May	Jun
Ammonium	Feb (12.2±2.9)				
	Mar (14.2±2.8)	Significant			
	Apr (14.0±4.0)	Significant	Not significant		
	May (11.6±4.6)	Not significant	Significant	Significant	
	Jun (12.2±5.2)	Not significant	Significant	Significant	Not significant
Chloride	Feb (7.7±6.1)				
	Mar (4.4±2.6)	Significant			
	Apr (1.1±1.2)	Significant	Significant		
	May (0.7±1.1)	Significant	Significant	Not significant	
	Jun (0.3±0.2)	Significant	Significant	Significant	Not significant
Nitrate	Feb (16.2±8.5)				
	Mar (26.7±8.8)	Significant			
	Apr (22.0±11.7)	Significant	Significant		
	May (17.3±11.8)	Not significant	Significant	Significant	
	Jun (16.7±12.8)	Not significant	Significant	Significant	Not significant
Organic	Feb (47.9±10.7)				
	Mar (45.9±10.2)	Not significant			
	Apr (46.5±14.2)	Not significant	Significant		
	May (52.9±17.0)	Not significant	Significant	Significant	
	Jun (52.6±18.7)	Significant	Significant	Significant	Not significant

Sulfate	Feb (16.0±9.1)					
	Mar (8.8±5.4)	Significant				
	Apr (16.4±8.2)	Not significant	Significant			
	May (17.5±6.6)	Significant	Significant	Not significant		
	Jun (18.2±8.0)	Significant	Significant	Significant	Not significant	
BC	Feb (3.0±2.8)					
	Mar (4.6±3.1)	Significant				
	Apr (3.2±2.6)	Not significant	Significant			
	May (2.8±2.1)	Not significant	Significant	Not significant		
	Jun (2.6±1.5)	Significant	Significant	Significant	Not significant	
HONO	Feb (0.73±0.70)					
	Mar (1.53±1.25)	Significant				
	Apr (1.38±1.35)	Significant	Not significant			
	May (1.31±1.00)	Significant	Significant	Not significant		
	Jun (1.35±0.80)	Significant	Significant	Not significant	Not significant	
NO _x	Feb (20.4±17.3)					
	Mar (40.5±24.0)	Significant				
	Apr (22.8±18.6)	Not significant	Significant			
	May (25.0±15.9)	Significant	Significant	Not significant		
	Jun (19.0±12.1)	Not significant	Significant	Significant	Significant	Significant
SO ₂	Feb (3.8±3.3)					
	Mar (12.1±13.0)	Significant				
	Apr (2.8±2.4)	Significant	Significant			
	May (1.8±1.7)	Significant	Significant	Not significant		
	Jun (1.3±1.2)	Significant	Significant	Significant	Not significant	
CO	Feb (959.6±554.6)					

	Mar (1075.0±571.8)	Significant			
	Apr (546.6±378.1)	Significant	Significant		
	May (554.1±336.9)	Significant	Significant	Not significant	
	Jun (583.4±286.2)	Significant	Significant	Not significant	Not significant
O ₃	Feb (22.6±14.6)				
	Mar (23.8±19.2)	Not significant			
	Apr (43.5±29.0)	Significant	Significant		
	May (42.5±28.3)	Significant	Significant	Not significant	
	Jun (57.2±30.7)	Significant	Significant	Significant	Significant

Note: “Significant” or “Not significant” denotes that the difference of the monthly mean fractions or concentrations is significant or not significant at the 0.05 level.

Tab. S2. Mean concentrations of HONO and PM_{2.5} in selected episodes

Episode No.	Duration	HONO (ppb)	Average PM _{2.5} concentration	NR-PM _{2.5} Concentration (%)									
				Chloride		Nitrate		Organic		Sulphate		Ammonium	
				(%)	($\mu\text{g m}^{-3}$)	(%)	($\mu\text{g m}^{-3}$)	(%)	($\mu\text{g m}^{-3}$)	(%)	($\mu\text{g m}^{-3}$)	(%)	($\mu\text{g m}^{-3}$)
1	Feb 2-5	0.38±0.28	9.3±4.5	4.0±2.3	0.26±0.39	12.3±5.6	0.80±1.17	51.1±10.0	2.68±3.00	20.6±9.2	0.69±0.24	12.0±3.2	0.54±0.49
2	Feb 8-9	0.90±0.72	44.5±3.5	6.3±2.9	1.59±1.46	15.8±7.9	4.20±3.87	49.9±4.8	9.63±7.64	17.3±8.8	2.31±1.42	10.8±1.0	2.14±1.69
3	Feb 10-12	0.31±0.40	9.0±0.8	5.2±3.5	0.18±0.22	6.8±3.9	0.30±0.44	48.6±10.6	1.75±1.72	28.1±11.5	0.74±0.38	11.2±2.5	0.35±0.23
4	Feb 16-19	1.38±0.86	101.5±26.8	15.5±4.2	9.04±4.94	25.0±4.1	13.15±7.73	32.2±3.8	18.21±8.25	14.4±3.7	7.82±4.39	12.9±1.5	6.85±3.78
5	Feb 21-24	0.64±0.58	24.3±7.0	5.5±4.1	0.60±0.51	14.9±6.3	1.80±1.38	56.3±10.0	5.83±2.94	11.8±5.0	1.17±0.67	11.6±2.8	1.24±0.77
6	Feb 25-28	0.87±0.64	108.8±42.9	5.2±1.4	2.94±1.97	27.1±3.9	15.3±8.77	42.5±6.8	22.83±9.68	10.4±3.8	6.44±5.78	14.7±1.8	8.34±5.30
7	Mar 2-3	1.41±0.84	120.0±47.0	8.3±2.2	4.23±1.72	26.5±4.8	15.29±9.44	44.4±6.2	23.40±10.49	7.2±1.9	4.36±3.37	13.5±1.9	7.74±4.76
8	Mar 8-10	1.36±0.89	88.7±34.2	4.8±1.8	1.87±1.09	28.3±5.2	11.00±6.20	43.0±7.0	15.65±7.15	9.0±2.8	3.10±1.42	14.9±2.0	5.58±2.92
9	Mar 11-14	2.27±1.68	170.3±75.4	3.5±0.9	2.48±1.32	34.8±4.3	28.32±19.09	36.8±5.0	27.90±15.78	8.1±1.8	6.60±4.72	16.8±1.5	13.57±8.99
10	Mar 16-19	1.88±1.38	66.0±25.7	3.8±1.7	1.99±1.18	30.2±6.3	17.40±12.45	35.9±2.8	20.87±10.52	13.5±5.1	7.00±4.92	16.5±1.0	9.17±5.86
11	Mar 21-23	1.41±0.72	83.7±22.1	5.3±2.8	2.54±2.30	31.5±3.8	12.23±5.22	45.1±6.7	18.02±5.46	4.4±1.0	1.67±0.92	13.7±1.6	5.38±2.08
12	Mar 25-27	2.22±1.34	129.5±51.9	2.0±0.7	0.94±0.64	35.3±3.6	16.32±9.90	41.5±5.4	20.46±10.18	5.7±1.2	2.56±1.68	15.6±1.6	7.11±4.37

1 Table S3. The summary of the HONO/NO_x ratio from vehicles in this study and the
 2 reported emission ratio of HONO/NO_x from vehicles in China.

No.	Time	$\Delta\text{NO}/\Delta\text{NO}_x$	$R_{\Delta\text{NO}/\Delta\text{NO}_x}$	$\Delta\text{HONO}/\Delta\text{NO}_x$	$R_{\Delta\text{HONO}/\Delta\text{NO}_x}$
1	2018/2/6 5:00-8:00	1.00	0.99	1.3%	0.92
2	2018/2/8 5:00-8:00	0.94	0.99	1.8%	0.96
3	2018/3/3 5:00-8:00	0.98	0.99	2.4%	0.96
4	2018/3/13 5:00-8:00	1.00	0.99	1.4%	0.86
5	2018/4/15 5:00-7:00	0.82	0.97	2.3%	0.99
Mean		0.95±0.08	-	1.8±0.5%	-
Time	Place	Methods	$\Delta\text{HONO}/\Delta\text{NO}_x$		Reference
			Range	Mean	
2015/9/1-2016/8/31	Ji'nan, Shandong	Empirical analysis of field data	0.19%-0.87%	0.53±0.20%	(Li et al., 2018)
2011/8/3-2012/5/31	Hongkong	Empirical analysis of field data	0.5%-1.6%	1.2±0.4%	(Xu et al., 2015)
2015/3/11-2015/3/21	Hongkong	Tunnel experiment	-	1.24±0.35%	(Liang et al., 2017)
2014	Beijing	Tunnel experiment	-	2.1%	(Yang et al., 2014)
2017	Beijing	Chassis dynamometer test	0.03%-0.42%	0.18%	(Liu et al., 2017)
2016/12/16-2016/12/24	Beijing	Empirical analysis of field data	-	1.3%	(Zhang et al., 2018)
2016/12/7-2016/12/13	Beijing	Low limit correlation of field data	-	1.41%	(Meng et al., 2019)
2018/2/1-2018/6/30	Beijing	Low limit correlation of field data	-	1.17%	This study
2018/2/1-2018/6/30	Beijing	Empirical analysis of field data	1.3-2.4%	1.8±0.5%	This study

3

4 **References:**

- 5 Fröhlich, R., Cubison, M. J., Slowik, J. G., Bukowiecki, N., Prévôt, A. S. H., Baltensperger, U., Schneider,
 6 J., Kimmel, J. R., Gonin, M., Rohner, U., Worsnop, D. R., and Jayne, J. T.: The ToF-ACSM: a portable
 7 aerosol chemical speciation monitor with TOFMS detection, *Atmos. Meas. Tech.*, 6, 3225-3241,
 8 10.5194/amt-6-3225-2013, 2013.
- 9 Li, D., Xue, L., Wen, L., Wang, X., Chen, T., Mellouki, A., Chen, J., and Wang, W.: Characteristics and
 10 sources of nitrous acid in an urban atmosphere of northern China: Results from 1-yr continuous
 11 observations, *Atmos. Environ.*, 182, 296-306, <https://doi.org/10.1016/j.atmosenv.2018.03.033>, 2018.
- 12 Liang, Y., Zha, Q., Wang, W., Cui, L., Lui, K. H., Ho, K. F., Wang, Z., Lee, S.-c., and Wang, T.: Revisiting

13 nitrous acid (HONO) emission from on-road vehicles: A tunnel study with a mixed fleet, *J. Air Waste*
14 *Manage. Assoc.*, 67, 797-805, 10.1080/10962247.2017.1293573, 2017.

15 Liu, Y., Lu, K., Ma, Y., Yang, X., Zhang, W., Wu, Y., Peng, J., Shuai, S., Hu, M., and Zhang, Y.: Direct
16 emission of nitrous acid (HONO) from gasoline cars in China determined by vehicle chassis
17 dynamometer experiments, *Atmos. Environ.*, 169, 89-96, 10.1016/j.atmosenv.2017.07.019, 2017.

18 Meng, F., Qin, M., Tang, K., Duan, J., Fang, W., Liang, S., Ye, K., Xie, P., Sun, Y., Xie, C., Ye, C., Fu,
19 P., Liu, J., and Liu, W.: High resolution vertical distribution and sources of HONO and NO₂ in the
20 nocturnal boundary layer in urban Beijing, China, *Atmos. Chem. Phys. Discuss.*, 2019, 1-34,
21 10.5194/acp-2019-613, 2019.

22 Tan, Z. F., Lu, K. D., Jiang, M. Q., Su, R., Wang, H. L., Lou, S. R., Fu, Q. Y., Zhai, C. Z., Tan, Q. W.,
23 Yue, D. L., Chen, D. H., Wang, Z. S., Xie, S. D., Zeng, L. M., and Zhang, Y. H.: Daytime atmospheric
24 oxidation capacity in four Chinese megacities during the photochemically polluted season: a case study
25 based on box model simulation, *Atmos. Chem. Phys.*, 19, 3493-3513, 10.5194/acp-19-3493-2019, 2019.

26 Tong, S., Hou, S., Zhang, Y., Chu, B., Liu, Y., He, H., Zhao, P., and Ge, M.: Exploring the nitrous acid
27 (HONO) formation mechanism in winter Beijing: direct emissions and heterogeneous production in
28 urban and suburban areas, *Faraday Discuss.*, 189, 213-230, 10.1039/c5fd00163c, 2016.

29 Williams, L. R., Gonzalez, L. A., Peck, J., Trimborn, D., McInnis, J., Farrar, M. R., Moore, K. D., Jayne,
30 J. T., Robinson, W. A., Lewis, D. K., Onasch, T. B., Canagaratna, M. R., Trimborn, A., Timko, M. T.,
31 Magoon, G., Deng, R., Tang, D., de la Rosa Blanco, E., Prevot, A. S. H., and Worsnop, D. R.:
32 Characterization of an aerodynamic lens for transmitting particles greater than 1 micrometer in diameter
33 into the Aerodyne aerosol mass spectrometer, *Atmos. Meas. Tech.*, 6, 3271-3280, 10.5194/amt-6-3271-
34 2013, 2013.

35 Xu, Z., Wang, T., Wu, J., Xue, L., Chan, J., Zha, Q., Zhou, S., Louie, P. K. K., and Luk, C. W. Y.: Nitrous
36 acid (HONO) in a polluted subtropical atmosphere: Seasonal variability, direct vehicle emissions and
37 heterogeneous production at ground surface, *Atmos. Environ.*, 106, 100-109,
38 10.1016/j.atmosenv.2015.01.061, 2015.

39 Yang, Q., Su, H., Li, X., Cheng, Y., Lu, K., Cheng, P., Gu, J., Guo, S., Hu, M., Zeng, L., Zhu, T., and
40 Zhang, Y.: Daytime HONO formation in the suburban area of the megacity Beijing, China, *Science*
41 *China-Chemistry*, 57, 1032-1042, 10.1007/s11426-013-5044-0, 2014.

42 Zhang, W., Tong, S., Ge, M., An, J., Shi, Z., Hou, S., Xia, K., Qu, Y., Zhang, H., Chu, B., Sun, Y., and
43 He, H.: Variations and sources of nitrous acid (HONO) during a severe pollution episode in Beijing in
44 winter 2016, *The Science of the total environment*, 648, 253-262, 10.1016/j.scitotenv.2018.08.133, 2018.

45